DESIGN, MODELING AND CONTROL OF AN AUTONOMOUS FIELD ROBOT FOR WHITE ASPARAGUS HARVESTING

Der Fakultät Maschinenbau der Otto-von-Guericke-Universität Magdeburg zur Erlangung des akademischen Grades

Doktoringenieurin / Doktoringenieur

(Dr.-Ing.)

von M. Eng. Fuhong Dong
geb. am 16.02.1978 in Shandong China
genehmigt durch die Fakultät Maschinenbau
der Otto-von-Guericke-Universität Magdeburg

Gutachter:
Prof. Dr.-Ing. Roland Kasper
Prof. Dr. Hans W. Griepentrog

Promotionskolloquium am 23.09.2014

In the memory of my mother

Acknowledgement

The past few years have been an impressive and challenging journey for me in the growth of my research as well as of myself. Much has changed since I joined Institute of Mobile Systems. I have been privileged to have worked with excellent colleagues, and to have got so much support of many people. I would like to take this opportunity to express my appreciation for all the help both in my research work and in my life.

First of all, I want to express my sincere gratitude to Prof. Dr. Roland Kasper who made this work possible in the first place. He accepted me as a PhD student in his group, and continuously guided me throughout my research with his valuable experience and knowledge, offered a permanent support and very much professional advice for me in my academic career. Without his guidance and persistence help this dissertation would not have been possible. I deeply appreciate Professor Dr. Griepentrog who has agreed to be the supervisor of my dissertation and given me a lot of insightful comments and constructive suggestions with his vast expertise in agricultural engineering.

I would like to acknowledge Dr. Wolfgang Heinemann for his great effort in the coordination of the project collaboration with the companies. I was always able to get immediate and skilled advice from him when I was stuck in difficulty with my work. To work with Wolfgang is really a great pleasure, especially for the successful experimental tests of the proposed navigation system on the prototype in the white asparagus field. Special thanks go to Dr. Olaf Petzolt, who gave me generous support on the Verilog programming and USB communication. He showed me how an excellent engineer should be. I am also thankful for the collaboration with the former college Thomas Fröhlich for his support on the prototype setup.

I am grateful to the group members of IMS who have contributed in making the environment enjoyable and stimulating and colored my experience with differing points of view in the last five years. In particular, special thanks go to Dr. Hans-Georg Baldauf for his help on the matters regarding computer and software. Hans, also thank you for sharing the happiness of your family and for the bicycle you lent me. It is rather a pity that I haven't had a chance for an institute bicycle tour with it. I would like to thank Dr. Stephan Schmidt, my first office colleague, for his kindness and endless help with my problems not only in my work but also in my everyday life. I have learned a lot from him "*Nur die Harten kommen in den Garten*!" I'll remember it. I want also to show my appreciation to the ex-colleague Shaowen for the illuminating discussions and the warm encouragement. I am also thankful for the advice given by Normann Borchardt. It is a great enjoyment to discuss with an optimistic. Special thanks go to Uwe Kuske, an expert at mechanical

techniques and a tour enthusiast, who is always ready to solve my problem in laboratory and eager to share his joy in journeys. My sincere gratitude goes to the group secretaries Frauke Heiduk, Angela Dorge, Corinna Kläger and Janine Daniel for their assistant work during these years. As a foreigner, I have sometimes trouble in understanding German and filling tables. They always made everything easier for me.

None of this work would have been possible without the generous support of the Loetec Elektronische Fertigungssysteme GmbH, in Lutherstadt Wittenberg, Germany and the specification of the cultivation features for white asparagus provided by SEYDAER AGROTECHNIK GmbH in Seyda, Germany. I would like to express my gratitude to the family Kalkofen in Cobbel, Germany for providing the white asparagus fields for our experimental tests. The generous treatment by Mr. Kalkofen with the dishes from fresh white asparagus for the lunch is totally unforgettable.

I would like to express my heartfelt appreciation to my husband, Suzhou, who has been always encouraging me to pursue my own career in the research field and providing continuous encouragement and inspiration to finish this dissertation. I am really fortunate to have him to always share all my laughter and tears. Without his support and love I could never have made it to where I am today. Now, we have made it!

Finally, my biggest debt is owed to father in China, and to my brother and sisters who provide me unending love and motivation to go my way. They supported me for all these years to whom I am pleased to dedicate my work.

Abstract

White asparagus harvesting is a typical highly repetitive and labor-intensive work which is carried out mainly by hand at present. The farmers of white asparagus suffer from high labor cost and lack of enough workers with the continuously expanding cultivation area. To partly release the hard work of the labors, this thesis is devoted to developing an autonomous robot which is capable of driving automatically following the target cultivation bed with high precision in the white asparagus field.

The mechanical design of the autonomous field robot is developed cost-effectively under consideration of the cultivation specialty and the application requirements. It has two drive wheels at the front and two casters at the rear to provide balance. The differential drive method is selected for the sake of the control flexibility and simplicity. Benefitting from the erected cultivation mounds of white asparagus over ground the ultrasonic sensors are adopted to determine the in-row position of the robot.

The movement of the field robot is not only affected by varied internal and external disturbances, but also strictly constrained by the limited working environment. Especially, the feasible area of the orientation angle is critical to be observed. The robot is expected to drive along a target row with a preset precision through a suitable guidance system. To achieve a row following operation with a high precision in rows, a hierarchical system, consisting of two independent speed loops of the drive motors against internal disturbance at the low level and a cascade structure at the high level to get rid of the external disturbance, is firstly proposed using conventional PID method based on the kinematics of the differential drive robot. To eliminate any following deviation as soon as possible and to achieve the optimal efficiency, the time-optimal control strategy is further investigated in the row following system. However, limited by the application of the optimal control solver from a third party, it is impossible to be implemented on the selected micro-controller. Fortunately, by referring the results of the time-optimal simulation studies we find a mapping between the time-optimal operating conditions and the orientation angle and lateral displacement. The time-optimal operation conditions can be expressed as a time-varying limitation on the orientation angle according to the actual lateral offset of the cascade system proposed previously. Through supplementing a time-varying limitation according to the actual lateral offset on the reference orientation angle, the previous

proposed hierarchical system based on PID method can perform the same function as the time-optimal controller, which allows an effortless implementation on a micro-controller. The row following effectiveness of the time-optimal control and the improved cascade system are thoroughly compared in the simulation studies. The results show the identical row following performance. In the practical applications, the suggested improved hierarchical algorithms are implemented on a micro-controller, and the processing data are saved and illustrated though USB communication on a laptop. Experiments are further carried out in laboratory as well as outdoors in the field to evaluate the proposed row guidance regime. The results show the satisfactory performance with high precision of ±0.03m in the field.

This field robot is capable of lifting and putting back the film automatically, autonomous drive along the target cultivation bed with high precision against varied disturbances, automatically turning to the next row according to the given geometrical relations. It can be used as a developing platform for the harvesting equipment to be a full automatic harvesting machine for the future research work. Also it can be directly applied as an assistant harvesting robot for white asparagus. Naturally, the automatic row following strategy with a hierarchical structure is suitable for any path-following systems especially for the systems with strict orientation constraints. Finally, the autonomous field robot for white asparagus harvesting is only economical minimal realization due to the financial issue. It could be improved by integration with other modern sensors like GNSS, machine-vision systems through a combination of them to acquire the absolute position of the cultivation beds as a useful supplement to the automatic navigation system.

Kurzreferat

Die vorlegende Arbeit behandelt den Entwurf und das spurgeführte selbstfahrende Regelungssysteme eines Elektronutzfahrzeugs, um die mühsame, arbeitsintensive und körperlich anstrengende Spargelernte möglichst zu erleichtern. Bei der Entwicklung der Maschine sind der sparsame Umgang mit der zur Verfügung stehenden Energie und die umweltfreundliche Technik die Hauptziele. Bei den Antrieben der Maschine werden zwei Elektromotoren eingesetzt, die separat auf zwei Vorderräder aufgebaut werden. Zwei Ultraschallsensoren, die jeweils vorne und hinten an der gleichen Seite eingebaut werden, werden zur Messung der Seitenabstände benutzt.

Der Roboter arbeitet unter dem Einfluss vielfältigen Störungen im Feld. Außerdem ist seine Bewegung durch die besonderen Arbeitsumgebungen streng eingeschränkt. Schließlich wird ein Kaskadensystem, der aus einem inneren Orientierungswinkelregel-kreis und einem äußeren Querverschiebungsregelkreis besteht, verwendet. Durch die weitere Untersuchung der zeitoptimalen Bahnplanung wird die Annährungszeit gegen Störungen deutlich verkürzt. Da die praktische Lösung des komplizierten zeitoptimalen Problems mittels Mikrocontroller zu zeitaufwändig ist, wird eine praktische Strategie auf Basis eines PID Reglers entworfen. Die Versuche werden weiter sowohl unter Laborbedingungen auf einem Modelldamm als auch unter realen Bedingungen auf einem Spargelfeld durchgeführt, um die vorgeschlagene Spurführung zu beurteilen. Die Ergebnisse zeigen eine sehr zufriedenstellende Leistung und Effizienz mit hoher Präzision sowohl im Labor als auch auf dem Feld.

Contents

List of Figures

Table Lists

Index of abbreviations

Abbreviation	Meaning
2D/3D	2-dimensions / 3-dimensions
3G	The third generation of wireless mobile networks
AC	Alternating Current
ARM	Advanced RISC Machines
CAN	Controller Area Network
CDMA	Code division multiple access
CRC	Cycle Redundancy Check
DC	Direct current
GLONASS	Global Orbiting Navigation Satellite Systems
GNSS	Global Navigation Satellite Systems
GPOPS	General Pseudospectral Optimization Software
GPS	Global Positioning Systems
GPRS	General packet radio service
GSM	Global System for Mobile
I2C	Two-wire interface to connect
ID	Identification
I/O	Input/output
IrDA	Infrared data association
MATLAB	Matrix laboratory
NLP	Nonlinear programming
PD	Proportional-Derivative
PID	Proportional-Integral-Derivative
PSoC	Programmable system on a chip
RISC	Reduced instruction set computing
RTK GPS	Real-Time-Kinematics Global Positioning Systems

SNOPT	Sparse Nonlinear OPTimizer
USB	Universal serial bus
WLAN	Wireless Local Area Network

Index of symbols

Symbol	Meaning	Unit
α	Gradient angle	rad
α_{max}	Maximal curvature of the track	rad
θ	Heading angle	rad
ω	Angular speed of the robot	rad·s^{-1}
$F_{grading,max}$	Maximal grading resistance	N
$F_{resistance,max}$	Maximal resistance	N
f_{roll}	Rolling resistance coefficient	-
g_{gear}	Gear ratio	-
$F_{roll,max}$	Maximal rolling resistance	N
G_{weight}	Total weight of the robot	N
v_{wheel}	Linear velocity of the wheel	m·s^{-1}
r_{radius}	Wheel radius	m
r_{min}	Minimal curvature radians	m
$T_{wheel,max}$	Maximal active torque on the wheel	Nm
$T_{resistance,max}$	Maximal resistance torque	Nm
L_a, L_b	Length and width of the robot	m
$\boldsymbol{r}_f, \boldsymbol{r}_r$	Position vector the front and rear ultrasonic sensors in robot coordinate system	-
$\boldsymbol{S}_F, \boldsymbol{S}_R$	Position vector of the front and rear ultrasonic sensors in global coordinate system	-
S_{Fy}, S_{Ry}	Lateral components of $\boldsymbol{S}_F, \boldsymbol{S}_R$	m
S_f, S_r	Front and rear side distances	m
S_f^{lb}, S_f^{ub}	Lower and upper bound of front side distance	m
S_f^{lbs}, S_f^{ubs}	Shrunk lower and upper bound of front side distance	m

S_{ref}	Desired side distances	m
S_r^{lb}, S_r^{ub}	Lower and upper bound of rear side distance	m
T	Transform matrix from robot coordination system to global coordination system	-
v_{ref}	Reference forward velocity	$m \cdot s^{-1}$
x, y	Actual position of the robot	m
x_d, y_d, θ_d	Desired position of the robot	-
e_x, e_y	Row following error in x- and y-direction	m
e_ω	Following error of the angular speed	$rad \cdot s^{-1}$
e_θ	Heading angle deviation	rad
e_S	Offset of the front side distance	m
v_L, v_R	Linear velocity of the left and right wheels	$m \cdot s^{-1}$
u_L, u_R	Control variable of the left and right motors	v
k_{ul}, k_{ur}	Transfer coefficient	-
v	Forward velocity of the robot	$m \cdot s^{-1}$
$\omega_{ml}^*, \omega_{mr}^*$	Reference angular speed of left and right motors	$rad \cdot s^{-1}$
ω_{mref}	Given angular speed	$rad \cdot s^{-1}$
ω_{diff}	Differential angular speed between motors	$rad \cdot s^{-1}$
G_{mcl}	Closed-loop transfer function of the motor speed	-
G_{mPI}	Transfer function of proportional-integral controller	-
J_m	Equivalent motor inertia	$kg \cdot m^2$
R_m	Motor electrical resistance	Ohm
L_m	Motor inductance	H
B_m	Viscous friction coefficient	$N \cdot m \cdot s \cdot rad^{-1}$
k_e	Back-emf constant	$V \cdot s \cdot rad^{-1}$
k_m	Torque constant	$N \cdot m \cdot A^{-1}$

1 Introduction

With the growing population and climate change, the agricultural productivity growth is too slow to meet the increased demand for food [10]. In the near future, advanced agricultural technologies, combined with intelligent, small-scale technologies, can contribute parched land bloom and alleviate the serious food crisis [51]. The incorporation of these technologies into agricultural production not only benefits productivity and environmental conditions, but also improves the working conditions of farmers, laborers, and vehicle operators. The work on the farm like sowing, planting, spraying, harvesting etc. is always labor-intensive, repetitive and monotonous due to the growing life cycle of the crops. This situation is encountered especially when the weather and moisture level are optimal and the price is favorable. The mental and physical fatigue is incurred and is increased through intensive and repetitive work or by the stress of steering accurately within tight rows and lanes without causing any damage to the crops.

Aiming at relieving the operator from continuously steering adjustments while operating or maintaining the field equipment, automated guidance systems have been developed and applied for most agricultural vehicles like tractors, combines, sprayers, etc. in many countries. Field robots are the application of robotics and automation in agriculture to relief the manual heavy tasks of labors. Unlike industrial robots that have been widely used and commercially available, field robots are still far from well-developed. Agricultural vehicles are typically operated in fields arranged into crop rows [68], [2], [21], orchard lanes [8], [42] or greenhouse corridors [48], [80], [25], [63], which are typically unstructured environment. Nowadays, with the increasing concern for environmental protection the use of inorganic chemicals that impact on soil health, food safety and water pollution are expected to be minimized. Therefore, automatic weeding robots are the preferable substitute for chemical herbicide to get rid of weeds. Another active research area of the field robots is automatic harvesting robot for different kinds of vegetables and fruits. Due to the varied cultivation features of different categories of vegetables and fruits, the requirements for the configuration, drive system and harvesting equipment are quite different.

1.1 Background and motivation

White asparagus is one of the most favorite vegetables in Germany as well as in Europe and known as “the royal vegetable”. In 2010, approximately 92,400,000kg (92,400 tons) of asparagus was harvested on 188,000,000m^2 (18,800 hectares) in Germany [61]. The cultivation area is approximated continuously to expand. White asparagus is cultivated in parallel trapezoidal mounds, which are heaped knee-highly with a height of about 0.5m, around the plants to prevent photosynthesis. Each mound is covered with a plastic film to keep humidity of the soil and to protect the crops from cold (see Fig. 1.1). To harvest the white asparagus stalks, the harvesters move firstly the film aside, cut stalks off with a special knife with a depth of 0.25m under the soil one by one, push the soil back and replace the film on the mound at the end. When the harvesters cut asparagus, care must be taken not to damage the shorter developing neighbor spears under the ground. The asparagus stalks need to be cut shortly after their spears emerge from the mound. Otherwise the tips will turn into light purple color with the sunlight, which decreases the product quality and results in significantly lower selling price. The harvesting season for white asparagus typically begins from early or mid-April and ends on June 24 every year. During these ten weeks, white asparagus tends to grow fast under ideal temperature and moisture. It is necessary harvested twice a day, once early hours in the morning and the other late hours in the afternoon, to minimize the vapor loss.

Fig. 1.1: Cultivation field and harvesting work of white asparagus.

White asparagus harvesting is a highly repetitive and labor-intensive task which is typically done by hand at present. With the cultivation area expanding, it becomes increasingly difficult to employ adequate workers during the harvesting season due to the

high task demand and the narrow harvesting time-frame. Approximately half of the selling price is contributed to the labor costs, which is reported to occupy about 25% of the cultivation investment [55]. Therefore, it is essential and urgent to explore an alternative solution for white asparagus harvesting to release workers from the laborious manual task and to lower the production cost. Researchers, engineers and entrepreneurs have been attempting to mechanize the harvesting process of white asparagus, and significant progress has been achieved.

1.2 Machinery for white asparagus harvesting

The existing machines for white asparagus harvesting according to the performing function, operating method, driving style or harvesting method can roughly be categorized into assistant harvesting or harvesting, manned or unmanned, diesel or electrical, selective or full-harvesting machine.

Assistant harvesting machine

Fig. 1.2: AspergeSpin A1 (from website of Engels Machines).

The assistant harvesting machine aids workers with film lift, replacement and the container carriage for the harvested spears. One of the most popular used assistant machines is AspergeSpin (shown in Fig. 1.2), which is developed by ENGELS MACHINES Innovatietechniek Company, Holland [87]. It has a frame of 3×2×1.6m (*l/w/h*). The film is lifted up in front, led over a channel and replaced behind the machine. After the workers have harvested all the spears under the frame, the machine is pushed forward for another distance. The assistant machines have generally two fixed wheels at the front and two casters at the rear. There are no additional sensors to sense the location of the machine. The row guidance is mechanically realized through contact by two leading wheels, which are

equipped on two arms in the front of the machine on the both sides of the target cultivation bed. AspergeSpin is designed to provide workers with harvesting assistance for one row or two rows. A commercial harvesting machine driven by diesel motor for five rows was reported [55], which also provides a cover for the workers against sun and rain.

Full harvester/non-selective

To greatly reduce the physical workload, full harvesting machine was also explored. The earliest literature available about mechanical harvesting of white asparagus, to our best knowledge, was presented in 1965 in America [37]. The full harvesting machine tears up the cultivation bed totally and cuts all the spears non-selectively with a certain depth under the ground. The machine is mounted on a high clearance tractor, cuts all spears at a depth of 0.25m with a band-saw type unit. A series of rolls successively lift the cut clay with spears so that a conveyor with meshes elevates the spears, which are manually sorted. The most soil falls down through the mesh openings. Thereafter, the cultivation bed is reshaped with the blade followed behind tractor. In June 2008, the French company Firma Kirpy presented a non-selective harvesting machine Type RGA for white asparagus [79], as is shown in Fig. 1.3. The design concept of the harvester Type RGA is similar to [37]. Type RGA is dragged by a tractor. The cultivation bed is cut through completely. The cutoff asparagus shoots together with soil are transferred over a sieve band in sequence. Workers on the tractor need to collect and sort the spears from the conveying band, and then put them into containers. The asparagus mound is reformed by the shaper installed behind the machine.

Fig. 1.3: Non-selective harvester Type RGA by Firma Kirpy for white asparagus (from website of ai-solution agrarmaschinen).

Obviously, the non-selective harvesting machine greatly improved the productivity and relieves the worker's manual task. However, it reduces the output of the products because the qualified shoots, as well as the developing ones under surface are harvested non-selectively at a time. We would like to note that the full harvesters are generally large in size. The film over cultivation bed must be removed before harvesting and replaced by hand thereafter.

Semi-automatic harvester/selective

In 2008, the German company ASM DIMANTEC invented a semi-automatic machine named Spargel-Panther [57]. Spargel-Panther is a tractor driven machine designed to harvest asparagus for three cultivation beds at a time. With the help of a laser beam, the driver locates the position of each asparagus tip by operating a joystick. The consequent harvesting procedure is performed automatically in series, which is composed of coordinating the position of the harvesting equipment, thrusting knife into earth with a certain depth, cutting off the target spear together with soil and taking it out with a gripper. The selected cutoff spear with soil is put on a slop band with meshes. The soil falls down automatically through mesh openings while the spear slides into container at the end of the slop band. ASM DIMANTEC harvesting machine gathers only white asparagus spears that emerge from bed surface without reforming the cultivation bed.

Fig. 1.4: Selective harvesting machine – Panther (from website of top agraronline).

Full-automatic harvester/selective

The Dutch company Brabantse Wal presented the first prototype of a full-automatic asparagus harvester in the world in 2008 [44] as is shown in Fig. 1.5. This full-automatic harvesting machine for white asparagus is driven automatically with electrical drive systems. The row guidance drive is realized using to guiding wheels in the front. The

identification of white asparagus spears and the harvesting process are performed automatically. The machine drives along one cultivation bed at work. If any spear to be harvested is detected, the machine stops and coordinates the harvesting apparatus to the desired location. According to the probe test, the thrust of the machine reported was less than 10 seconds per spear. Although Brabantse Wal has made pioneer endeavors, the detailed research and development information stays unavailable due to commercial reasons.

Fig. 1.5: Prototype of full-automatic asparagus harvester (from website of Fresh Plaza).

In the academic community only Chatzimichali et al. [13] recently have outlined a conceptual design of an advanced prototype robot for white asparagus harvesting. In their work, the structure of the prototype robot consisting of a caterpillar drive system, asparagus identification and harvesting system has been detailed. The realization of the proposed design is still ongoing.

In 2012 University of Bremen presented the development of an automatic asparagus harvester (shown in Fig. 1.6) [1]. This harvester was presented to identify the asparagus spears with the aid of an intelligent image data processing. The asparagus spears would be cut by mechanical positioning elements driven by electronic drive systems. It drives forward along the target cultivation bed through two leading wheels. It was expected to harvest six asparagus spears per minute. As the best of our knowledge, the available reports about the development of this machine were focus on the harvesting digger. It was described that the implementation of some technical solutions in terms of robustness and for safety aspects to be improved.

Fig. 1.6: Automatic asparagus harvester 'AutoSpar' (from University of Bremen).

Although researchers and engineers from commercial companies have made considerable efforts, the issue to automatically harvest white asparagus selectively is not yet completely solved. There are no full automatic machines for white asparagus harvesting on the market. To automate the process of the white asparagus harvesting is really a tough work due to the special cultivation features and needs extensive research. Two primary assignments need to be solved: autonomous row guidance and automatic device to perform harvesting work.

1.3 Aim and objectives

The task of this thesis aims at design, implementation and evaluation an autonomous vehicle for white asparagus harvesting with a safe, efficient and economic row guidance following operation. The objectives of this work in this thesis are composed of:

- Calculation and components selection including drive motor, driver, sensors, etc. for a cost-effective machinery under the consideration of costs of production for the future;
- Development of a control concept for a collision-free ridge following based on the kinematics of the field robot;
- Employing time-optimal control algorithms to find the time-optimal operating conditions;
- Establishment computational cost-efficient solution feasible for the realization on a micro-processor;

- Experimental verification of the proposed guidance system in laboratory as well as in field;
- Development of an experimental application design that is able to navigate the field robot freely.

1.4 Synopsis and organization

The remainder of this dissertation is outlined as follows:

Chapter 2 gives a broad literature review of current state of agricultural vehicles. The development of the applied sensors, autonomous drive systems and the steering control methods are overviewed.

Chapter 3 is focus on the principle and mechanical design of the field robot platform for white asparagus harvesting. The formulated requirements were investigated by SEYDAER AGROTECHNIK GmbH, Seyda, Germany. The field robot is determined in a differential-drive system with two active wheels at the front. The selection and installation of the sensors and components are detailed.

In Chapter 4 the system specification, including kinematics, robot movement description by ultrasonic sensors, is discussed. The working constraints on the robot's movement are illustrated. It signifies that both lateral offset and the orientation angle of the field robot subject to strictly constraints imposed by the working environment.

In Chapter 5, a cascade control system, composed of an outer lateral offset loop and an inner heading angle loop at the high level and two individual speed control loops of drive motors, is suggested for the row guidance control. The parameters of the controllers are determined based on the conventional PID algorithms. The desired value of the heading angle is constantly constrained to ensure a collision-free following. The efficiency of the developed cascade control system is evaluated in simulation studies.

Chapter 6 is devoted to investigating time-optimal row guidance control. The time-optimal control problem is formulated with constraints imposed by the working environments. The problem is numerically solved with help of time-optimal control software developed in MATLAB/Simulink. By analyzing the obtained numerical results, it is found that the operational operating conditions for minimum time control is to keep the rear side

distances at its boundary with non-zero lateral offset. Subsequently, a practical substitute is discovered to perform the time-optimal control functions by mapping the operating conditions onto orientation angle. It also allows for a simplified realization on a microprocessor for later use. It is verified by simulations that the practical substitute system fulfilled the time-optimal controller very well.

Chapter 7 constructs the illustration of the functional groups of the prototype driving system. The machine has a complete ability to drive in the field, such as automatic row following control, turning operation at the headland and function management. The proposed row following strategy in Chapter 6 is implemented on the micro-controller and evaluated in the fields. The experimental results and discussion are given.

Finally, conclusions and perspectives are given in Chapter 8.

2 State of the art

The farmer's growing awareness of advanced technology in electronics and information prompt to automate the machinery for agricultural applications since the manufacturing industry benefits a lot from well-engineered automated robots. In the past decades, automated agricultural machineries have been subjected to extensive studies due to labor shortage, food product quality and safety, as well as the environmental impact. A number of literatures presented systems that were developed to automate agricultural tasks. These machines vary in levels of automatic operation and task functions.

There are two directions for deploying vehicles for agricultural autonomous drive. One is retrofitting or redesigning existing vehicles with modern technology. Most of them are tractors driven by diesel engines which are developed for combines harvesting, fertilizer transporter machines to perform pesticides spraying mission, such as the harvesting tractor presented with the V2V system presented by Case IH[32], driverless tractor Machine Sync by John Deere [36], driverless grain cart with planting function by Kinze and the driverless model GuideConnect presented by German company Fendt [31]. These tractors are generally large in size and work in broad areas of land. The other is designing new vehicles unrestricted by ergonomics. The application area ranges from machines for weeding control [67, 2, 73, 47, 4, 62] to harvesters for radicchio [25], cucumbers [80], green asparagus [12], cherry [72], watermelon [78], tomato [49], mushroom [60] and so on. The development of the modern autonomous field robot depends entirely on the progress in sensors, which enables the vehicles aware of "where am I" and "where should I go" [9]. On the whole, sensors play a dominant role for the autonomous robots to identify the surrounding environment in the field and help the machines to make decisions on the performing of the consequent behavior.

2.1 Sensors

Since the automated manipulation of the agricultural machines entirely depends on the sensor information. The environmental sensing is the primary assignment, as well as a solid base for the reliable manipulation. The sensors used in agricultural vehicles are related to autonomous navigation and object identification for harvesting equipment. The

sensing devices most often used include mechanical feelers/tactile sensor, vision systems, Global Navigation Satellite Systems (GNSS), laser sensor, and ultrasonic rangefinders, etc.

Mechanical feelers/tactical sensors

Mechanical feelers and tactical sensors work by employing wherever interactions between a contact surface and the environment, such as the tactile row guidance system PSR TAC and PSR MEC for the corn harvester presented by Reichhardt GmbH. The signals of touch, force or pressure produced by any interactions are measured and sent to a processor. Since tactical sensors work by employing the contact information, it is difficult to work when the object is missing.

Machine vision

Machine vision is known to be classified as 2 dimensions (2D) and 3 dimensions (3D). 2D vision systems use cameras to scan area or lines for two characters being length and width. Images of 2D vision systems can be used to obtain the characteristics of an object such as edge, surface appearance and presence and relative location of the object in a two dimensional plain. 3D vision systems apply a specialized high speed camera and a projected laser line to provide three characters being length, width and depth. 3D vision systems are typically applied to get the object information in volume, flatness or shape and density.

The widely used machine vision technology thanks largely to the development of micro-processor which allows for a fast image processing. By analyzing the visual data acquired from camera or video systems, the objects of interest are filtered accordingly to the characters like monochrome, color, shape or brightness. Accordingly to the working principle of the machine vision, it has been widely used on the industrial robots to avoid obstacles. With the cost declination in recent years, machine vision systems are also adopted in agricultural applications, such as harvesting by making out and locating the object [42][49][60], weeding control by differentiating weeds from crops [2][67][5], the automated guidance control through identifying the crops of interest to construct crop ridges [3][7][21]. In machine vision based application, the real-time image processing is sometimes a challenge for micro-processing devices to execute complex image processing image algorithms. Besides, the effectiveness of the vision system is directly affected by lighting conditions and background interference. The performance of machine vision

system depends significantly on the signal-to-noise of the sampled images which varies considerably under different weather or illumination.

GNSS

GNSS is a satellite system that is used to pinpoint the geographic location of any receiver in the world. It provides the absolute location and information in all weather conditions. The most often used GNSS systems [35] are the United States' Global Positioning System (GPS), the Russian Federation's Global Orbiting Navigation Satellite Systems (GLONASS), Europe's Galileo and China's Beidou Navigation Satellite System (BDS). GNSS has become vital to many applications that range from military applications and route planning to the autonomous farming. With the development of the wireless communication and network systems, more precise planning in GNSS applications can be acquired. For example, the differential position corrections can be sent by the third generation (3G) wireless mobile networks integrated with GNSS for Real-Time Kinematic (RTK) network to the GNSS users [29]. GNSS-based applications in precision farming are being used for farm planning, field mapping, soil sampling, row guidance, crop scouting, etc. GNSS is widely available in the agricultural community and becomes the standard equipment on the modern agricultural vehicles due to the relatively inexpensive price. For precision farming the RTK GPS with a precision within 5 centimeters is preferable. The most frequently mentioned disadvantage of GNSS navigation is the up-front cost. A fully automatic navigation system that steers a tractor or vehicle with operator engagement only at field ends could range from $6,000 to $50,000 [29]. The satellite-based positioning system does not take account for unexpected obstacles.

Optical sensors

The most often used optical sensors are the optical encoder and laser sensors. The optical encoder is an electro-mechanical device that produces electrical signals to identify the angular position or the motion of a shaft. Optical encoders are widely adopted in electrical motors and wheels to get the information such as speed, position and distance. They are the most commonly used sensors for the positioning of wheeled mobile robots using odometry method.

Laser sensors currently available on the market use varied measuring principles as light time-of-flight and triangulation. Laser sensors using time-of-flight method are suitable for both short and far ranges. The triangulation laser sensors measure short distance ranges

from centimeter to a few meters with higher accuracy. The cost price of laser rangefinders ranges from 1,000€ up to one million Euros [18]. Laser rangefinders are now widely used in agricultural vehicles for volume measurement [77], [45], as well as for guidance control [69], [70]. It can also be used to create high resolution in 3D images by scanning [19]. The laser sensors are sensitive to bright background light patterns. An extra optical filter can be used to improve the detecting performance. Generally, sensors are supplied from the manufacturer with a 3B classification in order to perform measuring task outdoors even with intensive sunlight [18]. Although laser sensors are immune to background light, noise, wind, surface texture and color, their measuring range is easily affected by dust frog and rain.

Ultrasonic sensor

Ultrasonic ranging sensors use time-of-flight method to estimate distances to nearby objects. The distance is obtained by calculating the time it takes an ultrasonic pulse to travel from the Polaroid sensor to the object and then back to the sensor. It is also called transceiver because it includes both a transducer from emitting a high-pitched pulse of sound and a receiver for detecting the energy of the reflected pulse. The detecting efficiency of ultrasonic sensors is not affected by illumination of the environment, color or optical reflectivity of the object. Ultrasonic sensors are generally with digital outputs which have excellent repeat sensing accuracy. The price of ultrasonic sensors is much lower, from less than 50€ to 500€. Due to low cost and effortless realization, ultrasonic range sensors are widely used in automotive applications [11] and agricultural machinery for volume assessment [45],[77] and guidance [63]. The measuring of ultrasonic sensors is affected by the material and surface of the objects that absorb sound or have a soft or irregular surface may not reflect enough echo signals to be detected accurately.

2.2 Agricultural automatic guidance applications

Automatic drive or autonomous navigation is one of the most important characters for an automatic agricultural machine. In the past decades, it has been an interesting subject for agricultural researchers since early days of the tractor. In early 1920s, patent reported by Willrodt invented a steering attachment for tractors which allows tractor to follow furrows across a field [85]. In recent decades, the development of new technologies, such as machine vision analysis, GNSS and robotics, allows the improvement of automatic vehicle

guidance. The following requirements for row guidance systems were given by Åstrand as [68]:

- *Ability to track rows with an accuracy of a few centimeters.*
- *Ability to control a row cultivator and an autonomous agricultural robot in real-time, which means that both heading and offset of the row structure must be estimated at a sufficient fast rate.*

2.2.1 Guidance by contact or cable

The automatic guidance system through mechanical contact or cable is the main method adopted by earlier researchers for agricultural machines because it is simple and straightforward. For the guiding application with mechanical contact, the agricultural machine is guided by one or more mechanical arms that feel the boundary of the target trajectory by contacting with the crops. A major concern for this method is the substantial risk in damaging the crops. The control is lost in bare region without crops. An alternative is using cable that carries AC signal to get the guiding signal. When the vehicle moves over the cable, a coil on the vehicle base detects the magnetic fields generated by the cable to get the guiding information of the object track. This method works very well in orchards. The obvious drawback is the permanent installation of large structures, which improves the initial cost and required maintenance which increases over time. Besides, the cables require special attention by plowing, fertilizer and irrigation. With the advancement of sensor and electronics technology the researchers are drawn to the non-contact guidance method based on sensors due to the limitation of mechanical contact applications.

2.2.2 Odometry guidance system

Odometry is the most simplistic implementation of dead reckoning, which implies vehicle displacement along the path of travel is directly derived from some onboard "odometer"[9]. A common means of odometry instrumentation involves optical encoders directly coupled to the motor armatures or wheel axles. The principle idea of odometry is the integration of the incremental motion information over time. At the same time, the errors, if there is any, could be also integrated over time, which leads inevitably to the accumulation of errors. This method provides only good short-term accuracy in well structured environment. The successful application is reported by Feng et al. [23] and Wuwei et al. [88]. For the automated navigation systems of mobile wheeled robots based on odometry method, there are numerous disturbances arising from varied friction,

installation, diameters, resistance and ground surface of the two drive wheels. Therefore, the odometry positioning method is often applied with landmarks to get updates of the absolution position. Accordingly, there are some correction methods presented by Goel et.al [27] and Chung et.al [14]. In some cases, odometry is appealed only when no external reference is available or when other sensor subsystem fails to provide usable data.

2.2.3 Machine-vision guidance system

For automatic guidance system based on machine-vision, a real-time imagery process is essential to separate objects of interest from acquired field images. The most commonly used method for imaginary process is Hough transform [73], which is reported to be a computationally efficient procedure and capable of dealing with the situations where the crops stand is incomplete with gaps in rows. The extracted crops information is used to locate the actual position of the machine with respect to the target trajectory [73, 3, 7, 48]. However, in machine-vision based applications the real-time imaginary processing is always a serious challenge for the processing device to execute complex algorithms. Moreover, the effectiveness of the vision system is affected by lighting conditions and background interference [62].

3D/stereo vision systems are capable of providing depth perception of the surroundings, which provides more flexibility in the landmark identification and object location [34], [52], [65]. In the application for the crops with crown, stereovision can provide more precise information of the heading direction by identifying the ridges of the crops or fruit trees in field operations [84]. The more complete positioning information of 3D vision system can be obtained from the 3D field image by combining two monocular field images taken from a binocular camera simultaneously. Such a 3D image is reconstructed based on the difference between both monocular images, and therefore is less sensitive to ambient light changes. Kise et al. presented a crop row detection method based on stereovision system to guide an automated tractor in soya bean field [41]. Obviously, this application costs a greater deal of computational power than 2D vision system. The successful application of 3D vision systems in automatic navigation significantly depends on the advances in electronics and processor speed. It is worth noting that 3D vision system is not feasible for the navigation application without any landmark like planting, fertilizer before planting.

2.2.4 GNSS guidance system

Alternatively, the efficiency of GNSS-based guidance system does not depend on the landmarks after the initial mapping of the environment. It provides the absolute positioning information of the field vehicle. The Real-Time Kinematic GPS (RTK GPS) with precision of a few centimeters is commercially available for some tractors [29]. Stoll and Dieter Kutzbach [66] developed an automatic steering system for a self-propelled forage harvester using RTK GPS as the only positioning sensor. Kise et al. proposed an RTK GPS guidance system for a field autonomous vehicle traveling along a curved path with a maximal tracking error of 13 cm for curve path [39]. Nørremark et.al presented an autonomous RTK GPS-based system for intra-row weeding machine which succeeded in following the target row with an accuracy of ±0.022m at 0.52 m/s [54]. The most obvious advantage of RTK GPS is that RTK GPS provides absolute positioning information and its efficiency is not affected by light conditions and status of crops. But additional investigation is needed for Base (reference receiver) and Remote (roving receiver). The Base transmits measurement or correction information through a radio link to the Remote. The Base and Remote must communicate with each other at all times during vehicle operation in order to maintain good accuracy. This guidance method suffers from some limitations. It is difficult to guarantee consistent positioning accuracy for varied field conditions. Another drawback is the inherent time delay of the system [43]. The price ranges from $40,000 to $50,000 with no annual subscription fees [29], which is rather than economical for the agricultural applications.

2.2.5 Sonar sensor guidance system

Middle-range and short-range sensors were reported by Sánchez-Hermosilla et al. to sense the distances between robot and plant rows in greenhouse [63]. With the distance information provided by ultrasonic sensors, the autonomous robot succeeds in following along plant rows automatically among greenhouse corridors.

This technology is limited by the features of surfaces and the density or consistency of the material. The signal returned from natural, diffusely reflecting, surfaces is of much smaller amplitude than that from a smooth reflecting surface such as a laboratory wall. Further difficulties in the applications include stability of movement and ambient ultrasonic noise which may be generated by nearby machinery [30].

2.2.6 Remote control guidance system

With the technological advancement of wireless communication, remote control or tele-operation is subject to prosperous research in agricultural applications. The development of wireless communication varies from short-range, point-to-point infrared data association (IrDA), point-to-multi-point communication tools like Bluetooth and ZigBee, mid-range, multi-hop wireless local area network (WLAN) to long-distance cellular phone systems as GSM/GPRS and CDMA. The movement of the field vehicle is supervised and controlled remotely through wireless communication in real-time. An obvious advantage using remote control is the comfortable environment of operation and safety. The major challenge is the time delay in communication. The application of wireless communication in agriculture was reviewed in detail by Wang et.al [83].

Obviously, there is no sensor that is perfect for all applications. What the engineers need do is to find the proper solution for each application. By combining sensors we can benefit from their advantage and compensate their disadvantage. Zhang and Reid developed an autonomous on field navigation system with one vision sensor, a fiber optic gyroscope and RTK GPS [90]. The results illustrated that the multi-sensor navigation system worked very well both in rows and out rows. An autonomous navigation system using multi-sensor information fusion was reported by Liu et al. through combining the information of GNSS, ultrasonic sensors and laser scanner [46].

2.3 Automatic steering control

Agricultural vehicles vary widely from dimension (from tractor combines to small size electric robot for one row), driving concept (track, caterpillar, wheels) and driving mode (diesel machine or electrical drive motor, front-wheel-drive, rear-wheel-drive, full-wheel-drive) to steering type (with or without steering wheel, one or more steering wheels). It is difficult to setup a universal model or control systems for all machines. But all the automatic guidance systems for agricultural vehicles have the common objective that they must follow the command path with a certain precision under proper steering control all the time. The most often used control variables are the orientation angle and lateral deviation. By comparing the information of vehicle actual position measured by sensors to the desired values, the controller supplies steering signals to the actuator in order to eliminate the guidance error and to allow the machine back to the right position in the path.

The outputs of the vehicle's position supervised are generally orientation error and lateral deviation. Several control methods have been presented in the previous literature.

The simplest controller available was based on ON/OFF control presented by Yekutieli and Pegna in 2002 [89]. The ON/OFF controller was designed to guide a crawler tractor using a curved bar arm to sense the distance to the side crops in a vineyard. It was reported that this controller provided fast responsibility, but also considerable overshoot was observed. More sophisticated strategy was expected to improve the guidance performance. As Proportional Integral Derivative (PID) control strategy is widely and successfully used almost for all industrial processes, a PD controller presented by Marchant et.al to perform an autonomous row-following task for a weeding machine that preserved a differential-drive system [47]. The PD controller sent the differential speed of the drive wheels as control signals according to the actual errors of orientation angle and lateral displacement. Zhang et.al suggested a controller of PID plus feed-forward function for a wheel-drive tractor using multi-sensors [91]. The feed-forward segment was supplemented due to a large time-delay of the steering system. Some researchers also tried using intelligent control strategy to steer field vehicles. Benson et.al adopted fuzzy logic algorithms to steer a combine. In a typical field, the combine was guided automatically to pursuit the desired path with a comparable accuracy with manual operation. Neural network was reported by Noguchil et. al [53] by considering the nonlinear characters of the system and [92] for sloping terrain. Genetic method was used by Ryerson and Zhang to steer a field machine to follow the planned optimal path. Kise et.al developed an optimal controller for a tractor steering that identified the position using RTK GPS and an IMU sensor [40]. The optimal control strategy was compared with PI control that the optimal controller performed high-speed guidance more precisely.

2.4 Discussion

Although the research activities in developing new autonomous field vehicles have attracted great interest, the autonomous agricultural vehicles are still far from well-developed since the development of agricultural machines must take the special application purpose. The harvesting machines, especially for vegetables and fruits, are not commercially available due to several hurdles. Most importantly of all, the complexity of the manual operations is difficult to be replaced by mechanized systems. Hand work incorporates high efficient visual image processing, intelligent directions, delicate and

skillful activities. The intellectual manual versatile manipulation is a serious challenge to be replaced by a mechanical system. Another reason is the possible mechanical damage incurred during automatic harvest, which has another major deterrent to continue the development of automatic harvesting system for fresh fruits and vegetables. If the damage caused by mechanical systems for processed crops cannot be tolerated by farmers or growers, they will not be commercially produced. Lastly, there is lack of uniform maturity in technical criteria for harvest. The harvesting technology for one kind of products may not be adopted by another because of the unique characters of growing and cultivation. Besides, divergence exists between different horticultural crops, and even between species and varieties, which makes it very complicated to substitute machines for human judgment and dexterity.

The development of robotics and the advancement of the sensor technology, especially the visual sensors and the image processing algorithms, allow for the possibility to design specialized robotics. The electric drive systems are preferred for the actors due to higher energy efficiency, continuous speed and torque regulation and environmental friendliness.

3 Prototype

3.1 Applications requirements

Function requirements

The functions of the robot are specified through discussion and consultation with the agricultural company Seyda for white asparagus planting. The robot platform is expected to possess the following abilities and to be designed under consideration of cost-efficiency.

- Manual/automatic operation models
- Automatic turn to the next row at the end of rows
- Ability to work day and night
- Drive automatically in the direction given by the target bed against varied disturbances
- Lifting film from cultivation bed before replacing film onto cultivation bed automatically during forward operation
- Reserved place to install automatic harvesting equipment for future development
- Load capacity for 200kg
- Maximal working velocity 0.5/s (1.8kmh)

Configuration requirements

The cultivation bed for white asparagus is about 0.6m tall, 1.0m wide at the bottom, and the interval space between beds is 0.8m. The robot is required to be capable of operating by striding one bed at a time.

3.2 Overall principle

3.2.1 Traction, drive and steering

Electric traction has significant environmental advantages over conventional gasoline or diesel power with higher power-to-weight ratio, quieter operation, higher efficiency, lack of dependence on crude oil as fuel, zero CO_2 emission, etc. A design with wheels is preferred over caterpillars to make enough room for the cultivation bed and also to reduce

the damage to the soil in sharp turns in rows due to skid steering. Therefore, electric traction using electrical drive motors is decided for the robot platform.

The important properties required by the robot are steering precision, low power consumption and low cost. Moreover, the working environment of the white asparagus field imposes special constraints on the dimensions of the traction equipment. The electrical wheel-drive is decided for the traction since it has significant advantage in cost-efficient, flexible mobility, steering flexibility, speed regulation and skidding over caterpillar track. The robot is developed as a platform for sustainable operation in white asparagus cultivation field. Since the crop rows are mostly straight, there is no drastic curve in crop rows. The automatic guidance system is expected to get rid of the disturbance caused by uneven surface and small deviation of the target row. As a result, a differential-drive system using two front wheels is decided due to its simplicity. The steering is achieved by adjusting the differential velocity of the drive wheels. Therefore, it doesn't need additional steer equipment. The two rear wheels are casters to provide balance.

3.2.2 Robot platform

The development of the robot platform takes the required functions into account. The working environment is the major consideration for the dimension of the platform. As was discussed in Section 1.1, white aspragus is planted in parallel beds which are erected up the ground surface with a height of 0.6m and has a trapezoidal cross-section. The cultivation bed is 1m wide at the bottom, and about 0.6m wide at the top. The interval space between beds is about 0.8m. As a result, The dimensions of the robot base are specified 3.1×1.8×1.6m (l/w/h) as shown in Fig. 3.1. The platform frame has a hollow space of 3.1×1.6×0.73m (l/w/h) under the machine. It has a weight of 430kg with a maximal load capacity of 200kg. The roller at the front of the machine is designed to lift film covering the cultivation bed. Over the sliding track on the top of the machine, the film is replaced over the supporting frame at the rear top onto the cultivation bed . These operations are performed automatically during the forward operation. The area of the cultivation bed between front wheels and rear casters is workspace. Track is preserved inside of the chassis's frame to install the harvesting equipment for future use. Loading platform is arranged at one side of the machine for harvested asparagus spears.

Differential-drive robot is one of the most popular designs and is composed of two active wheels and one or two casters. This design has simple mechanical structure and a simple

kinematic model. The most obvious advantage of this design is low fabrication cost. The platform of the field robot has two active wheels at the front and two passive casters at the rear to provide balance. According to the kinematics of the differencial-drive wheeled robots, the turning point of the harvester lies in the middle point of the front drive axle. The two front active wheels with a radius of 0.3m are actuated independently. The rear casters with a radius of 0.15m is fixed to the chassis with an swivel radius of 0.15m. The passive rear casters have no influence on machine velocities.

(a) Mechanical design

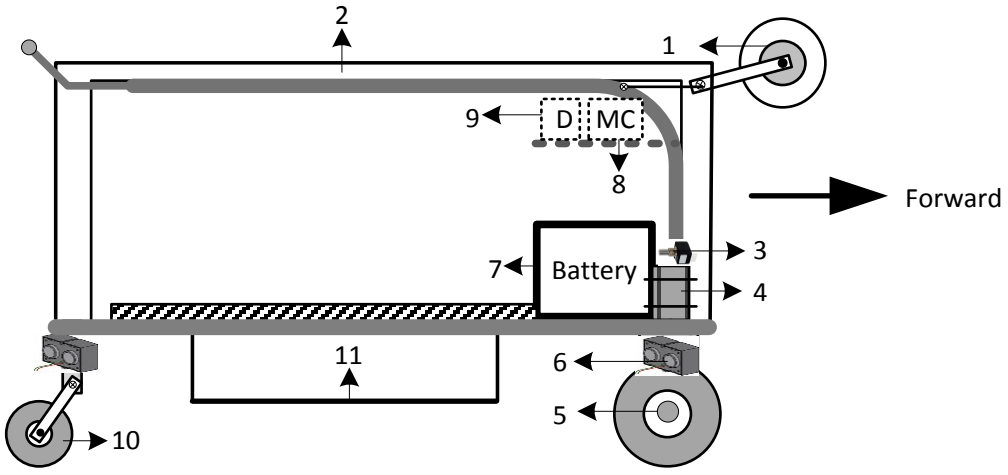

(b)Schematic illustration (1.Film roller 2. Sliding channel for the film 3. Incremental optical encoder 4. DC motor 5. Front drive wheel 6. Ultrasonic sensor 7.Battery 8. Micro-controller 9. Drive board 10. Caster/rear wheel 11. Loading platform 12. Track for harvesting arm)

Fig. 3.1: Platform of the robot.

The field robot should be capable of following the target row automously with electrical DC motors. Therefore, it is essential for the robot to own power supply not only for the drive motors, but also for the sensors and control accessories. As a result, two rechargable

batteries (12V38AH×2) are choosed to supply power. They are able to contineously work for 8 hours.

3.3 Drive transmission

In order to find a proper electrical motor providing sufficient drive power, the resistance for the robot to overcome should be estimated as well as with forward velocity in mind. The gross weight of the vehicle is approximately 430kg with all accessories. The robot is capable of taking 200kg payload. The exactly rolling resistance is very hard to determine because it is affected by tire pressure and soil conditions. Some literature [20] suggests rolling resistance coefficients as high as 0.3 for 0.5 diameter tyres on sand and 0.1 to 0.15 on firm soil. In agricultural notes rolling coefficients for tractors on up to 0.15 to 0.25 under very difficult conditions are found. Since the robot operates in soil field with sand, the resistance $F_{resistance,max}$ is mainly composed of rolling resistance $F_{roll,max}$ and grading resistance $F_{grading,max}$. The rolling resistance coefficient f_{roll} ranges from 0.1 to 0.30 for the vehicles in field [20]. In this application the climbing slope $tan(\alpha)$ is estimated by 5%. The maximal resistance force is calculated as:

$$\begin{aligned} F_{resistance,max} &= Fr_{roll,max} + Fr_{grading,max} \\ &= G_{weight} \cdot f_{roll} \cdot cos(\alpha) + G_{weight} \cdot tan(\alpha) \\ &= 2161N \end{aligned} \tag{3.1}$$

where G_{weight} is the total weight with loading in Newton.

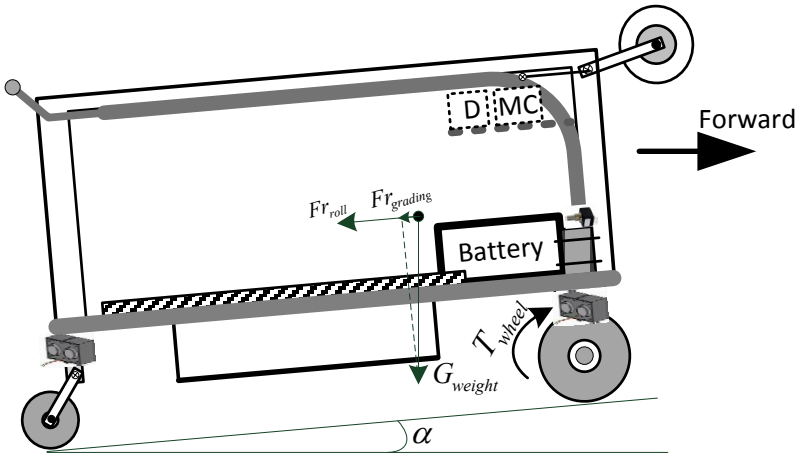

Fig. 3.2: Forces acting on a vehicle.

The maximal torque on the wheel shaft is calculated using Eq. (3.2) as follows:

$$T_{resistance,max} = \frac{F_{resistance,max}}{2} r_{radius} = 324Nm \tag{3.2}$$

The motors for the robot platform must be easy to control, supply and install. Another preferrable performer is cost-efficiency for the agricultural application. DC motors mostly meet the demands above. Considering the application of the robot platform for white asparagus harvesting for future use, the forward general forward velocity is under 0.5m/s. It is extremly difficult to find a qualified motor that drives the wheels directl with low velocity operation area and the requirement of high torque. There are no qualified DC motors available to meet the requirements on speed and torque directly. As a result, gears are adopted to improve the drive force and to reduce rational speed of the motor. Finally, a 500W DC motor (MY1020Z2, Zhejiang Unite Electric Motor Co., Ltd., China) integrated with a spur gear with the rating rational speed of 375rpm, a rating torque of 12.6Nm and a maximal torque of 20.8Nm. A second-order chain gear box with a translation of 16:1 was applied to increase the torque and to lower the rotational speed. The montage of the drive transimission is shown in Fig. 3.3.

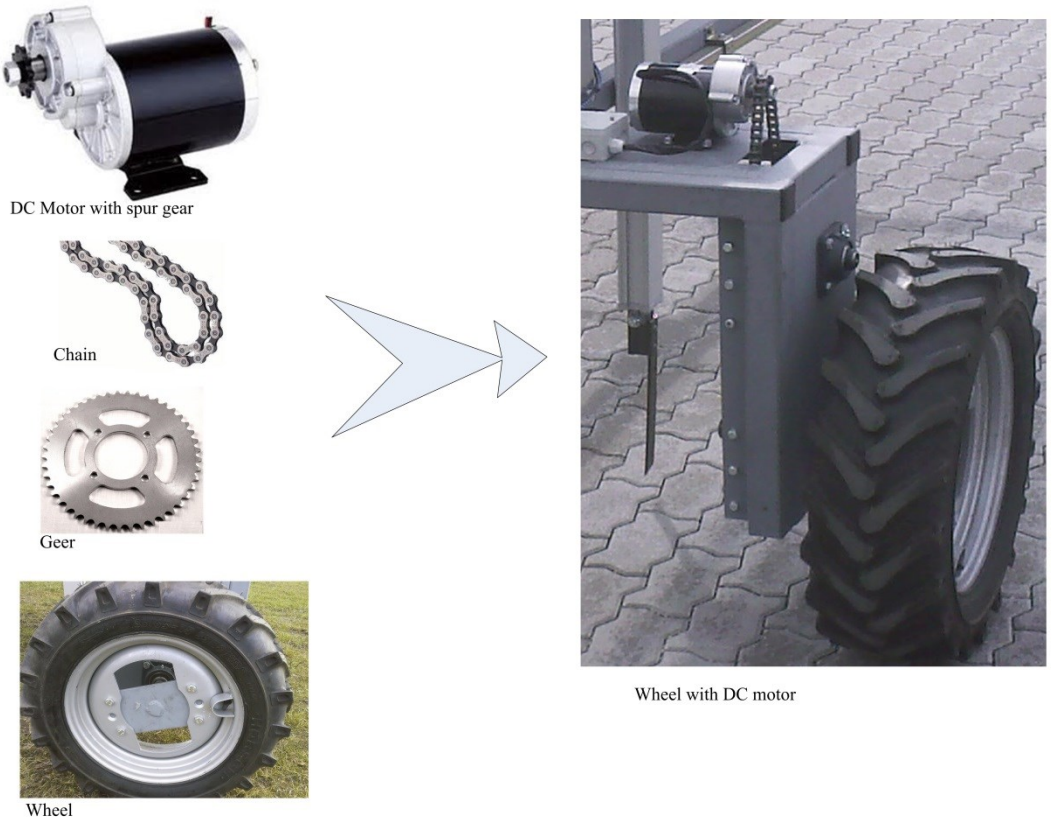

Fig. 3.3: Drive transmission.

The maximal torque on the wheel will be

$$T_{wheel,max} = T_{motor,max} \times g_{gear} = 332.7Nm \tag{3.3}$$

with a chain gear ratio g_{gear} of 16:1. Since the efficiency of the chain drive is approximated over 98% [86], the maximal active toque on the wheel $T_{wheel,max}$ is higher than the maximal resistance torque, which satisfied the expected requirement. The rational velocity v_{wheel} on the wheel is accordingly,

$$v_{wheel} = \frac{n_{motor}}{60 g_{gear}} \times 2\pi \times r_{radius} \times 100 = 0.74m/s \tag{3.4}$$

3.4 Motor control

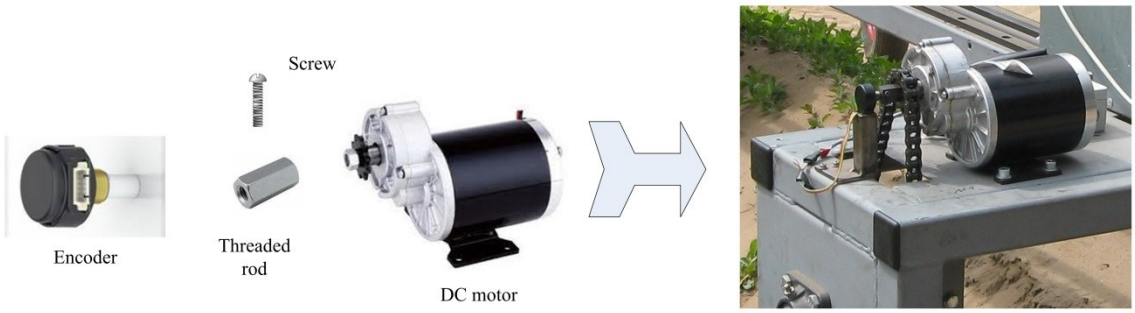

Fig 3.4: Motor and sensor.

To control the speed of the drive motors, sensor is needed on the motors to get the rotatory information. Because the selected drive motor does not have any integrated sensor, an incremental optical encoder Model 120E with 128 pulses per turn is choosed. The encoder works with 5V norminal voltage and outputs digital signal. The encoder provides a quadrature encoded signal. The motor speed is estimated by measuring the pulse width or by counting the numbers of pulse within a certain time span. The encoder is simply installed on the DC motor by attaching the shafts of them together using a screw (see Fig 3.4). To stablilize the movement, the handle of the sensor is held by a frame that is fest mounted on the machine frame.

Sabertooth motor driver (2×50HV) is applied to actuate two DC motors. It works with input voltage from 12V to 48V. The output current is up to 50A continueous per channel. Peak loads may be up to 100A per channel for a few seconds. It is suitable to drive dual

motors for high powered robots. The speed regualtion and the a can be easily realized through adjusting a 0~5V control signal.

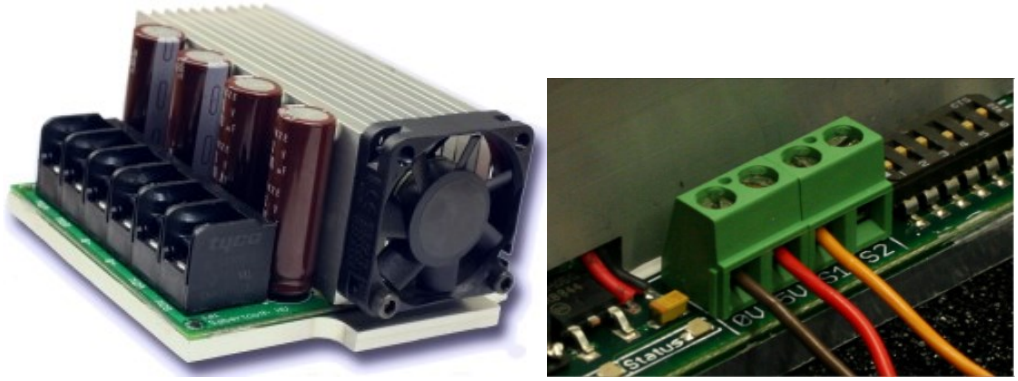

Fig. 3.5: Sabertooth motor driver and the 5V terminal.

3.5 Positioning system in rows

The main sensors used for positioning the robot were reviewed in detail in Section 2.1. In the application of the guidance method based on GPS, the mapping of the distribution of rows is required to be done previously besides the considerable investiment for the equipment. The machine-vision based guidance method works well for the applications with ideal lighting conditions where the array of crops are contineously well arranged. The field robot for white aspragus harvesting works partly under a plastic film early in the morning or late in the afternoon. At that time, the natural lightness is always insufficient for the application of machine-vision systems. Besides, the white asparagus spears to be harvested commonly discontineously scatter in a 0.8m band area. There is no evident hint or border of crop rows. Sonar sensors have overwhelming advantage in price and simplicity over machine-vision and RTK GPS. Simutaneously, the ultrasonic sensors are reported to be successfully applied to measure the distance between robot and aimed crop ridges although the reflecting surface of the crops is irregular. In our application, the field robot is required to follow the crop hills that is heaped over ground surface as discussed in Section 1.1, which provides an natural plain surface for the application of ultrasonic sensors. Resultantly, the Parallax PING)))^{TM} ultrasonic distance sensor [33] was adopted for cost-effectiveness and high efficiency.

The PING))) sensor works by transmitting an ultrasonic burst and providing an output pulse that corrsponds to the time reqired for the burst echo to return to the sensor. By measuring the echo pulse width, the distance that the ultrasonic burst traveled to target can easily be calculated. The working pricinple of PING))) sensor is shown in Fig. 3.6. The range of measurement of PING)) sensor is approximately from 0.02m to 3m. The angular

aperture is approximately 45° by measuring, which satisfies the application for sandy surface.

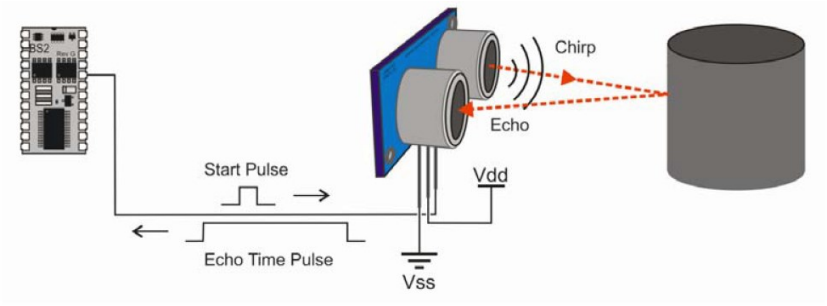

Fig. 3.6: Working principle of PING))) sensor.

To supervise the movement of the find out the in-row position of the robot, two PING))) sensors are used to sense the front and rear side distance between robot and the cultivation bed it follows. PING))) is enclosed in a box with a handle to enable a out-door application as is shown in Fig 3.7. The PING))) box is fixed on a metal bracket and further equipped on the robot. As is know from the working principle of ultrasonic sensors, the sensing precision and efficiency depend entirely on the verticality of the sensor and the object surface it measures. To allows a flexible modification of the verticality, the angle and height of the box with PING))) sensor can be conveniently adjusted by hand according to the height of the cultivation bed and the inclination of the side surface. One of them is installed through near the front wheel and the other near the rear at the right side of the machine. The actual position and orientation of the robot with respect to the target row can be computed using the front and rear side distances measured by the two ultrasonic sensors.

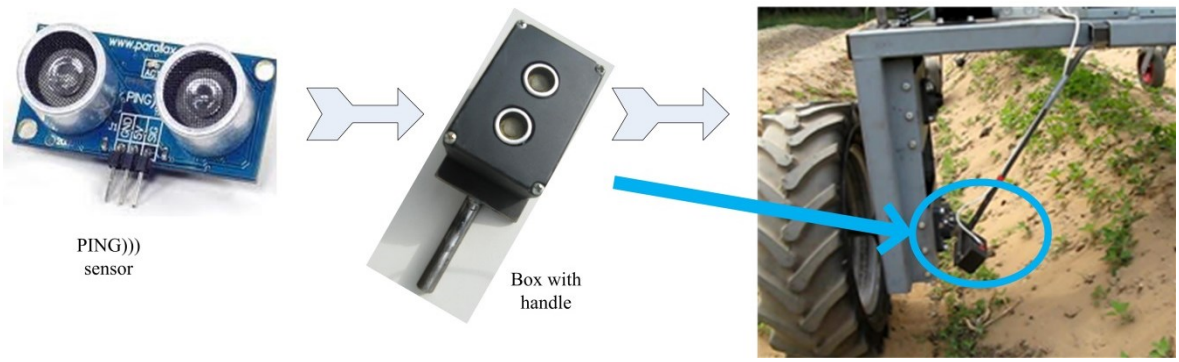

Fig 3.7: Installation of ultrasonic sensors.

3.6 Controller

The hardware is required to process the signals of sensors and perform the suggested row guidance strategy. PSoC (Cypress Semiconductor Corporation, USA) is a programmable embedded system on a chip integrating configurable analog and digital peripheral functions, memory and a microcontroller on a single chip. With an extremely flexible visual embedded design methodology that includes preconfigured, user-defined peripherals and hierarchical schematic entry in PSoC Creator programming environment. PSoC CY8C55 is integrated with 32-bit MHz ARM Cortex-M3 processor and capable of handling larger, more complex applications easily. More conveniently, PSoC CY8C55 works with the CY8CKIT-001 PSoC Development Kit, which is designed to aid hardware (CAN, I2C, USB, etc.), firmware, and software developers in building applicable systems. PSoC system satisfies all our requirements and the most preferable due to cost-efficiency.

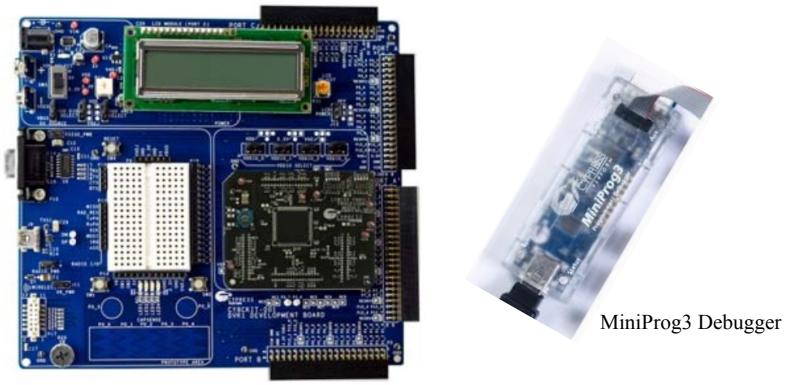

Fig. 3.8: PSoC development board.

3.7 Conclusion

In this chapter, the overall principle of the field robot was given.

- The dimension of the robot platform was determined by referring the application environment, which allows it to be capable of an in-row operation in typical fields for white asparagus.
- The differential-drive concept was adopted due to steering simplicity and cost-effective realization.
- DC motors were chosen to drive the robot. Chain gears were applied to improve driving power and lower the rotary speed.

- Ultrasonic sensors were decided to determine the actual in-row position of the robot by utilizing the natural reflecting surface of the cultivation bed erected over ground surface.
- The micro-controller CY8CKIT-001 PSoC Development Kit with PSoC 5 architecture presented by CyPress was selected to develop the automatic row guidance algorithms due to cost-effectiveness and powerful integrated modules.

The design concept in this part was suggested for a prototype. There may be modified or improved with new modules or components. All the modules and components can be flexibly to be replaced and changed on the platform.

4 System Specification

4.1 Kinematics of the robot

The differential-drive mobile robot is a classical locomotion system that is constituted by two parallel driving wheels. The movement of the driving wheels is controlled by two independent motors. Casters are normally adopted to ensure the robot stability. To model kinematics of the differential-drive wheeled mobile robot, some assumptions suggested by [50] should be given:

- The robot is composed of rigid bodies;
- The translational friction at the point-of-contact on the wheel is large enough so that no translational slip may occur;
- The rotational friction at the point-of-contact on the wheel is small enough so that rotational slip may occur;
- The robot moves on a plenary surface.

The turn point of the differential-drive mobile robot lies in the middle of the axle of the active drive wheels. Therefore, in this application the midpoint of the front axle for drive wheels is chosen as the reference point of the robot. Its coordinates with respect to the original fixed frame are denoted by (x, y). The heading direction of the vehicle is the orientation angle θ. With L_b designating the distance between the two driving wheels, the movement of the robot is expressed by:

$$\begin{pmatrix} \dot{x} \\ \dot{y} \\ \dot{\theta} \\ \dot{v_L} \\ \dot{v_R} \end{pmatrix} = \begin{pmatrix} \frac{1}{2}cos(\theta) & \frac{1}{2}cos(\theta) \\ \frac{1}{2}sin(\theta) & \frac{1}{2}sin(\theta) \\ \frac{1}{L_b} & -\frac{1}{L_b} \\ k_{vl} & 0 \\ 0 & k_{vr} \end{pmatrix} \begin{pmatrix} v_L \\ v_R \end{pmatrix} + \begin{pmatrix} 0 & 0 \\ 0 & 0 \\ 0 & 0 \\ k_{ul} & 0 \\ 0 & k_{ur} \end{pmatrix} \begin{pmatrix} u_L \\ u_R \end{pmatrix} \tag{4.1}$$

with v_L, v_R the translational velocities of the drive wheels, and u_L, u_R bounded control variables. k_{vl}, k_{vr} and k_{ul}, k_{ur} the parameters in terms of motors and wheels. By setting

$$v = \frac{v_L + v_R}{2} \tag{4.2}$$

$$\omega = \frac{v_R - v_L}{L_b} \tag{4.3}$$

we get the kinematic model from the 5-dimensional system in Eq. (4.1) in a 3-dimensional system as follows:

$$\begin{bmatrix} \dot{x} \\ \dot{y} \\ \dot{\theta} \end{bmatrix} = \begin{bmatrix} cos(\theta) & 0 \\ sin(\theta) & 0 \\ 0 & 1 \end{bmatrix} \begin{bmatrix} v \\ \omega \end{bmatrix} \tag{4.4}$$

It is assumed that the wheels are non-deformable and there is no slip between wheels and ground surface. Subsequently, the movement of the vehicle is subjected to the non-integral differential constraint,

$$-\dot{x}sin(\theta) + \dot{y}cos(\theta) = 0 \tag{4.5}$$

4.2 Dynamic description using side distances

As discussed the actual position and heading angle of the robot with respect of the target cultivation bed was determined by the front and rear side distance measurements of the ultrasonic sensors. Pseudo measurements of the ultrasonic sensors are formulated to model the system.

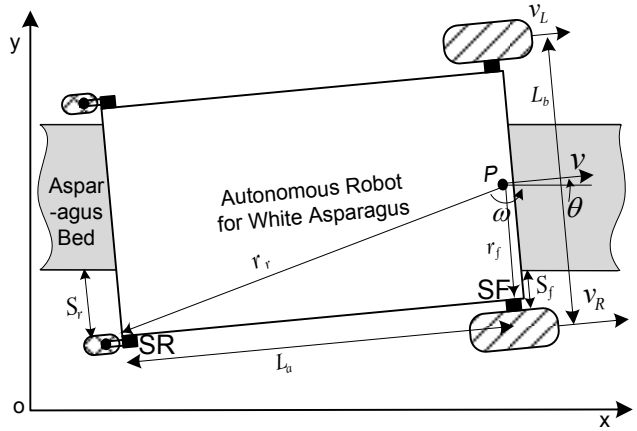

Fig. 4.1: Top view of the harvesting robot.

In the robot moving frame shown in Fig. 4.1, the positions of the front and rear ultrasonic sensors are described by vector $\boldsymbol{r}_f$ and $\boldsymbol{r}_r$ as follows:

$$\boldsymbol{r}_f = \begin{bmatrix} 0 \\ -\frac{L_b}{2} \\ 0 \end{bmatrix},\ \boldsymbol{r}_r = \begin{bmatrix} -L_a \\ -\frac{L_b}{2} \\ 0 \end{bmatrix} \tag{4.6}$$

with L_a length of the robot platform.

With the help of transformation matrix T from the moving frame to the base frame, the linear velocity vector $\boldsymbol{v}$ and angular speed vector $\boldsymbol{\omega}$:

$$T = \begin{bmatrix} cos(\theta) & -sin(\theta) & 0 \\ sin(\theta) & cos(\theta) & 0 \\ 0 & 0 & 1 \end{bmatrix}, \tag{4.7}$$

$$\boldsymbol{v} = [\dot{x} \quad \dot{y} \quad 0]^T,\ \boldsymbol{\omega} = [0 \quad 0 \quad \omega]^T \tag{4.8}$$

the velocity vectors of the sensors $\boldsymbol{S}_F$ and $\boldsymbol{S}_R$ can be derived as:

$$\dot{\boldsymbol{S}}_F = \boldsymbol{v} + T \cdot (\boldsymbol{\omega}_v \times \boldsymbol{r}_f) = \begin{bmatrix} v \cdot cos(\theta) + \frac{L_b}{2} \cdot \omega \cdot cos(\theta) \\ v \cdot sin(\theta) + \frac{L_b}{2} \cdot \omega \cdot sin(\theta) \\ 0 \end{bmatrix} \tag{4.9}$$

$$\begin{aligned} \dot{\boldsymbol{S}}_R &= \boldsymbol{v} + T \cdot (\boldsymbol{\omega} \times \boldsymbol{r}_r) \\ &= \begin{bmatrix} v \cdot cos(\theta) + \frac{L_b}{2} \cdot \omega \cdot cos(\theta) + \omega \cdot L_a \cdot sin(\theta) \\ v \cdot sin(\theta) + \frac{L_b}{2} \cdot \omega \cdot sin(\theta) - \omega \cdot L_a \cdot cos(\theta) \\ 0 \end{bmatrix} \end{aligned} \tag{4.10}$$

4.3 Environmental specifications

The differential-drive robot platform is inherently capable of tracking any trajectory. If the non-zero velocity of the drive motors is the same with $v_L = v_R$, the robot will drive straightly forward. If the non-zero velocity of the motors is the same in value but opposite in symbol with $v_L = -v_R$, the robot will turn around the reference point. To the best of our knowledge, all the differential-drive mobile robots are considered as a point in the

applications. However, the geometrical configuration cannot be neglect due to the limited free space. Differently from industrial robots or robotics in laboratory, this field robot has a rather long shaft. Its movements are strictly constrained by the limited space between cultivation beds.

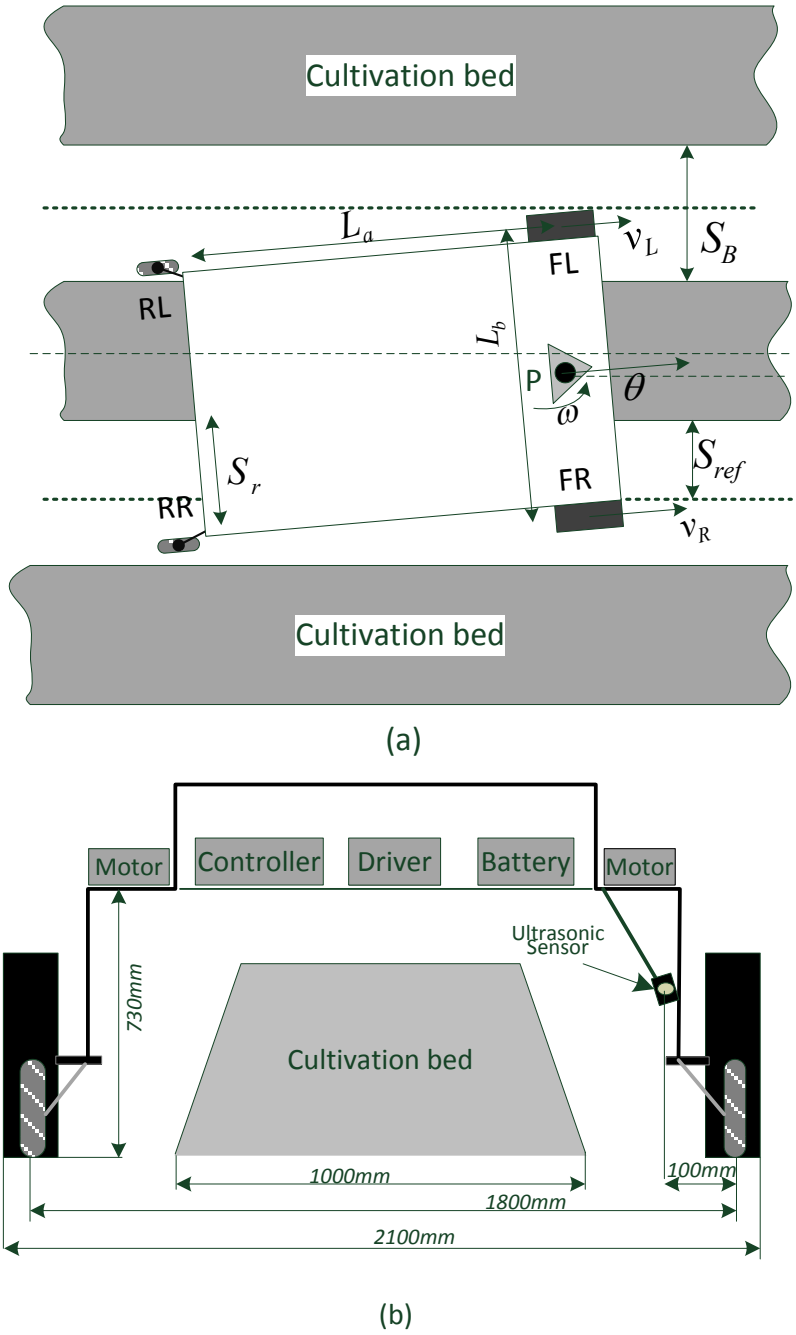

Fig. 4.2: Description of the robot position with respect to cultivation beds in field, (a) Top view (b) Side view.

The harvesting robot is demanded to drive by striding one row at a time as is shown in Fig. 4.2. The interval space ($S_B = 0.8m$) limits the robot movement on both lateral offset and orientation angle. The location of the robot with respect to its target row is supervised by

the front and rear side distances noted by S_f and S_r measured by the installed ultrasonic sensors SF and SR (shown in Fig. 4.2(a)). Because of the symmetry of the spatial arrangement, only side distances on one side are necessary to be sensed. The movement in row direction is free. The working environment is described by:

- harvesting robot 1.8m wide
- cultivation bed 1m wide at the bottom
- interval space between beds 0.8m
- free space between wheels is 1.6m wide
- swivel radius of rear casters is 0.15m

The reference side distance is set $S_{ref} = 0.3m$ with a sufficient margin for rear casters. The desired location of the robot can be subsequently expressed using side distance $S_f = S_r = S_{ref}$. The left region for the robot in lateral direction is $S_{ref} \pm 0.15m$ that is the strictly constraints on the vehicle by:

$$S_f^{lb} \leq S_f \leq S_f^{ub} \tag{4.11}$$

$$S_r^{lb} \leq S_r \leq S_r^{ub} \tag{4.12}$$

Fig. 4.3 illustrates the movement of the robot following a curve path. It can be concluded that the maximal curvature α that the robot follows in rows equals the orientation angle θ and is achieved with $S_f = S_f^{lb}$ and $S_r = S_r^{ub}$ by:

$$\alpha_{max} = atan\frac{S_r^{ub} - S_f^{lb}}{L_a} \tag{4.13}$$

In our application, θ is within 5^o. The arc length in Fig. 4.3 can be approximated using L_a. The curvature radians is consequently given by $r_{min} = L_a/\alpha_{max}$. It is observed from Eq. (4.13) that the allowable arc span that the robot can follow is determined by the length of the platform L_a and the width of the cultivation bed. If L_a and the width of cultivation bed approach zero, α_{max} will go to $\pi/2$. On the other side, if L_a goes to infinite or the width of the cultivation bed approximates L_b, α_{max} will go to zero. Under this condition, the robot can only go straight. It is worth noting that the steering control is significantly affected by the allowable orientation angle, i.e. curvature arc, which is to be discussed in the following.

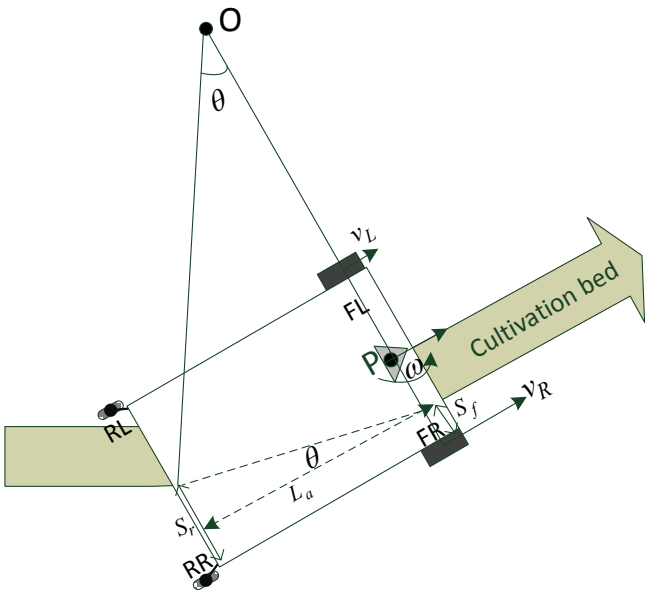

Fig. 4.3: Operation following curve path.

4.4 Conclusions

In this chapter, the mathematical kinematic model for a differential-drive mobile robot was firstly given. And then the dynamic model of the ultrasonic sensors was deduced based on the robot kinematics to establish pseudo-measurements. The working environment and the constraints impacted on the robot were discussed in detail. The feasible region of the side distances was strictly limited by the width and the interval space of the cultivation bed. However, the steering flexibility depends on the limit of the adjustment of the orientation angle which is determined by the dimensions of the robot and the width of the bed width. The configuration of the platform could be further optimized to shorten the robot length.

5 Row Guidance System

Differently from the robot working in well-structured indoor environments, the agricultural vehicles operating in fields are suffered from varied disturbances, which can largely be classified into two categories: internal disturbance and external disturbance. The internal disturbance arises mainly from different parameters, such as time constants of drive motors and loop gains of drive systems, and bearing frictions. External disturbance comes from wheel misalignment, different contact area, wheel slippage, diverse diameters of the drive wheels and varied resistances when the robot moves due to unlike ground surface. In the path following problem of differential-drive mobile robots, the path deviation that detected in real-time is also considered as external disturbance. Both internal and external errors will be applied to drive motors, which affect motor response more or less. The differentiation of the motor speeds would result in error in the path.

The internal disturbances can be detected by the wheel motion information, while the external disturbances are only apparent through absolute robot motion measurements. The errors can be further divided into systematic errors and non-systematic errors. Systematic errors exist when the robot moves without changing their characteristics over time, such as time constant of the drive motor, loop gains of the drive system, diverse diameters etc. Non-systematic errors arise in a random fashion and can only be described in a statistical sense. Many researchers suggested varied strategies for the differential-drive mobile robots.

5.1 Control strategies

Control research for differential-drive wheeled mobile robots has been subjected to extensive studies for industrial and service applications. The basic motion task for a differential-drive mobile robot, in the absence of obstacles, is moving between two postures and following a given trajectory [17].

One of the most popular solutions is wheel-based odometry, which is known as relative or local localization method. For wheel-based odometry technique, robot location is incrementally calculated from an initial point. Then, the position and orientation of the robot with respect the original point in the initial frame are geometrically calculated by

using integration of wheel velocities measured by encoders. This method is mostly often adopted for wheeled mobile robots working in well-structured environments. A primary control method named cross-coupling controller was proposed by Feng et al. [23] to coordinate the velocities of the two wheels. Feng et al. [24] improved cross-coupling controller by adopting a model-reference adaptive strategy in the compensation of motion errors. Some advantage control techniques considering kinematics and dynamics, such as back-stepping like feedback linearization [15], dynamic feedback linearization [17], were employed to improve stability of the system. Intelligent method like fuzzy logic was also presented by Espinosa et al. [22] and Tso et al. [76]. The main drawback of wheel-based odometry is that it causes an unbounded growth of the error along the time and distance since encoder measurements are integrated simultaneously with the noise. Moreover, the efficiency of odometry method depends on the assumption that wheel revolutions can be converted into linear displacement. But this assumption is not necessarily true especially for off-road vehicles.

Alternatively, the application of beacons or landmarks is rather attractive because it is capable of providing actual location information of robots with respect to a reference frame. But additional sensors like vision system, GNSS sensors, sonar sensors etc. are necessary to get the actual information of the working environments. For the application of off-road robots with differential-drive system, the PID control strategy is mostly often desired not only due to computational efficiency but also reliability [15]. For example, Marchant et al. [47] suggested a PD controller for the row tracking system of an autonomous machine-vision agricultural vehicle. Sánchez-Hermosilla et al. succeeded in driving their autonomous mobile robot in greenhouses by feeding back the linear combination of position offset and orientation error [63].

All the previous control strategies consider position error and orientation error together. It means that there is no special requirement for orientation angle. However, the differential-drive mobile robot in this application was developed specially for white asparagus harvesting. The working environment imposes strictly constraints not only on the lateral offset but also on the orientation angle as was discussed in section 4.3. Special consideration must be taken in the development of the row guidance system.

5.2 Problem formulation

5.2.1 Formulation of the following error

The objective of the path following problem is to bring the robot from its current configuration to a target configuration through a path specified by a curvature to avoid any collision. The differential-drive mobile robot is assumed to follow a reference path $\mathcal{T}$ as is shown in Fig. 5.1. X_DDY_D is a moving frame on the reference path. The original point D of the moving frame is the projection of the reference point P of the robot onto the reference path. The moving frame is defined such that the X_D axis is tangent to the path and oriented in the robot moving direction, Y_D axis passes through P. Since the robot drives by striding over the reference path, the distance between D and P is much smaller than the momentary curvature radius. The projection point D is consequently unique.

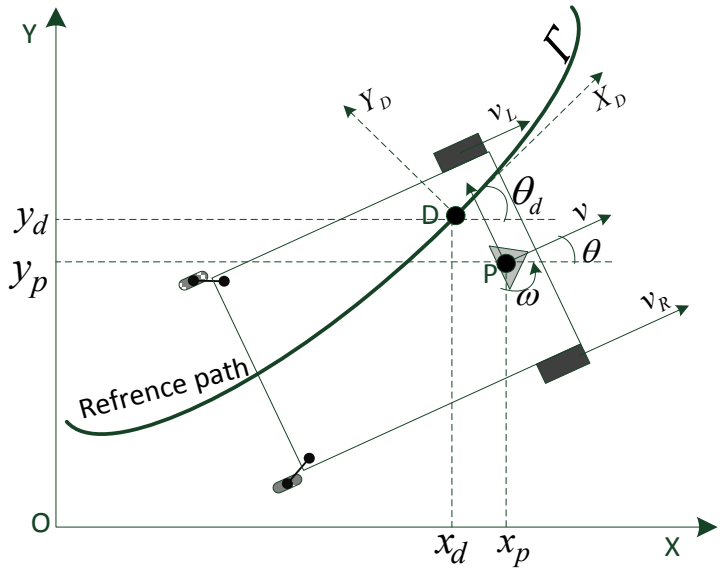

Fig. 5.1: Path following error.

The following error can be expressed by the path following deviation e_x, e_y and the orientation error e_θ as follows:

$$\begin{bmatrix} e_x \\ e_y \\ e_\theta \end{bmatrix} = \begin{bmatrix} cos(\theta_d) & sin(\theta_d) & 0 \\ -sin(\theta_d) & cos(\theta_d) & 0 \\ 0 & 0 & 1 \end{bmatrix} \begin{bmatrix} x - x_d \\ y - y_d \\ \theta - \theta_d \end{bmatrix} \tag{5.1}$$

where $[x_d \quad y_d \quad \theta_d]^T$ is the desired location of the machine in the generalized coordinate frame by making a numerical projection of the current location of the robot onto the target

path. $[x \quad y \quad \theta]^T$ is the actual position and orientation of the robot in the original frame. The dynamics of the open-loop error for the robot is derived as:

$$\begin{bmatrix} \dot{e}_x \\ \dot{e}_y \\ \dot{e}_\theta \end{bmatrix} = -\begin{bmatrix} v_d \\ 0 \\ \omega_d \end{bmatrix} + \begin{bmatrix} \cos(e_\theta) & sin(e_\theta) & 0 \\ -sin(e_\theta) & cos(e_\theta) & 0 \\ 0 & 0 & 1 \end{bmatrix} \begin{bmatrix} v \\ 0 \\ \omega \end{bmatrix} + \begin{bmatrix} 0 & \omega_d & 0 \\ -\omega_d & 0 & 0 \\ 0 & 0 & 0 \end{bmatrix} \begin{bmatrix} e_x \\ e_y \\ e_\theta \end{bmatrix} \tag{5.2}$$

where v_d and ω_d are the forward and angular velocity of the desired point D in the original coordinate with $\omega_d = \dot{\theta}_d$. In this application, the forward velocity of the robot v is non-zero constant and does not converge to zero. Since Y_D passes through the original point P of the moving robot frame, there is $e_x \equiv 0$ and $\dot{e}_x \equiv 0$. Finally, the error dynamics for the path following problem can be expressed using the second and third variables in Eq.(6.2) as follows:

$$\begin{aligned} \dot{e}_y &= v \cdot sin(e_\theta) \\ \dot{e}_\theta &= e_\omega \end{aligned} \tag{5.3}$$

where $e_\omega = \omega - \omega_d$.

To further simplify the expression, we define the frame $X_D DY_D$ as the generalized coordinate, and the axis X_D is in the tangential direction of the target path. For the forward operation, the reference frame is defined according to the direction of the cultivation bed, which gives $y_d = 0$ and $\theta_d = 0$. We get

$$\begin{aligned} \dot{y} &= v \cdot sin(\theta) \\ \dot{\theta} &= \omega \end{aligned} \tag{5.4}$$

5.2.2 Row guidance problem

The objective of row following control is to develop a proper controller that drives the vehicle along the target row without collision or damage to the crops. In fact, the row following problem can be categorized into the pure-pursuit problem for the robot. As is known, the differential-drive wheeled mobile robots subject non-holonomic constraints. They cannot correct errors with respect to the nearest point of the path that followed. The

most often strategy for the pure-pursuit control is assuming that the vehicle pursuits a point on the aimed path with certain distance ahead of it. A smooth vehicle response can be achieved by selecting a proper look-ahead distance. If the look-ahead distance is selected too small, the steering flexibility will reduce. If the look-ahead distance is too larger, the robot will cut the corner in curve path. The selection of the look-ahead distance is affected by the traveled path and the velocity of the robots. Unfortunately, there are no solid rules on the selection of a proper look-ahead distance. The most often used method is trial and error.

Most of the research work on the pure-pursuit control is based on the look-ahead distance. It is naturally to assume that the moving aim point is ahead of driver. Comparably, some researchers tried path following strategy based on look-behind method. Wang et. al [81] presented that the similar control performance was achieved using look-ahead and look-behind distance on a car-like vehicle. Pham and Wang [58] succeeded in controlling a platoon of two car-line vehicles both forward and backward tracking by properly selecting a look-ahead and look-behind distance.

5.2.3 In-row location

As was discussed in Chapter 3, two ultrasonic sensors were applied to identify the in-row location of the robot. The front and rear side distances S_f and S_r are respectively sensed by SF and SR as is illustrated in Fig. 5.2. According to the geometric relations, the actual orientation angel of the robot with respect to the target row is calculated by:

$$\theta = arctan(\frac{S_r - S_f}{L_a}) \tag{5.5}$$

The actual lateral position of the reference point of the robot P can be achieved as follows:

$$y = e_S + sign(e_S) \cdot \frac{L_b}{2} \cdot (1 - \cos(\theta)) \tag{5.6}$$

where $e_S = S_f \cdot cos(\theta) - S_{ref}$ is the actual lateral offset of the ultrasonic sensor SF, and S_{ref} is the desired value of SF and SR.

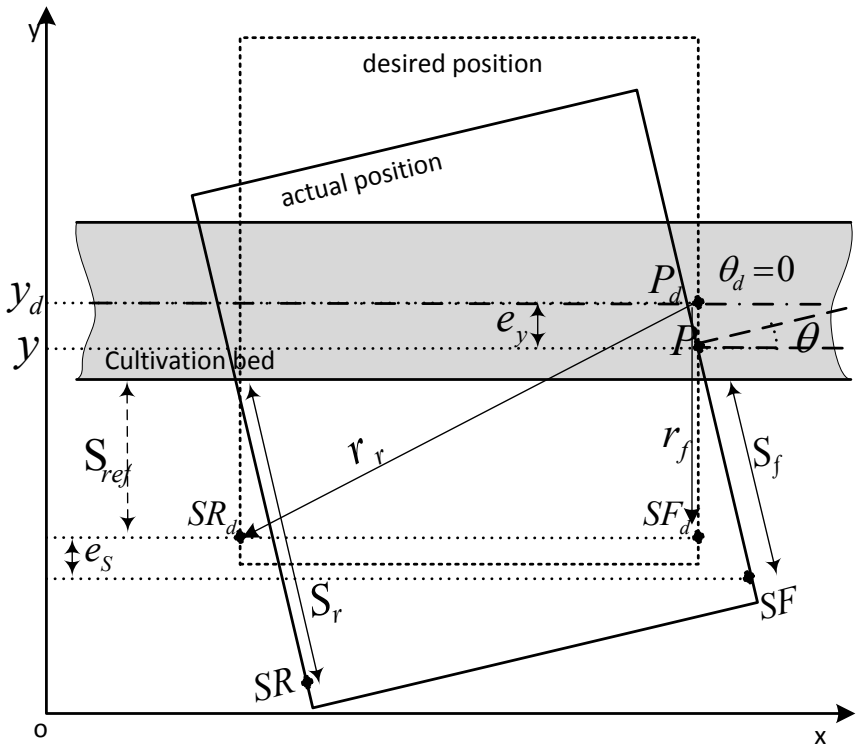

Fig. 5.2: Graphic representation of the tracking deviation.

The robot developed for white asparagus harvesting in this work is driven by front wheels. The actual location and orientation angle of the robot are determined with help of the rear side distance S_r, which is behind P. It is considered that the assumed point on the target path that the robot should follow is behind the robot reference point with a distance of L_a.

5.3 Cascade guidance control system

Since the agricultural robot suffers varied disturbance in field, a proper guidance controller must be developed to drive the machine along the given cultivation bed. The internal errors can be detected by the wheel speed information. The external errors can only be perceived by absolute robot motion measurement. In order to overcome internal and external errors, the guidance controller with a typical multilayer structure (shown in Fig. 5.3) is most often adopted, as was reported in [28], [24], [22], [16] and [88]. The low level is composed of two independent speed control loops for the drive motors to ensure the drive motor speed as desired. The controller at the high level is to get rid of the row following deviation that is caused by external disturbances or divergence of the target cultivation bed. The motion of the robot can be decomposed into the orientation angle deviation e_θ and the lateral offset e_θ as is shown in Eq. (5.3). The orientation angle error is seriously concerned in

motion accuracy control because the orientation error will result in a lateral offset, which grows with the distance traveled. Since the lateral offset is the direct result of the orientation error, both errors cannot be controlled at the same time. Therefore, we decide in a cascade control structure, consisting of an inner orientation angle controller and an outer lateral displacement controller, in that the lateral offset does not have a very significant effect on the motion accuracy of the robot. We can control the guidance error by adjusting the input so that the field robot follows the desired track.

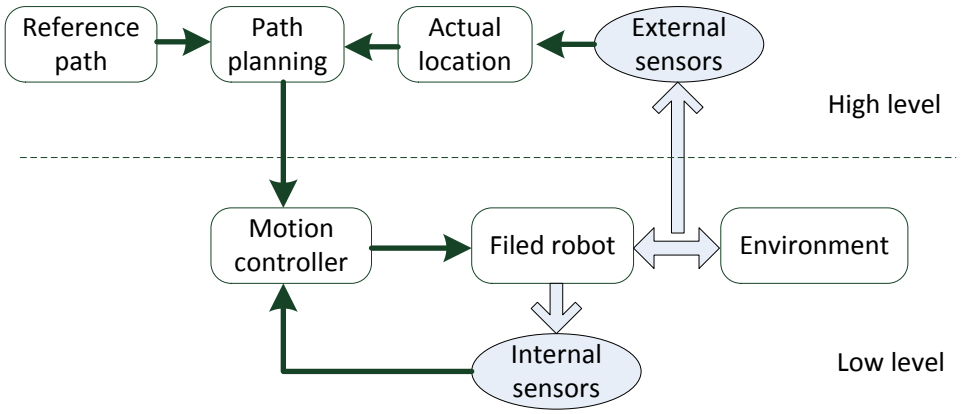

Fig. 5.3: Block diagram of row guidance control.

As was discussed in Section 4.3, the movement of the robot subjects concrete constraints imposed by the working environment. Because the robot drives mostly along straight lines or soft curvature with large radius, the forward operation is the primary assignment, and the adjustment in lateral direction is a supplementary. Therefore, the desired revolutions of the left and right drive motors ω_{ml}^{*} and ω_{mr}^{*} are formulated as follows:

$$\begin{aligned} \omega_{ml}^{*} &= \omega_{mref} - \omega_{mdiff} \\ \omega_{mr}^{*} &= \omega_{mref} + \omega_{mdiff} \end{aligned} \tag{5.7}$$

Obviously, the command angle velocity of each motor consists of two components: a primary angular speed ω_{mref} and a differential component ω_{mdiff}. ω_{mref} is obtained according to the predetermined forward velocity v_{ref} using

$$\omega_{mref} = \frac{g}{r} v_{ref} \tag{5.8}$$

and ω_{mdiff} is determined by the cascade controller at the high level in terms of the actual guidance error. If the following error is zero, i.e. $e_y = 0$ and $e_\theta = 0$, then $\omega_{mdiff} = 0$.

The vehicle drives straightly forward with the motors operating at the same speed. Otherwise, by $\omega_{mdiff} \neq 0$, the trajectory controller is activated. The machine then orients itself through the adjustment of the motor speeds simultaneously to eliminate the tracking error.

5.3.1 Low level control

The low level controller consists of two independent speed loops for drive motors. The speeds loops are employed to ensure that the actual motor speed ω_m always follow its reference precisely. The open loop transfer function of the drive motor from the rotational speed ω_m to the input voltage u is

$$\frac{\omega_m}{u} = \frac{k_e}{J_m \cdot L_m \cdot s^2 + (L_m \cdot B_m + J_m \cdot R_m)s + B_m \cdot R_m + k_e \cdot k_m} \tag{5.9}$$

where L_m and R_m are the inductance and resistance of the motor, B_m the viscous friction coefficient, and J_m the equivalent motor inertia together with its drive wheel and chain gears, k_e and k_m are the motor voltage constant and torque constant, relatively. There is no special requirement on the dynamics of the motor control system because the robot has a much larger time constant than the drive motor and works with a low speed. As a result, a single speed loop with a proportional-integral controller is suggested for motor speed as:

$$G_{mPI} = k_{p\omega} + \frac{k_{i\omega}}{s} \tag{5.10}$$

with $k_{p\omega}$ and $k_{i\omega}$ the proportional and integral gains. The closed-loop transfer function of the speed loop is obtained:

$$G_{mcl} = \frac{k_e(k_{p\omega} \cdot s + k_{i\omega})}{J_m \cdot L_m \cdot s^3 + (L_m \cdot B_m + J_m \cdot R_m)s^2 + (k_e \cdot k_{p\omega} + B_m \cdot R_m + k_e \cdot k_m)s + k_e k_{i\omega}} \tag{5.11}$$

The step response of the DC motor with suggested PI controller is shown in Fig. 5.4.

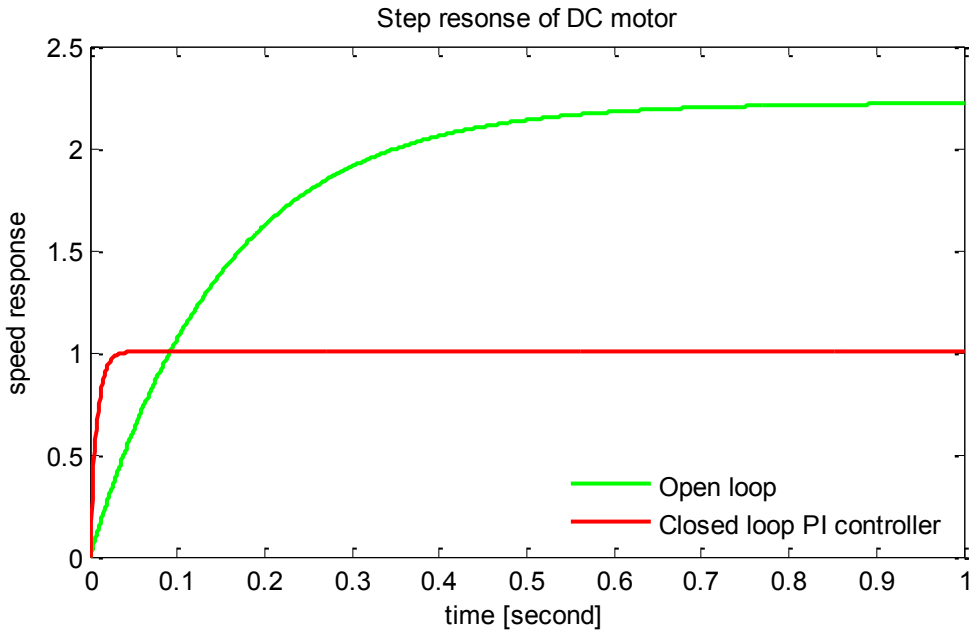

Fig. 5.4: Step response of the DC motor with suggested PI controller.

5.3.2 High level control

At the high level, a guidance controller with cascade structure to eliminate following error caused by external disturbances which can only be observed by external sensors. It is observed from Eq.(5.4) that the lateral offset $\dot{e}_y$ is the integration of orientation error $sin(\theta)$. Because of the constraints of the working space, the orientation angle is always limited within 5^o. Therefore, it is reasonable to make an approximation with $\theta \approx sin(\theta)$. We get:

$$\dot{y} = v \cdot \theta$$
$$\dot{\theta} = \omega \tag{5.12}$$

That means that $\dot{e}_y$ can only be eliminated by adjusting θ with a constant forward velocity v. For that reason, e_θ was also considered as the most significant error by Feng et al. [23]. Based on the analysis of the following error in Eq. (5.4), we apply a cascade control strategy by taking the orientation loop as inner loop and the lateral displacement as the outer loop. The set-point of θ is given by the lateral offset controller in the outer loop as is shown in

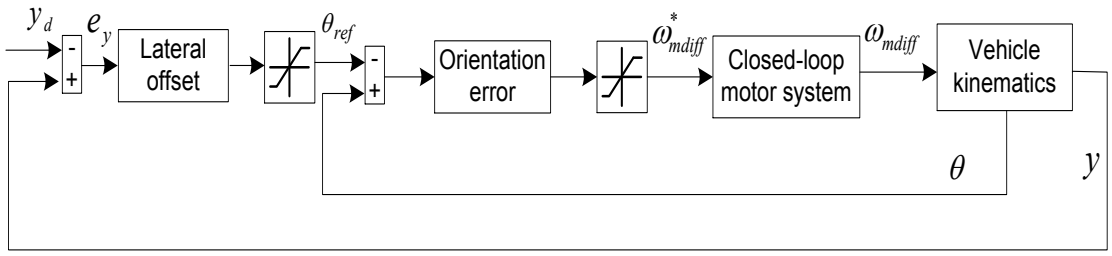

Fig. 5.5: Block diagram of the cascade control system.

The step response in Fig. 5.4 for the motor PI control can be approximated using a first-order system. To simplify the controller design at the high level, the third-order model in Eq. (5.11) is simplified into a first-order system as follows:

$$\frac{\omega_{mdiff}}{\omega^*_{mdiff}} = \frac{k_{ms}}{T_{ms} \cdot s + 1} \tag{5.13}$$

with k_{ms} the equivalent loop gain and T_{ms} the equivalent time constant. Note that this approximation is only considered to estimate parameters of the controller design on high level.

The open-loop transfer function of the orientation angle contributes the integral role. With a proportional controller, the objective of a zero steady-state error was achieved for the orientation control. Given proportional gain $k_{p\theta}$, the closed-loop transfer function is described as:

$$\frac{\theta}{\theta_{ref}} = \frac{k_{p\theta} \cdot k_{ms} \cdot r}{L_b \cdot T_{ms} \cdot g \cdot s^2 + L_b \cdot g \cdot s + k_{p\theta} \cdot k_{ms} \cdot r} \tag{5.14}$$

Similarly, a proportional-derivative is adopted for lateral offset with k_{py} and k_{dy} the proportional and derivative gains,

$$G_{PDy} = k_{py} + k_{dy} \cdot s \tag{5.15}$$

The resulting closed-loop transfer function is given by:

$$\frac{y}{y_d} = \tag{5.16}$$

$$\frac{k_{p\theta}k_{ms}rv(k_{dy}s + k_{py})}{L_b \cdot T_{ms} \cdot g \cdot s^3 + L_b \cdot g \cdot s^2 + k_{p\theta} \cdot k_{ms} \cdot r(1 + k_{dy} \cdot v)s + k_{py} \cdot k_{p\theta} \cdot k_{ms} \cdot r \cdot v}$$

The parameters and values of the robot control system are summarized and illustrated in *Table 5.1* whereby the parameters of the drive motor were experimentally determined.

Table 5.1: System parameters

Parameter	Value
Wheel radius r (m)	0.3
Gear ratio g	16:1
Vehicle width L_b(m)	2.1
Supply voltage motor u (V)	24
Equivalent motor inertia J_m (kg·m^2)	0.0738
Motor resistance R_m (Ohm)	0.4
Motor inductance L_m (H)	1e-4
Viscous friction coefficient B_m (N·m·s·rad^{-1})	4.3e-3
Back-emf constant k_e (V·s·rad^{-1})	0.45
Torque constant k_m (N·m·A^{-1})	0.45
Simplified forward gain k_{ms}	1
Simplified time constant T_{ms} (s)	0.137
Proportional gain speed controller $k_{p\omega}$ (V·s·rad^{-1})	9
Integral gain speed controller $k_{i\omega}$ (V·s·rad^{-1})	65.6
Proportional gain orientation controller $k_{p\theta}$ (s^{-1})	204
Proportional gain lateral offset controller k_{py} (rad·m^{-1})	10
Integral gain lateral offset controller k_{dy} (rad·m^{-1})	3

5.3.3 Constraints

The strict constraints imposed by the environment were detailed in Section 4.3. But we observed that the robot cannot proceed with some special positions like $S_f = 0.45m$ and $S_r = 0.45m$ or $S_f = 0.15m$ and $S_r = 0.15m$ since the robot is only permitted to drive forward. This problem is avoided by shrinking softly the feasible region of S_f by 0.05m. The feasible region of S_f becomes $S_f^{lbs} \leq S_f \leq S_f^{ubs}$ whereby $S_f^{lbs} = 0.2m$ and $S_f^{ubs} = 0.4m$.

In this cascade guidance system, the side distances S_f and S_r cannot be directly constrained because they are not the controlled variables. But they can be constrained by setting proper limit to the orientation angle θ by regarding to the geometrical relations in Eq. (5.5). The range of orientation for all $S_f \in [S_f^{lbs}, S_f^{ubs}]$ and $S_r \in [S_r^{lb}, S_r^{ub}]$ is

If $S_f \geq S_{ref}$ $$\theta \leq arctan(\frac{S_r^{ub} - S_f^{ubs}}{L_a}) \tag{5.17}$$

If $S_f \leq S_{ref}$ $$\theta \geq arctanarctan(\frac{S_r^{lb} - S_f^{lbs}}{L_a}) \tag{5.18}$$

To prevent uncontrollable movement of the vehicle caused by sudden change of the wheel velocity and skidding, the differential term is also constrained as follows

$$\omega_{mdiff} \leq 0.1\omega_{mref} \tag{5.19}$$

5.4 Simulation studies

The performance of the suggested row guidance system with constant constraints on the orientation angle was tested against varied initial error and disturbance of following deviation. There is geometrical symmetry in the movement of differential-drive wheeled mobile robots, which was discussed in detail by Balkcom and Mason [6]. There is unnecessary to list all the situations. Only the row guidance performance with three representative locations at one side ($e_y \geq 0$) is examined which are named Case I $(S_f(t_0), S_r(t_0)) = (0.4m, 0.45m)$, *i.e.* $(e_y(t_0), e_\theta(t_0)) = (0.1m, 0.92^o)$, Case II $(S_f(t_0), S_r(t_0)) = (0.35m, 0.25m)$, *i.e.* $(e_y(t_0), e_\theta(t_0)) = (0.05m, -1.84^o)$.

Two simulation studies with different initial positions were carried out for $v_{ref} = 0.12m$. A following deviation of $0.05m$ is introduced and added onto S_f at 50s. The simulation results are shown in Fig. 5.6 and Fig. 5.7.

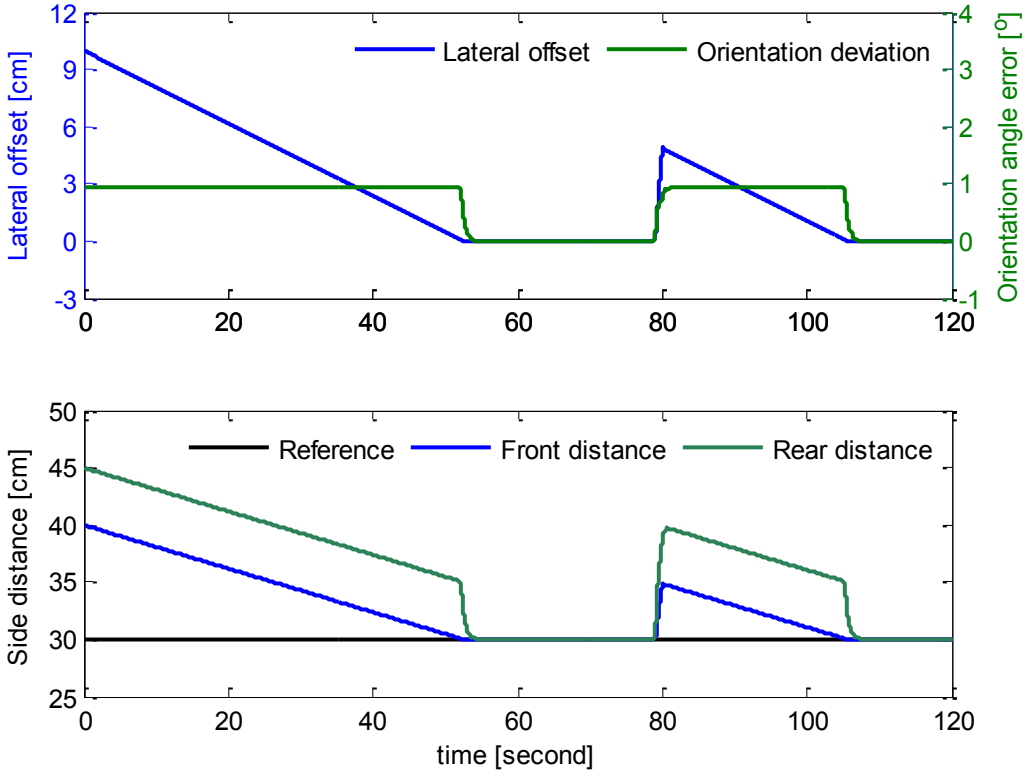

Fig. 5.6: Guiding performance for case I with $v_{ref} = 0.12m/s$.

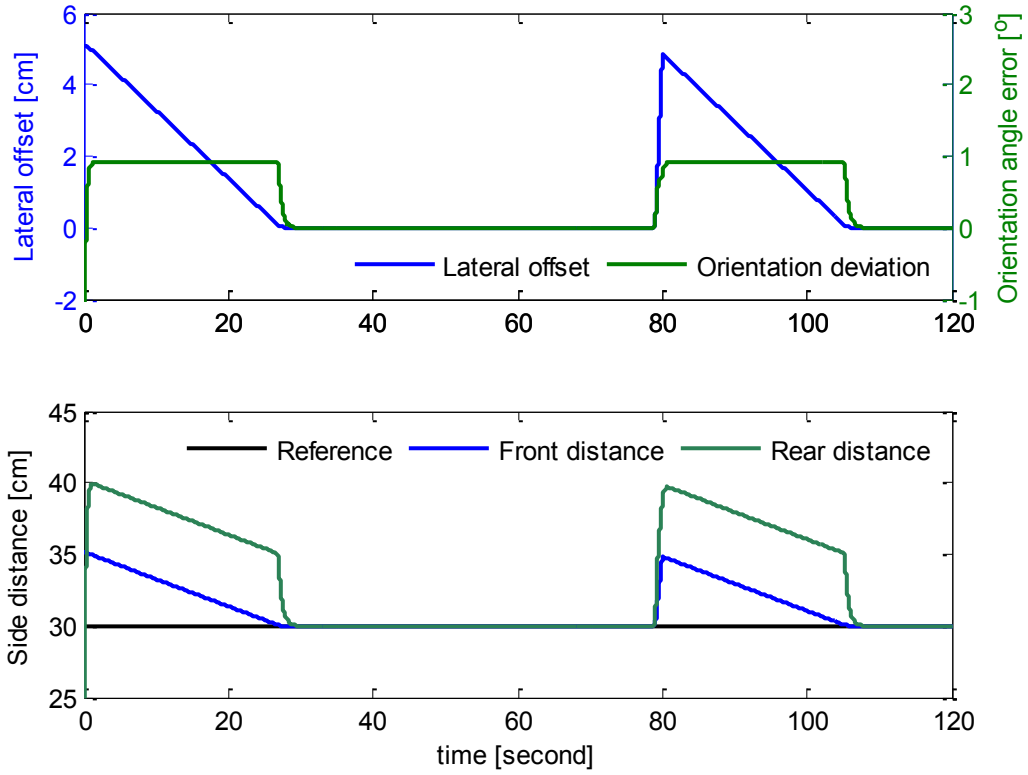

Fig. 5.7: Guiding performance for case II with $v_{ref} = 0.12m/s$.

Fig. 5.6 shows the guidance performance with the initial position of $(S_f(t_0), S_r(t_0))$ = $(0.4m, 0.45m)$ where the front and rear side distances were both at their upper bound and the orientation was at its maximal value. It is observed that the lateral offset e_y decrease continuously to zero with orientation deviation e_θ stays at its maximal value thanks to the saturation of the inner loop of the cascade structure. Thereafter, θ declines rapidly to zero. As the guidance deviation of $0.05m$ arose at 80s, e_θ decrease slightly, then rose quickly and was kept at its upper bound to remove the introduced disturbance. The similar results were also seen in the side distance plot. Firstly, S_f and S_r decline continuously in parallel by at its maximal value until S_f reaches its desired value S_{ref}. After that, S_f decreases exponentially to S_{ref}. As the guidance deviation was detected at 8s, S_r rises drastically to orientate itself in order to clear up the guidance offset. In plot Fig. 5.7, the robot started with the initial location of $(S_f(t_0), S_r(t_0))$ = $(0.35m, 0.25m)$, i.e. $(e_y(t_0), e_\theta(t_0))$ = $(0.05m, -1.84^o)$, where $e_\theta(t_0)$ is negative and contrary to $e_y(t_0)$. The initial location allows the tendency to enlarge e_y. Therefore, the robot must firstly orientate itself towards the right direction to compensate the initial error. It is observed that e_θ increases rapidly to θ_{max}, and thene_y falls gradually to zero. The developing process of variables in Fig. 5.7 coincides with that of Fig. 5.6 after e_θ reaches θ_{max}. We would like to note that e_y in Fig. 5.7 rises slightly at the beginning by $e_\theta \leq 0$, which can also be seen by S_f in side distances plot.

The critical case for the startup of the machine is $(S_f(t_0), S_r(t_0))$ = $(0.4m, 0.15m)$, i.e. $(e_y(t_0), e_\theta(t_0))$ = $(0.1m, -4.62^o)$, where $S_f(t_0) = S_f^{ubs}$ and $S_r(t_0) = S_r^{lb}$. Fig. 5.8 shows the simulation results of the critical case. This situation is basically similar to that in Fig. 5.7. The vehicle should also orientate itself firstly, and then adjust the orientation error. But it takes longer time than that of Fig. 5.7 due to the larger lateral deviation and smaller $e_\theta(t_0)$. As a result, e_y overshoots slightly by 0.018m at the moment $e_\theta = 0$ in the startup stage. In the side distance plot, S_f and S_y are observed going beyond their boundaries S_f^{ubs} and S_r^{ub} by 0.018m and 0.019m, respectively. The overshoot is generally acceptable.

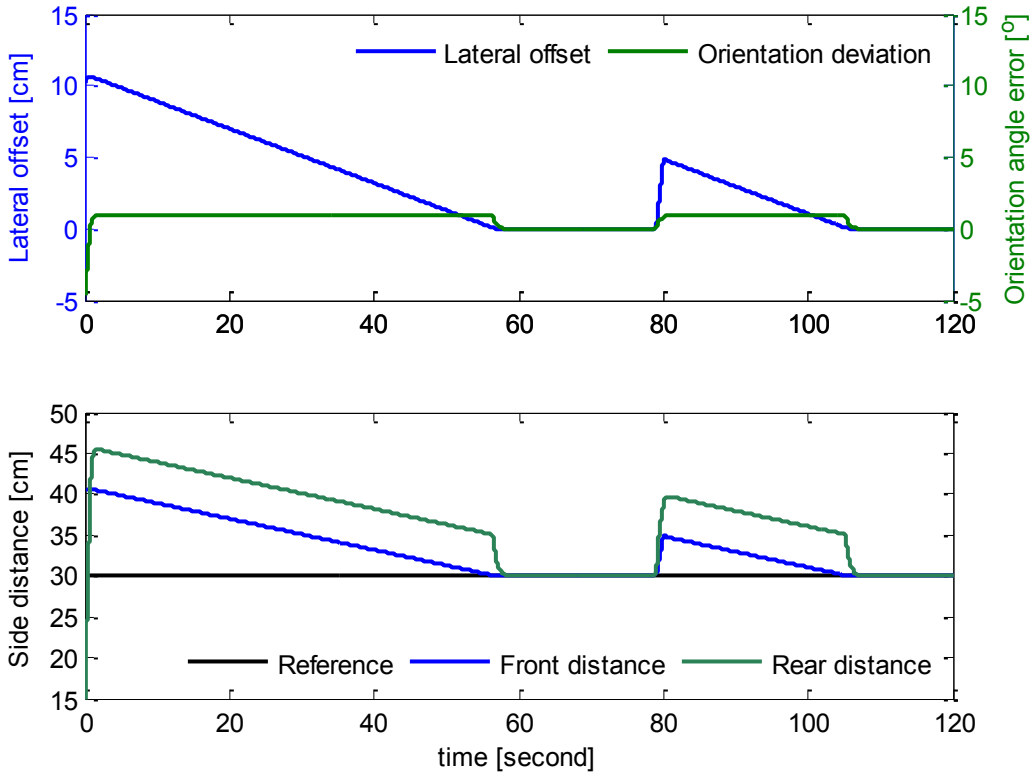

Fig. 5.8: Guiding performance for a critical case with $v_{ref} = 0.12m/s$.

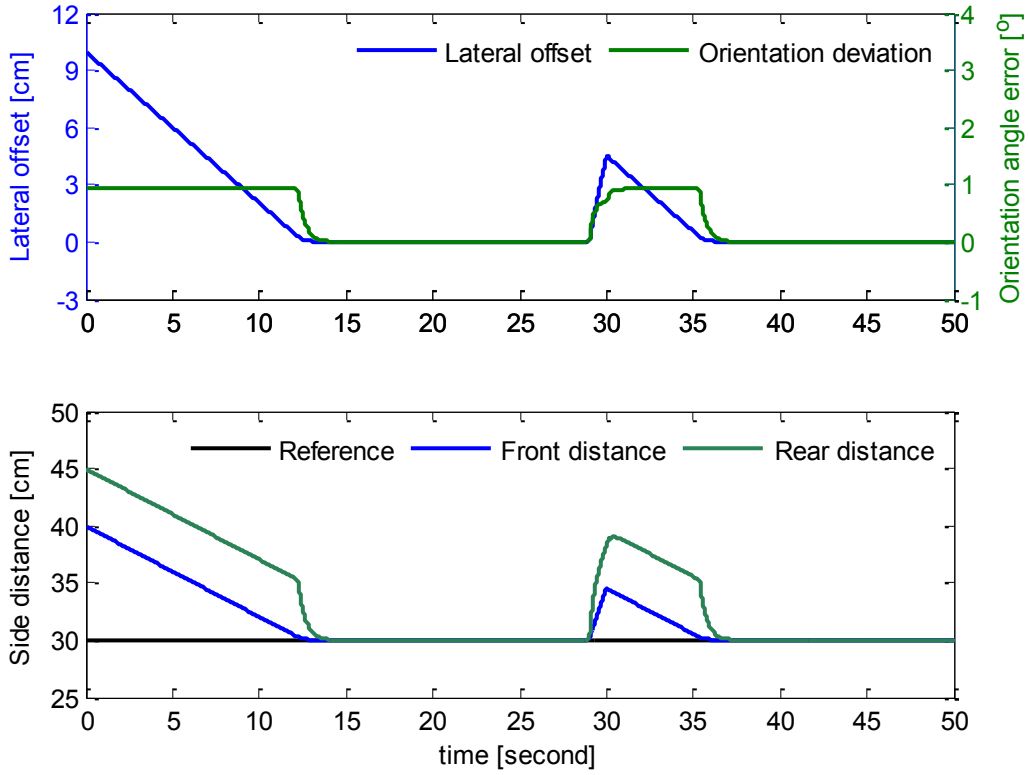

Fig. 5.9: Guiding performance for case I with $v_{ref} = 0.5m/s$.

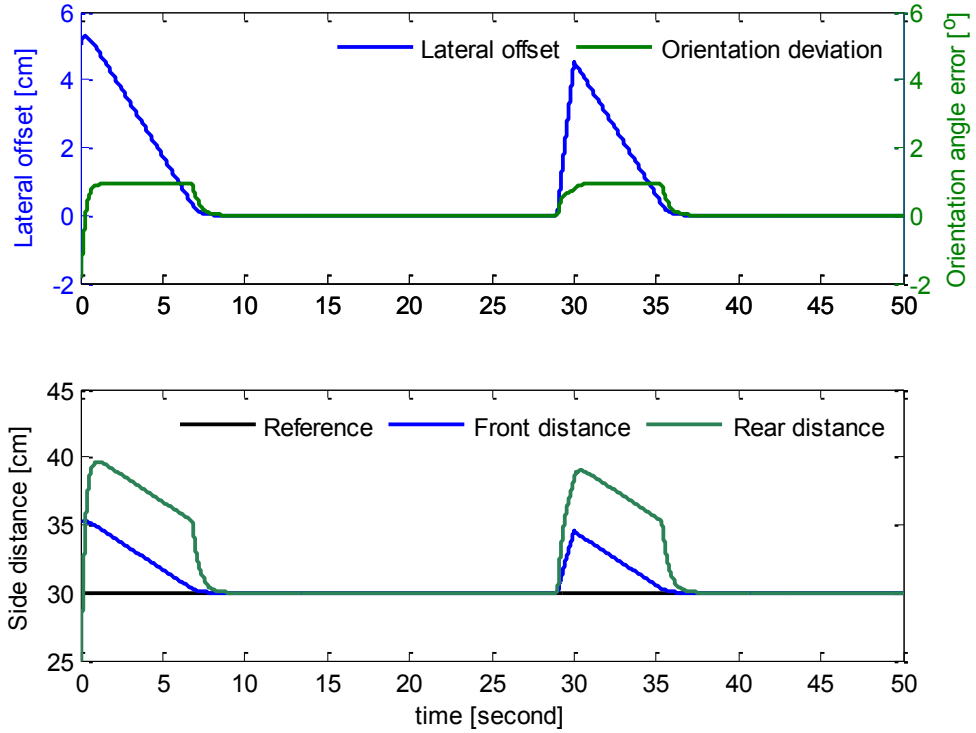

Fig. 5.10: Guiding performance for case II with $v_{ref} = 0.5m/s$.

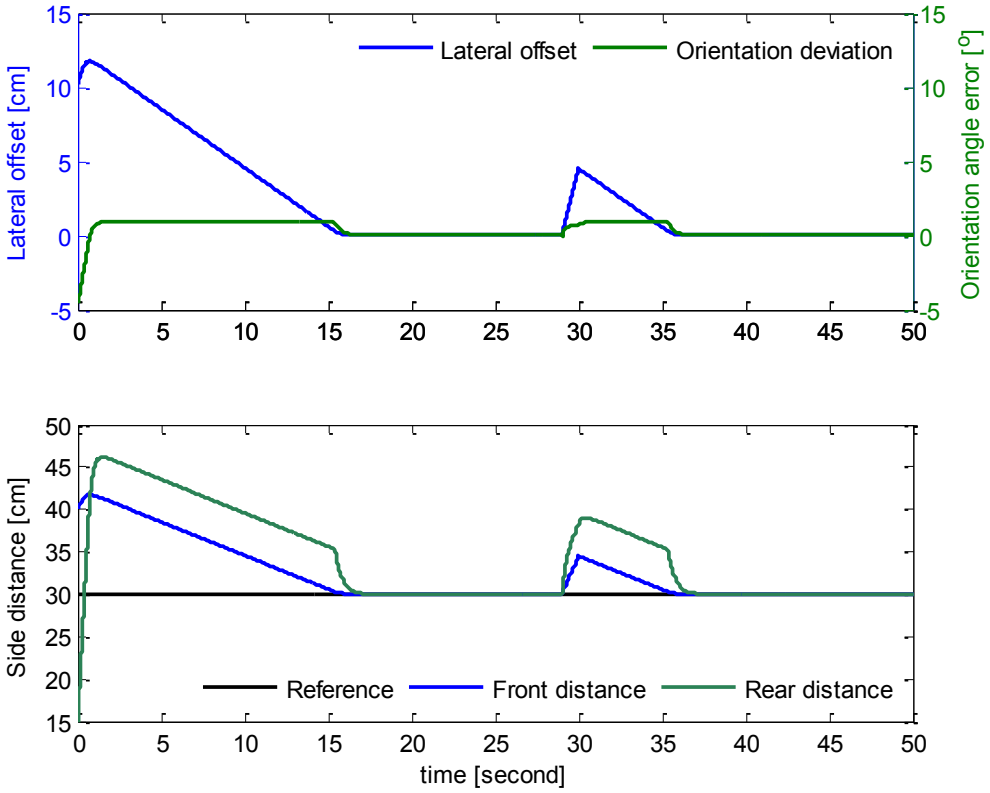

Fig. 5.11: Guiding performance for a critical case with $v_{ref} = 0.5m/s$.

Fig. 5.9 to Fig. 5.11 illustrate the simulation results for $v_{ref} = 0.5m/s$ with the same initial positions as that in Fig. 5.6 to Fig. 5.8. We observed that the development of the plots is completely coincident. But the converging time becomes approximately one-quarter as the machine drives much faster with v_{ref} from $0.12m/s$ to $0.5m/s$. The overshoot of e_y for the critical situation in Fig. 5.11 becomes larger by $0.01m$ than that in Fig. 5.9.

It is concluded from the simulation results that the initial location errors and the deviation of row following system has been successfully eliminated with the proposed cascade guidance strategy through setting a proper limitation onto the orientation angle. The field robot operates in the direction given by the target row. However, some overshoot is observed by the situation with the critical initial position. It is acceptable from practice view.

It is worth noting that the converging response of the following deviation depends on the value of the orientation angle. If their symbols are coincident, the following error decreases monotonously. If their symbols are different, the symbol of the orientation error is firstly altered to reduce the following error under the developed control function. The following error is kept increasing before their symbols are the same. The reason for this is the selected look-behind reference point. Generally, a reference point ahead of the robot's reference point with a certain distance is selected to formulate a look-ahead pattern for the path following control of differential-drive wheeled mobile robots. Comparably, the front wheels were adopted as drive wheels in this application. The rear side distance was used to determine the orientation angle, the developing process of which is behind the robot's reference point P with a distance L_a. As a result, the row following system is built based on a look-behind pattern, which leads to the simulation result that the following error did not always decrease continuously. Obviously, the application of the rear side distance to calculate the robot's in-row location has one overwhelming advantage that the rear part of the robot is observed in real time, and the possible collision with rows are avoided.

5.5 Conclusions and discussion

In this chapter, the row guidance problem was firstly formulated. It belongs to the path following control for differential-drive wheeled mobile robots. The specialization was the strict constraints on the robot's movement imposed by the working environment and the

dimensions of the machine. Benefiting from raised cultivation beds of white asparagus over ground surface, two ultrasonic sensors was adopted to measure the front and rear side distances which are used to calculate the actual location of the robot with respect to the target bed.

For the guidance system, a typical hierarchical controller with two levels was suggested based on the kinematics of differential-drive wheeled mobile robots. At the low level the speeds of the drive motors were independently stabilized through two control loops designed based on PID algorithms. At the high level, a cascade structure with an inner orientation loop and an outer lateral offset loop was proposed to compensate following errors. The heading angle of the machine was constrained conveniently by setting proper limit to the output of the controller in outer lateral offset loop. The guidance performance of the developed row following strategy was examined through simulation studies. The simulation results illustrated the efficiency of the guidance controller against initial errors and tracking deviation.

Although some satisfactory has been achieved, the development of the side distances, especially the rear side distance, by the critical situation overshot the boundary by 2 or 3 centimeters depend on the given forward velocity. Therefore, a time-optimal control design will be discussed in the following Chapter 6.

6 Time-optimal guidance control system

For the field robot, the efficiency of the guidance control system is significantly affected by the path planning strategy. The off-road structure and environmental situations are totally different. To improve the efficiency of field operations, researchers and engineers have devoted themselves to the optimal control methods. Oksanen and Visala proposed an optimal control regime to create a path for a tractor-trailer combination in specified headland [56], where the vehicle's mechanical and the field's geometrical constraints were considered and the solutions were approximated with Bézier curves. Torisu et al. presented the minimal time control strategy for the tractor in lateral motion and headland using optimal control theory in 1996 [75] and 1997 [74], respectively.

In the cascade control system discussed in Chapter 5, the lateral displacement and orientation angle of the robot's reference point were considered as system outputs. However, the constraints on the robot in rows are directly described by the front and rear side distances. The dynamics of the side distances are typical nonlinear, which makes it difficult to be solved using the traditional control strategy. In the last Chapter, they were transformed into expressions of lateral displacement and orientation angle. In this Chapter we investigate time-optimal guidance control strategy to drive the robot back to the target trajectory in minimum time in consideration of front and rear side distances as outputs. The objective of the time-optimal control for the row following system is to find an optimal control profile that minimizes the cost function without destroying the constraints. To allow for a practical implementation on a micro-controller, the cascade system discussed in Chapter 5 is improved as a substitute to realize the time-optimal control. The row following performance of the two systems are compared in detail.

6.1 Introduction

The goal of optimal control is to find solutions that are optimal with respect to a given cost function under constraints. For kinematic models of wheeled mobile robots, the optimal control of path planning and time-optimal control problems have been studied most often. For optimal control of path planning, solutions from an initial configuration q_0 to a desired configuration q_d are searched that give the minimal path coverage

$$l = \int_{t_0}^{t_f} |v(t)| dt \tag{6.1}$$

where $|v(t)|$ is the absolute translational velocity. Time-optimal control problem of wheeled mobile robots deals with the solutions from an initial configuration q_0 to a desired configuration q_d in minimal time T. The performance measure to be minimized is

$$J = t_f - t_0 = \int_{t_0}^{t_f} dt \tag{6.2}$$

with t_f the first instant of time when q_0 reaches q_d. If t_f is unspecified, this application is called time-optimal control problem with free end time. By the transformation of time $s = 1/(t_f - t_0) \cdot t$ for $t_f > t_0$, such problems are converted into problems over a fixed interval $[0, 1]$. The transformed problems can be solved using fixed end time problems [38]. As discussed in contributions [64], [71] and [82], the solutions of time-optimal control are equivalent to those of shortest paths for kinematic models of wheeled mobile robots with constant absolute translational velocity and positive minimal turning radius, i.e., for robots which cannot turn on the spot.

6.2 Formulation of the time-optimal control

The time-optimal control for the row following system is formulated based on the kinematic model of the harvesting robot platform which was discussed in Chapter 4. The object of time-optimal guidance control is to find an admissible control law that gives the minimal value of converging time from any permitted starting state to the target state.

In the application of row following problem, the forward velocity v is constant, and there are no sharp curves during operation. Only the movements in lateral direction are required to be regulated. The movements of the robot in lateral direction can be described by the dynamics of the front and rear ultrasonic sensors in lateral direction.

According to the dynamic description of the robot movement using ultrasonic sensors in Eqs. (4.9) and (4.10), only the lateral components are greatly concerned. The variables of the control system are written as:

$$\dot{S}_{Fy} = v \cdot sin(\theta) + \frac{L_b}{2} \cdot \omega \cdot sin(\theta) \tag{6.3}$$

$$\dot{S}_{Ry} = v \cdot sin(\theta) + \frac{L_b}{2} \cdot \omega \cdot sin(\theta) - \omega \cdot L_a \cdot cos(\theta) \tag{6.4}$$

with S_{Fy} and S_{Ry} are the lateral components of S_F and S_R.

The constraints imposed by the working environment are expressed as boundary conditions of the time-optimal control problem:

$$\begin{gathered} 0.2m \leq S_{Fy}(t) \leq 0.4m \\ 0.15m \leq S_{Ry}(t) \leq 0.45m \end{gathered} \tag{6.5}$$

and the desired configuration is

$$\begin{gathered} S_{Fy}(t_f) = S_{ref} \\ S_{Ry}(t_f) = S_{ref} \end{gathered} \tag{6.6}$$

with limited control input

$$|\omega| \leq 0.1\omega_{mref} \tag{6.7}$$

6.3 Solutions

General Pseudospectral Optimization Software (GPOPS) is applied to solve the time-optimal guidance control problem [59]. GPOPS is an open-source software for optimal control written in MATLAB that implements the Gauss and Radau hp-adaptive pseudospectral collocation methods. This software has a build-in forward mode automatic differentiation and generates derivative estimates as efficiently as possible by adopting sparse finite-differencing of optimal control problem. The continuous-time optimal control problem is transcribed to a finite-dimensional nonlinear programming problem (NLP) that is solved using a restricted version of NLP solver SNOPT [26].

The emphasis of the time-optimal control for the row guidance system is to find an operation method that is able to eliminate the guidance error in a minimum time. Therefore, the only thing we need to care about is how to construct the problem to be tackled according to GPOPS syntax, but not the complex algorithms in solving optimization problem. All the conditions such like initial guess, final states, cost function, constraint function etc., are to be formulated using the vectorization capabilities of MATLAB. The problem is solved using the built-in automatic differentiator which is preferred in that it provides highly accurate derivatives and already included as part of the GPOPS software.

To allow for a fair comparison between the cascade system discussed in Chapter 5 and the time-optimal method, the same initial positions of the robot is selected in the simulation studies of time-optimal row following control. The two initial locations are named as Case I $(S_f(t_0), S_r(t_0)) = (0.4m, 0.45m)$, i.e. $(e_y(t_0), e_\theta(t_0)) = (0.1m, 0.92^o)$), and Case II $(S_f(t_0), S_r(t_0)) = (0.35m, 0.25m)$, i.e. $(e_y(t_0), e_\theta(t_0)) = (0.05m, -1.84^o)$). The simulation results of the comparison studies are illustrated in the figures that follow.

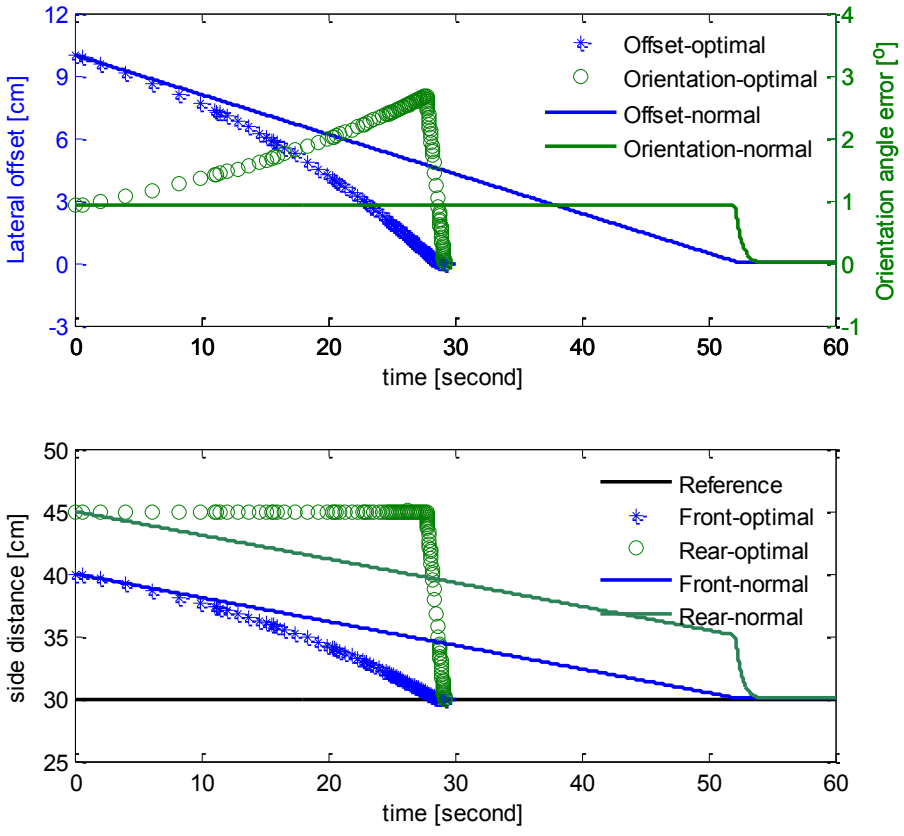

Fig. 6.1: Comparison of row guiding performance case I with $v_{ref} = 0.12m/s$.

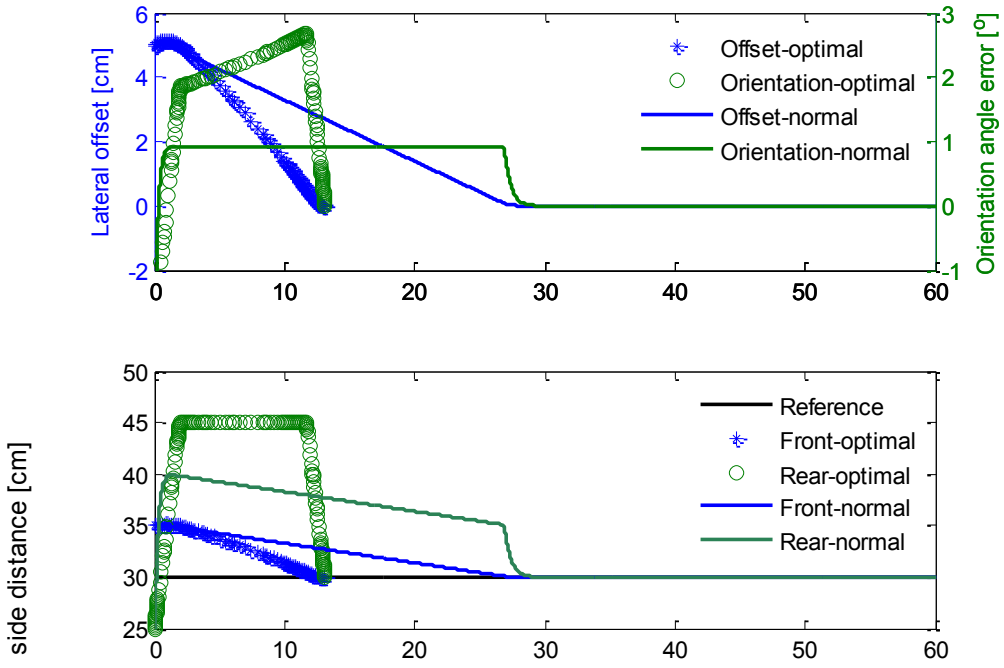

Fig. 6.2: Comparison of row guiding performance case II with $v_{ref} = 0.12m/s$.

In Fig. 6.1, the plots illustrate the simulation results of comparison for the robot with an initial position of Case I. As is observed, the converging tendency of the lateral offset for the time-optimal control and the cascade system appears identical. The significant difference is the changes of the orientation angle or the rear side distances. Differently from being kept constant for the cascade controller, the orientation angle of the time-optimal control system increases with the decrease of the lateral offset, which is shown in the side distance plot that S_r is kept at its upper boundary for the time-optimal control. That accelerates the converging process by 25s.

Fig. 6.2 shows the results of the time-optimal controller with an initial position of Case II, where $e_\theta(t_0)$ is negative and contrary to $e_y(t_0)$. The development of the time-optimal solutions is comparable to that of the normal cascade guidance controller. The orientation angle is firstly adjusted drastically to the right direction and then increases until S_r arrives at its upper limit. With the reduction of S_f the orientation deviation e_θ rises slowly. e_y increases slightly before e_θ comes to zero. Then e_θ rises gradually until e_y approaches to zero after that e_θ decreases rapidly to zero.

Fig. 6.3 and Fig. 6.4 illustrate the row guidance performance of the field robot with a forward velocity of 0.5m/s. The robot starts up with the same initial positions as that in Fig. 6.1 and Fig. 6.2, respectively. The similar developing process of the row following is

observed. The only difference is that the converging time decreases significantly with improved forward velocity.

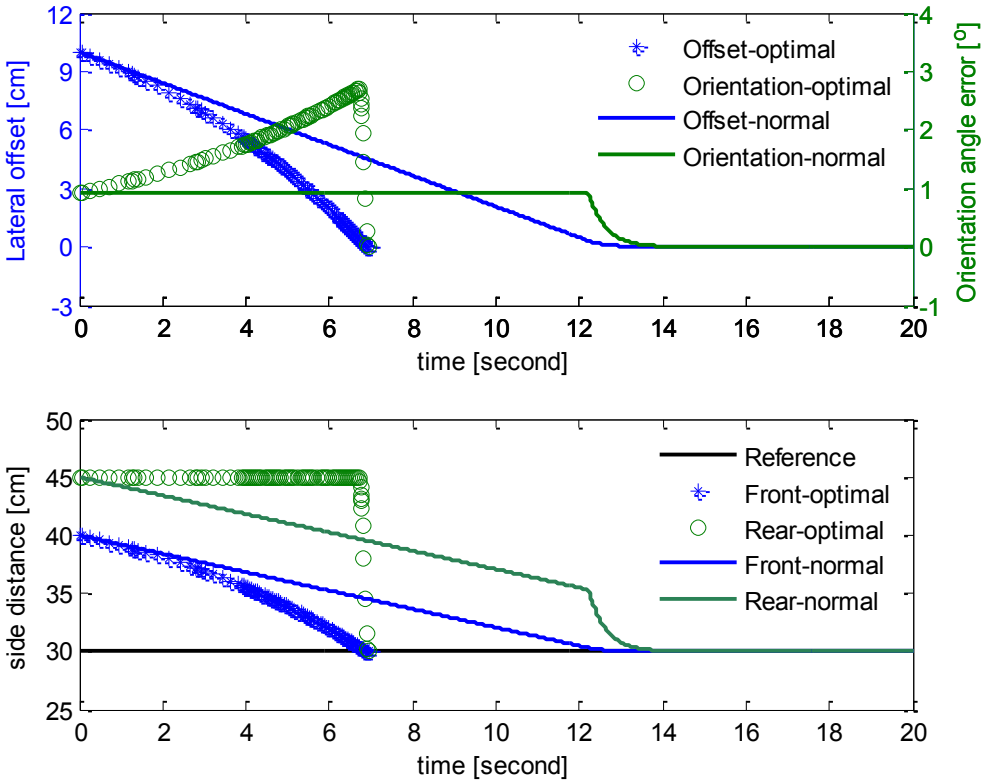

Fig. 6.3: Comparison of row guiding performance case I with $v_{ref} = 0.5m/s$.

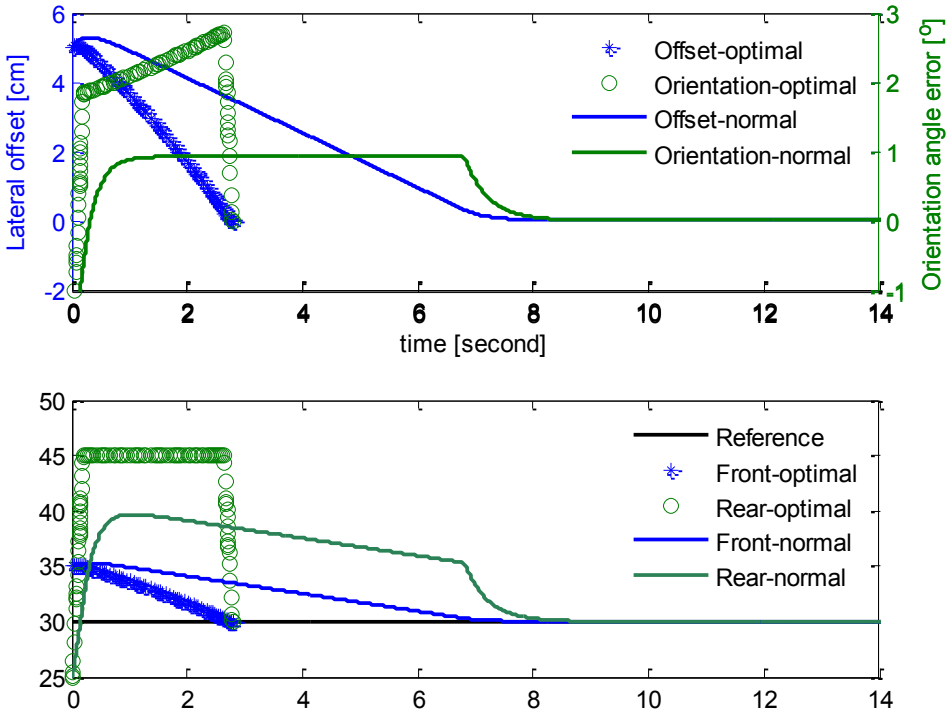

Fig. 6.4: Comparison of row guiding performance case II with $v_{ref} = 0.5m/s$.

It is concluded from the simulation results in Fig. 6.1 to Fig. 6.4 that time-optimal guidance controller accelerates the converging process dramatically in comparison to the normal cascade controller. The time-optimal guidance strategy exploits the full potential by maximizing the orientation angle, which is observed in the side distance plot that the rear side distance S_r is set to its upper boundary if $S_f \neq S_{ref}$ or $e_y \neq 0$. While the normal cascade guidance controller in Chapter 4 directly set the limit on the orientation angle constantly. With the constant limit on the orientation angle, the converging process slowed significantly down. Note that the time-optimal control simulation studies with critical initial positions are not possible since the front side distance would exceed its predefined constraints that must be strictly satisfied.

To use time-optimal control strategy, an advanced solver is necessary to solve the finite dimensional optimization problem obtained by discretizing the time domain of the time-optimal control problem. Unfortunately, the application of the time-optimal control algorithms on the selected micro-controller is difficult due to computational efficiency and algorithm complexity.

6.4 Practice substitute system

As discussed in Section 6.2, our guidance system is governed by a set of nonlinear state equations and furthermore the original time optimal control problem is subjected to various constraints, such as initial and target conditions, state and control input constraints, which makes it difficult to get an analytical solution. The time-optimal control problem is then numerically resolved using well-developed optimal control software GPOPS. GPOPS integrates a third-party solver SNOPT. The original time-optimal control problem is converted into a constrained nonlinear programming problem. It is worth noting that the implementation of such complex optimization algorithm in a typical low-cost hardware for agricultural machine is unrealistic since the selected micro-controller PSoC 5 offers very limited memories and the clock frequency of the CPU is in MHz range. All these limitations motivate us to explore computational cost-effective solutions. Enlightened by the simulation results of time-optimal row following control, we seek a comparable cost-efficient solution that is suitable for the practical implementation on a micro-controller as PSoC 5.

6.4.1 Improved cascade control system

The time-optimal solution of the rear side distance was accomplished on its upper or lower boundary by $e_y \neq 0$. In time-optimal control guidance method, S_f and S_r were the controlled variables. However, the direct controlled variable is y and the indirect controlled variable is θ in the normal cascade control method. With the inspiration of the numerical results of the time-optimal control, if a mapping relationship between side distances and the constraints on the orientation angle would be established, the normal cascade guidance controller can realize the time-optimal following function. At the same time, we observed that there is a mapping of side distances (S_f, S_r) onto (y, θ) according to Eqs. (5.3) and (5.4). We resort to improve the cascade system to realize the time-optimal control function by adjusting the limitations of the orientation angle.

By referencing the constraints on the orientation angle in Eqs. (5.17) and (5.18), the limits on θ can be adjusted with the actual front side distance S_f accordingly to:

$$\text{If } S_f \geq S_{ref} \qquad arctan(\frac{S_r^{lb} - S_f}{L_a}) \leq \theta \leq arctan(\frac{S_r^{ub} - S_f}{L_a}) \tag{6.8}$$

$$\text{If } S_f \leq S_{ref} \qquad arctan(\frac{S_r^{lb} - S_f}{L_a}) \leq \theta \leq arctan(\frac{S_r^{ub} - S_f}{L_a}) \tag{6.9}$$

The improved cascade controller for row guidance system is shown in Fig. 6.5 by which the limit on the orientation angle is modified with the actual S_f according to Eqs. (6.8) and (6.9). The parameters of the controllers in motor speed loops, lateral offset loop and orientation angle loop are identified with that in Table 5.1.

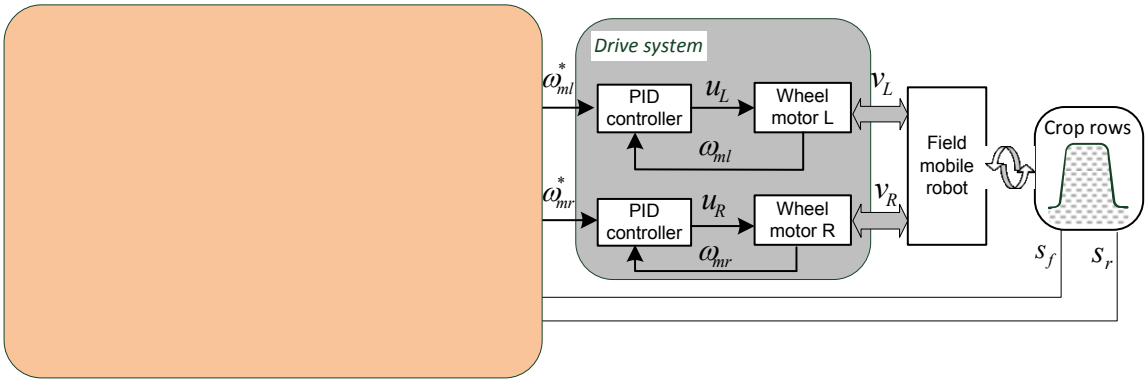

Fig. 6.5: Substitute cascade row guidance system for time-optimal control.

6.4.2 Comparison studies

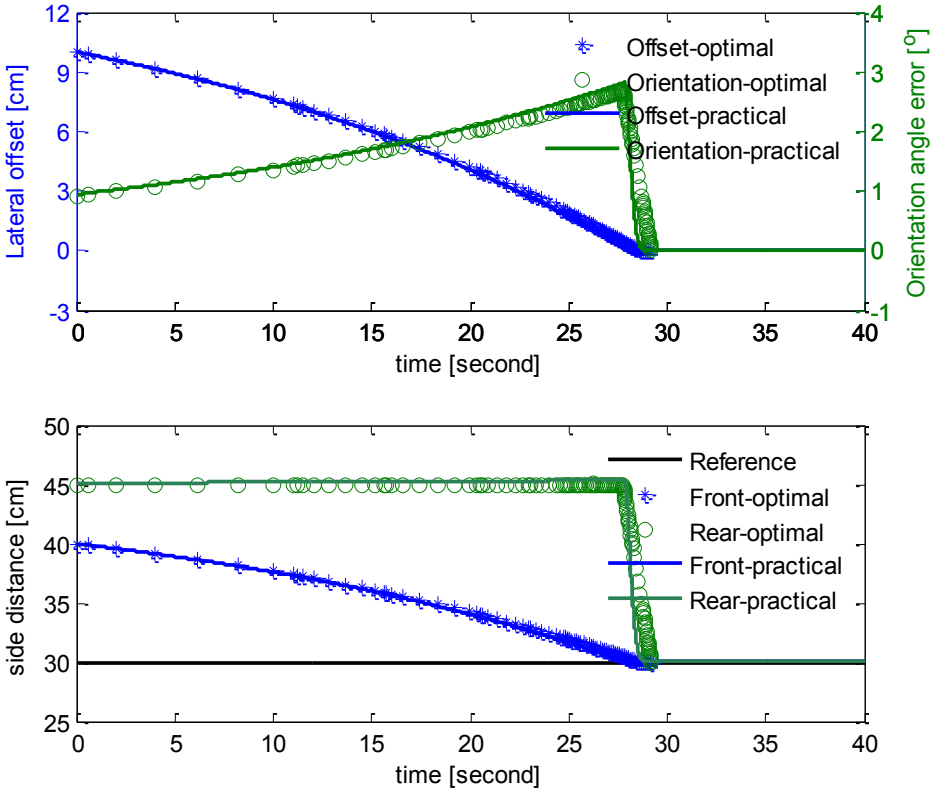

Fig. 6.6: Comparison of row guiding performance for case I with $v_{ref} = 0.12m/s$.

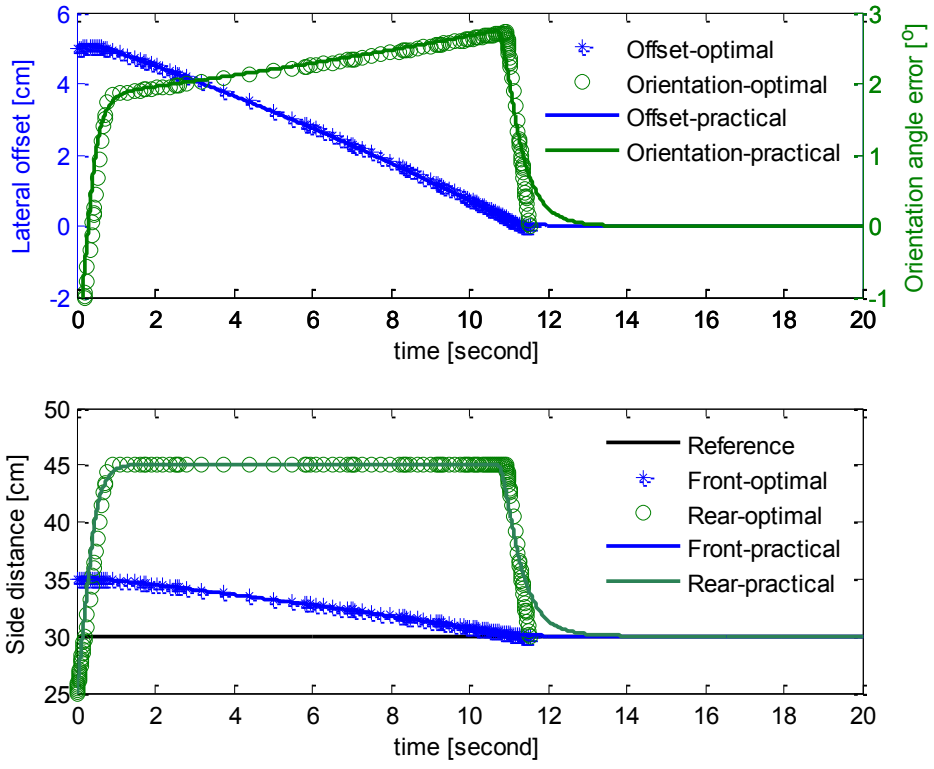

Fig. 6.7: Comparison of row guiding performance for case II with $v_{ref} = 0.12m/s$.

The guidance performance of the proposed substitute controller for time-optimal control was firstly examined in simulation studies. The simulation results of the improved cascade control system are shown in Fig. 6.6 to Fig. 6.9 compared with the results of time-optimal guidance controller.

Fig. 6.6 and Fig. 6.7 show the simulation plots with a forward velocity of 0.12m/s where the field robot starts with the two representative initial positions $(e_y(t_0), e_\theta(t_0)) = (0.1m, 0.92^o)$ and $(e_y(t_0), e_\theta(t_0)) = (0.05m, -1.84^o)$, respectively. Fig. 6.8 and Fig. 6.9 illustrate the results for the robot with a forward velocity of 0.5m/s. It is shown that the simulation plots of the improved cascade guidance controller and the plots of the time-optimal controller almost overlap one another. The only difference between them is that the deviation of the orientation angle e_θ of the substitute time-optimal controller begins to decrease as soon as the lateral offset e_y reduces to zero, while e_θ and e_y go down to zero simultaneously for the time-optimal control system. It is explained by the cascade control structure: only when the lateral offset of the outer loop reduces to zero the inner loop can retreat from saturation. Comparably, in the time-optimal control method, the front and rear side distances S_f and S_r are the controlled variables to be optimized. The similar developing process can be also observed in the side distance plots. Accordingly, for the improved cascade controller S_r begins to reduce from is upper limit for $e_y \geq 0$ only after S_f comes to zero.

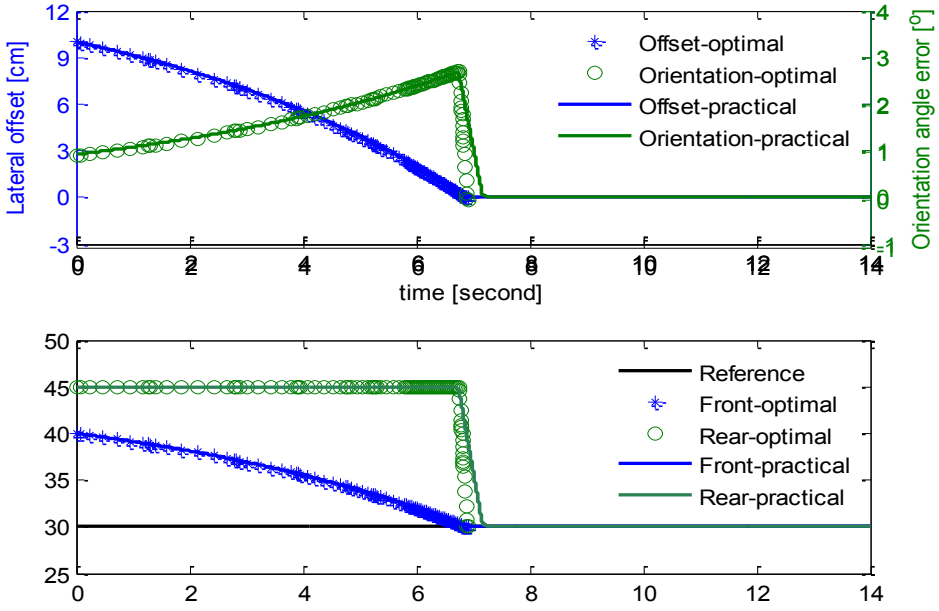

Fig. 6.8: Comparison of row guiding performance for case I with $v_{ref} = 0.5m/s$.

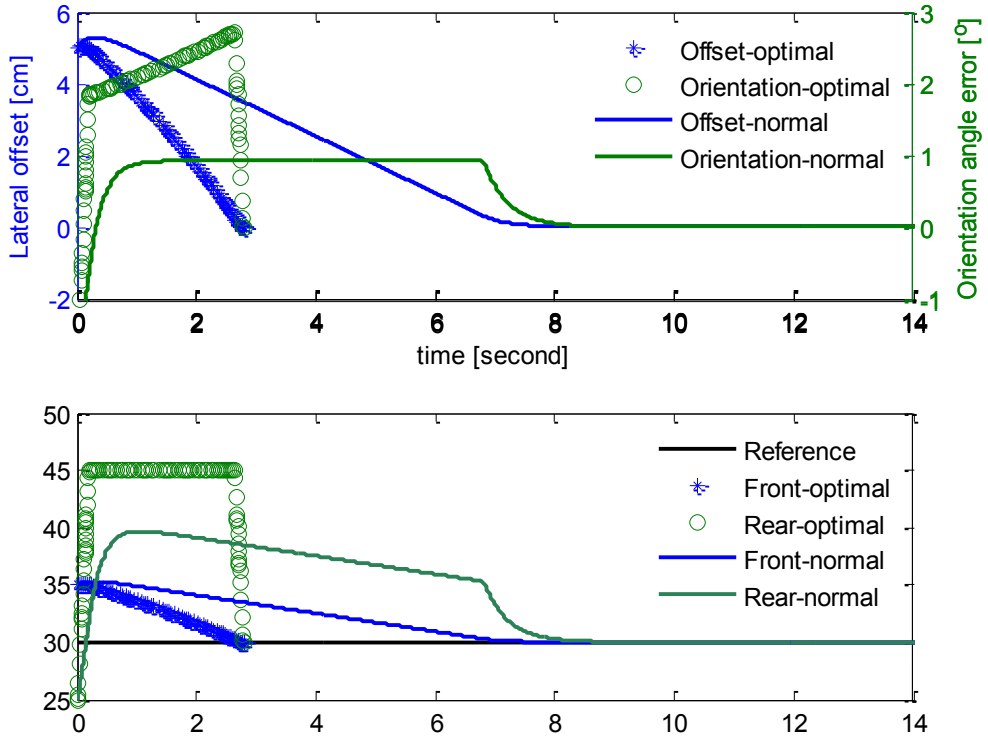

Fig. 6.9: Comparison of row guiding performance for case II with $v_{ref} = 0.5m/s$.

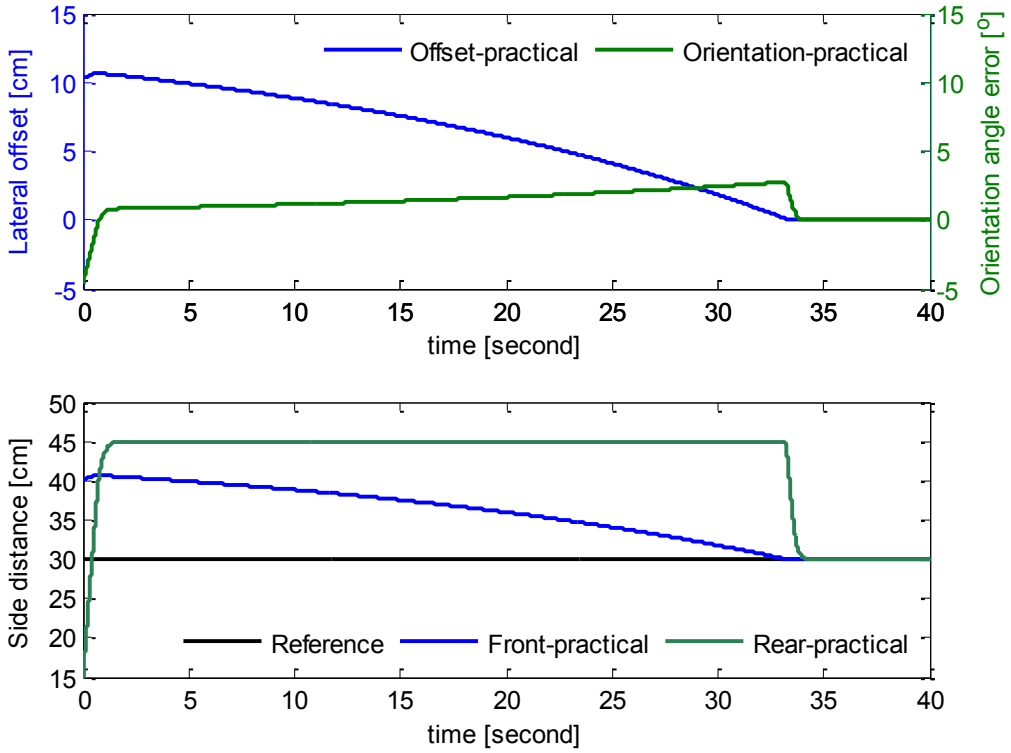

Fig. 6.10: Guiding performance with an initial position for critical case with $v_{ref} = 0.12m/s$.

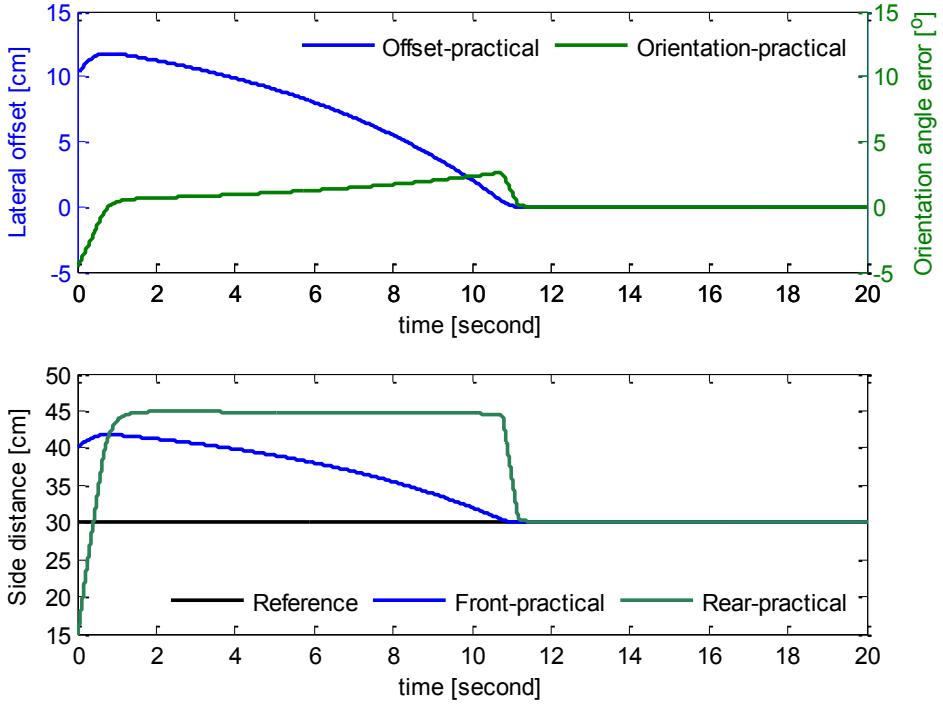

Fig. 6.11: Guiding performance with an initial position for critical case with $v_{ref} = 0.5m/s$.

The critical situation $(S_f(t_0), S_r(t_0)) = (S_f^{ubs}, S_r^{lb})$, i.e. $(S_f(t_0), S_r(t_0)) = (0.4m, 0.15m)$, was also studied. The numerical results were shown in Fig. 6.10 and Fig. 6.11 for forward velocity $v_{ref} = 0.12m/s$ and $v_{ref} = 0.5m/s$. Since this field robot in this application has no steerable axle, it cannot proceed without destroy the soft limit on S_f by the critical situation. In the normal cascade guidance system, S_f and S_r overshoot by 0.01m by $v_{ref} = 0.12m/s$ and 0.025m by $v_{ref} = 0.5\text{m/s}$, respectively. Obviously, S_r goes beyond the critical constraints 0.45. In the time-optimal control application, the solving program cannot proceed by the critical situation. However, the simulation results in Fig. 6.10 and Fig. 6.11 show that the machine drives successfully forward without destroy the critical constraint imposed on the S_r and comes back to the desired track faster.

6.5 Conclusions

The time-optimal control for the field harvesting robot with constraints of the working environment was firstly investigated. The time-optimal control problem for row following system was formulated using the front and rear side distances as the controlled variables, and then solved with a well-developed optimal-control solver GPOPS. With the instructive conclusions drawn from the time-optimal control results, a substitute with cascade

structure was proposed. The substitute system was developed based on PID method and conveniently implemented on any micro-controller. The cascade system improved the computational efficiency because the complex optimization that was essential in solving time-optimal control problem was avoided. It allows for an effortless realization on a micro-processor. The comparison studies of following performance illustrated that the substitute controller accomplished the same performance of the row following of the time-optimal guidance controller.

7 Experimental verification

This Chapter is focus on the experimental verification of the developed row following strategy. The setup of the experimental platform on the prototype is firstly detailed. The tasks for the robot to undertake are explained in the function management. The design of software and hardware is detailed. The aforementioned practical substitute system for the time-optimal row following control is verified extensively in laboratory as well as in fields.

7.1 Experimental platform

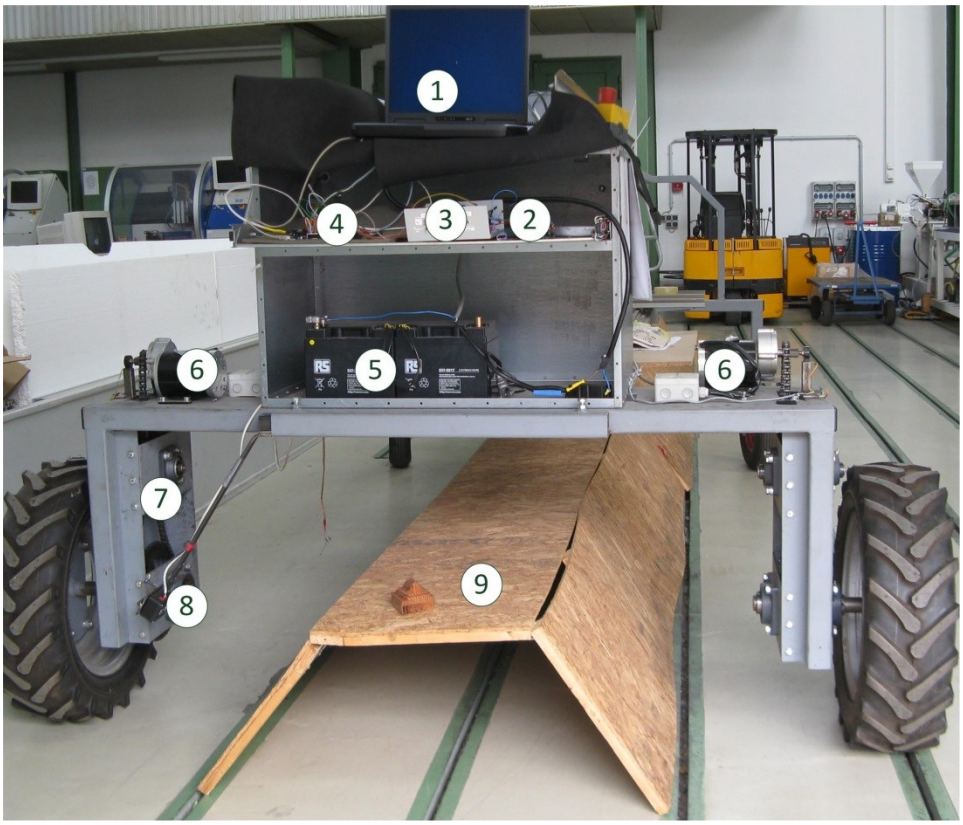

Fig. 7.1: Experimental platform.
(1.laptop, 2. Joystick, 3. Sabertooth 2×50AH, 4. PSoC CYCKIT-001 with CY8C55 processor, 5,Battery 2×15V, 6. DC drive motor MY1020Z2, 7. Chain gear box 16:1, 8 Ultrasonic sensor PING))), 9. Model of cultivation mound.)

The experimental platform (shown in Fig. 7.1) consists of drive systems, sensors, PSoC controller, Sabertooth driver, incremental encoders, ultrasonic sensors, battery and a joystick. The configuration of the prototype was discussed in detail in Chapter 3. The motor speed is regulated by the voltage supplied from Sabertooth. The regulation of the output voltage of Sabertooth driver is achieved by adjusting a 0~5V analog control signal

or PWM signal. The control signal is provided by micro-controller in the automatic operating mode and by the joystick in manual mode. An emergency stop is performed by the red button at the right side. A laptop is applied as the user interface to adjust the parameters in real-time and save processing data. The laptop communicates with the controller through USB cable.

7.2 Function management

The robot locates itself with the help of front and rear side distances with respect to the target cultivation bed. There are no other sensors except for the two ultrasonic sensors to provide the absolute position of the robot. The automatic row following control strategy works effectively only for the in-row drive when the side distances satisfy the constraints discussed in Section 4.3. If the side distances dissatisfy the imposed constraints or are unavailable out rows, it is impossible for the robot to orient the direction. Besides, constrained by the working environments the initial position for the robot startup in the autonomous row guidance control is strictly limited to prevent any collision. Under these conditions manual operation is essential to modify the machine to the right location. Therefore, the platform is expected to capable of executing manual and automatic operation. Although the robot works only with forward drive, backward operation is also considered to locate the vehicle in the experimental tests more conveniently. The function management of the system is illustrated in Fig. 7.2.

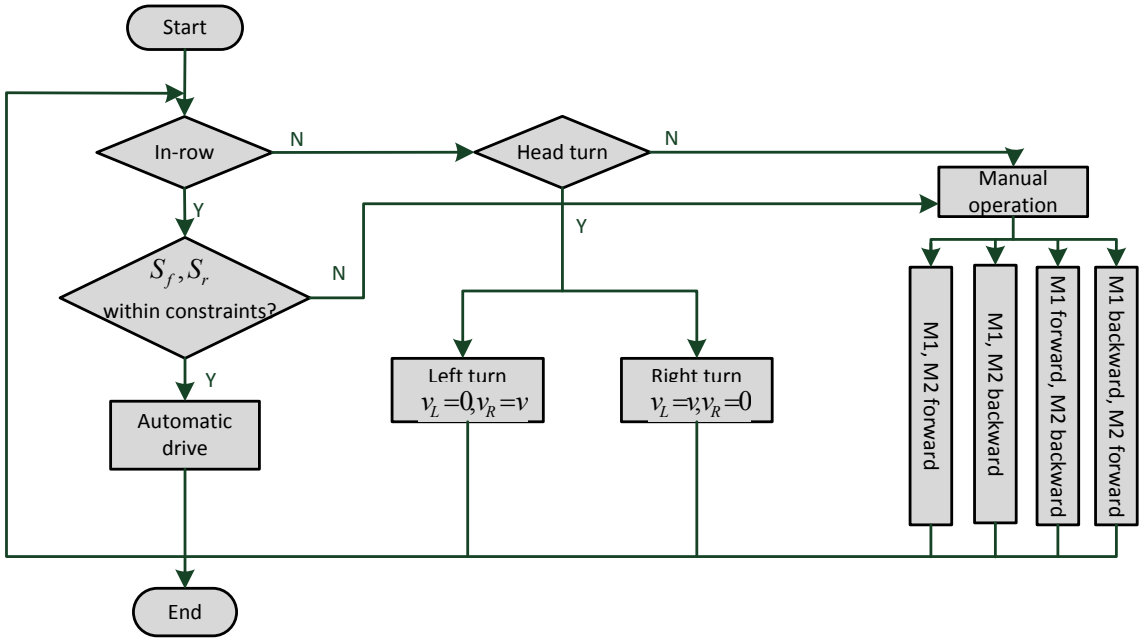

Fig. 7.2: Function management.

7.2.1 Manual operating mode

For the manual operation, the robot's movement is controlled by a two-axis joystick. The joystick is capable of controlling the two drive motors forward or backward separately or together at will. And then the robot can be operated to follow any curve path. The manual operation is essential under situations:

- The information of cultivation rows is not available
- The robot starts with the special positions discussed in the Section 5.3.3

whereby the automatic operation is impossible. The manual method is used to adjust the robot to the correct location that is suitable for automatic operation.

7.2.2 Automatic row guidance

In the automatic driving mode, the control signals of Sabertooth driver for the drive motors are provided by the micro-controller. The motor speeds are regulated according to the sensed side distances by the programmed row following control algorithms on the controller. The autonomous guidance can be conducted only in the field with the cultivation bed. To start up the field robot in the autonomous operating mode, the front and rear side distances must satisfy the predefined constraints. To get more precise distance measurements, the ultrasonic sensors are required to be oriented vertically to the surface to be measured.

7.2.3 Turn at the end of rows

Turn operation at the headland is also an important task. The first step is to determine if the robot reaches the headland. The measurements of the ultrasonic sensors are applied to determine whether the robot arrives at the headland. When the robot drives in the field, the side distances measured by ultrasonic sensors between robot and the cultivation bed are within a certain scope. Sudden increased distance measurements do not necessarily mean that the vehicle drives out of field. Only when the both side distance measurements are beyond a predefined value over a certain time scope, it signifies that the robot arrived at the headland. Although there is no testing information about the absolute location of the robot, the allocation of the cultivation beds are kept unchanged. If there is enough space at the headland, the turn operation to the next cultivation bed can be conveniently performed according to the symmetrical allocation of the cultivation beds using odometry method.

Fig. 7.3 shows the left-turn operation at the headland. The current target row is *Cultivation bed II*, and the next target is *Cultivation bed III*. The turn operation can be started until S_r is beyond the preset measuring scope to reserve sufficient place for the rear wheels. For the right-turn, the left motor stands still and the right motor drives a curve length of πL_b around the left wheel. And then both motors operate forward with the same speed until S_f and S_r are detected within the preset measuring scope. Thus, the shift of the target row from *Cultivation bed II* to *Cultivation bed III* is finished. It is easily to imagine that for the right-turn operation the right wheel stands still and the left wheel drives a curve length of πL_b around the right wheel. We would like to note that the turn of the robot at the headland is executed by using the given geometrical arrangement of the cultivation beds since there are no any global positioning sensors. Since there is no additional landmarks available, the adoption of odometry navigation method using the installed incremental encode on the drive motor at the headland is the most cost-effective alternative. It is observed that the space of two vehicle length and two vehicle width is needed at the headland for the robot to perform the turn operation.

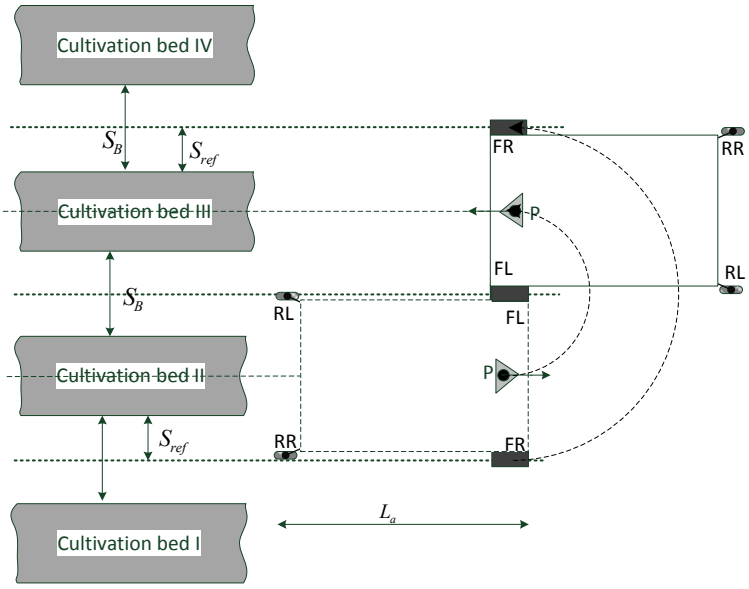

Fig. 7.3: Turn operation at the headland.

Since this automatic turn operation for the robot at headland was developed on the basis of geometrical distribution of the cultivation beds, it is worth noting that this method is effective only for the fields with well-structured cultivation bed, and that there is no slip between wheels and the ground surface. To achieve a more precise drive for the switch of target cultivation beds at the headland, additional sensors are necessary to feed back the relative locating information for the robot with respect to the cultivation bed.

7.3 Functional modules

7.3.1 Signal acquisition

Signal acquisition includes mainly output of sensors, ultrasonic sensor PING))) and incremental encoder Model120. Ultrasonic sensors are essential to be used to calculate the actual location of the robot. The signal of incremental encoder provides the actual rotation speed of drive motor.

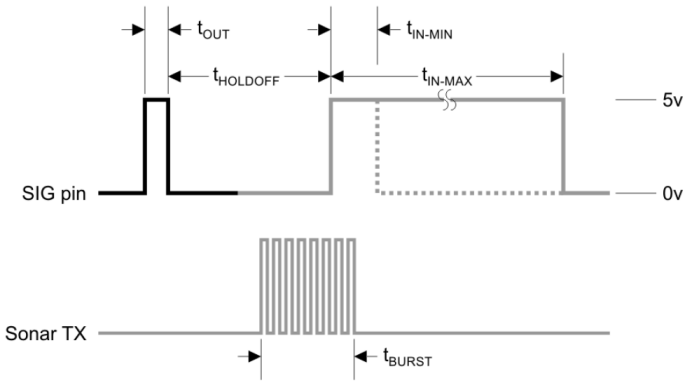

Fig. 7.4: Sensing principle of PING))) sensor.

Table 7.1: Event sequence and time span of PING))) sensor

Input Trigger Pulse	t_{OUT}	2 µs (min), 5 µs (min) typical
Echo Hold-off	$t_{HOLDOFF}$	750 µs
Burst Frequency	t_{BURST}	200 µs @40 kHz
Echo Return Pulse Minimum	t_{IN-MIN}	115 µs
Echo Return Pulse Maximum	t_{IN-MAX}	18.5 µs
Delay before next measurement		200 µs

The basic principle of operation of PING))) sensor is shown in Fig. 7.4. The PING))) ultrasonic sensor detects objects by emitting a short ultrasonic burst and then “listening” for the echo. Under control of a host microcontroller (trigger pulse), the sensor emits a short 40 kHz ultrasonic burst, which travels through the air, hits an object and then bounces to the sensor. PING))) sensor provides an output pulse to the host that will terminate when the echo is detected. The width of this pulse corresponds to the distance between PING))) and the target.

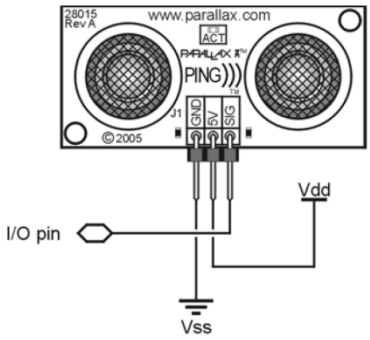

Fig. 7.5: PING))) ultrasonic sensor.

The trigger and the echo signals are both transmitted and captured at the same I/O pin (see Fig. 7.5) over different time spans. Therefore, the event occurred at I/O pin must be efficiently managed according to time. The time management of events at I/O pin is accomplished using the component developed using Verilog in PSoC Creator. PSoC Creator allows user to define components in Verilog. The Verilog based components developed by user offer more flexibility and scope to optimize the resource utilization. The signal acquisition is developed using Verilog and encapsulated with the combined API functions.

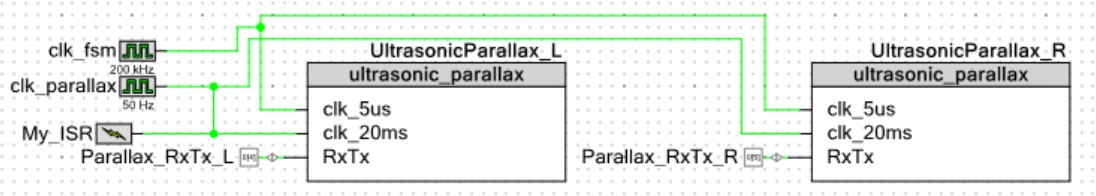

Fig. 7.6: Encapsulated PINP))) block.

The encapsulated PING))) block is shown in Fig. 7.6. *Parallax_RxTx* is the bidirectional signal interface for the ultrasonic sensors to send signal and to accept the echo signal. There are two clocks are applied for this module. *clk_fsm* generates the trigger signal for 5µs every 20ms controlled by the 50Hz *clk_parallax*. The distance measurement is read out each 20ms. The detected distance is calculated with:

$$d = C_{air} \frac{CounterNumber_{ultra}}{CounterFrequency_{ultra}} \tag{7.1}$$

with C_{air} the speed of sound in air in m/s.

The detecting precision of the ultrasonic sensor is significantly affected by the roughness of the measuring surface because the route of the echo signal could be changed more or

less by the irregular detecting surface. The detecting performance was investigated in laboratory.

Incremental encoders are adopted to detect the movement of the motor and further to calculate the motor speed. It is also used to quantify the covering path. A 1MHz counter is used to timing the pulse width of the encoder.

$$\omega_m = 2\pi \frac{CounterFrequency_{motor}}{CounterNumber_{motor}} \tag{7.2}$$

The distance travelled for each pulse is

$$\Delta distance = \frac{WheelCircumference}{PulseNumber \cdot GearRatio} = 0.9mm \tag{7.3}$$

The distance change is added to a variable after each pulse to record the total travelled path. The detection would accumulate considerable error in the calculated distance if drive wheels suffer from slippage or spin, which cannot be detected currently. As for the application of this agricultural robot, the motor operates with a relatively low speed (60rpm~250rpm). It is not reasonable to count pulse numbers with a certain time span. Therefore, a counter in micro-second frequency is used to count the time duration of every pulse.

7.3.2 Controller module

The controller module deals with the in-row automatic drive. The time-optimal row following performance was achieved through a cascade guidance system as was discussed in Section 6.4. The substitute control system is preferred due to computational cost-efficiency and practical implementation on micro-controller. As a result, only the improved cascade system is implemented on the micro-controller PSoC 5.

For the revolution control of the drive motors a PI controller is adopted.

$$u_m = k_{p\omega} \cdot e_\omega(k) + \alpha \cdot k_{i\omega} \sum_{j=0}^{k} e_\omega(j) \cdot \tau_{s\omega} \tag{7.4}$$

where $e_\omega(k) = \omega_m^*(k) - \omega_m(k)$, α is the anti-saturation coefficient of the integration function, $\tau_{s\omega}$ the sample time of the motor speed control system.

A simple P controller is applied for the orientation angle loop. For the lateral offset with PD controller

$$u_y(k) = \theta_d(k) = k_{py} \cdot e_y(k) + \frac{k_{py} \cdot \tau_{dy}}{T_{sy}} (e(k) - e(k-1)) \tag{7.5}$$

Where $e_y(k) = y(k) - y_d(k)$, τ_{dy} is the derivative time constant and T_{ys} the sample time. The saturation are set by referencing Eqs. (6.8) and (6.9). The sample time constants for the low and high levels are appointed as 5ms and 50ms, respectively.

7.3.3 Communication

To record experimental results and to analyze system performance in the experimental tests, the process data are necessary to be saved and observed on a computer. The CY8CKIT-001 PSoC Development Kit provides communication interfaces such as USB, I2C, CAN, wireless. Only one interface is required to connect the micro-controller to a computer in this application. USB devices are easy to use because of a systematic design process. And USB communication is accordingly selected to transfer data between micro-controller and computer. USB communication is composed of a series of transfers. There are four transfer types are defined in USB module: Control, Interrupt, Bulk and Isochronous. The selection of transfer type depends on the end application. Bulk transfer is preferred for transference of large amounts of non-periodic burst data. It uses idle time on the bus that is not used by Interrupt and Isochronous transfers. The more available the bus is, the faster the data is transferred until to the bus speed limitation. Bulk transfer is only supported on full speed and high speed devices, but not on low speed devices.

The USB transference comprises multiple stages. The Bulk transfer type is composed of three steps: Token transaction, Data transaction and Handshake transaction as is shown in Fig. 7.7. In the Token stage, the packet to be transferred is setup where the actual request is made. In the Data transaction, the descriptor information including Packet IDs, Data and Cycle Redundancy Check (CRC) is sent to the host. In the final Handshake stage, the host acknowledges receiving the packet.

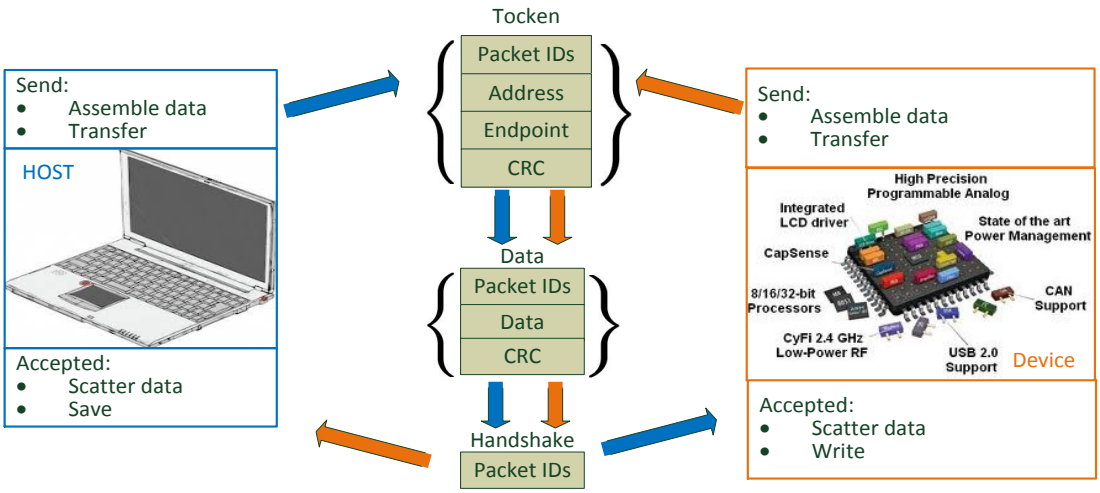

Fig. 7.7: Data transfer structure.

The developed application of USB communication is bidirectional. The process data on the micro-controller including motor speeds, control signals, side distances etc., are transferred to the host computer and saved. Some reference information such as forward linear velocity and desired side distance, and the parameters of controllers can be online adjusted through the user interface program on the Host and sent to the controller device.

7.4 Test results in laboratory

Experiments were firstly executed in laboratory to evaluate the practical substitute for time-optimal row guidance strategy discussed in the Section 6.4. The cultivation bed for white asparagus was modeled using some pieces of solid woods in accordance with the desired dimensions. The control regime of the cascade development was programmed and downloaded onto the PSoC CY8C55 processor (shown in Fig. 7.8). The control loops at low level were performed with a frequency of 200 Hz. The cascade system at the high level was performed with a frequency of 20 Hz. The forward linear velocity of the machine is set to 12cm/s. The processing data were saved on a computer through USB cable. The following performance was investigated against initial position errors and introduced lateral offset. Each experiment was executed repeatedly, and the similar results were achieved.

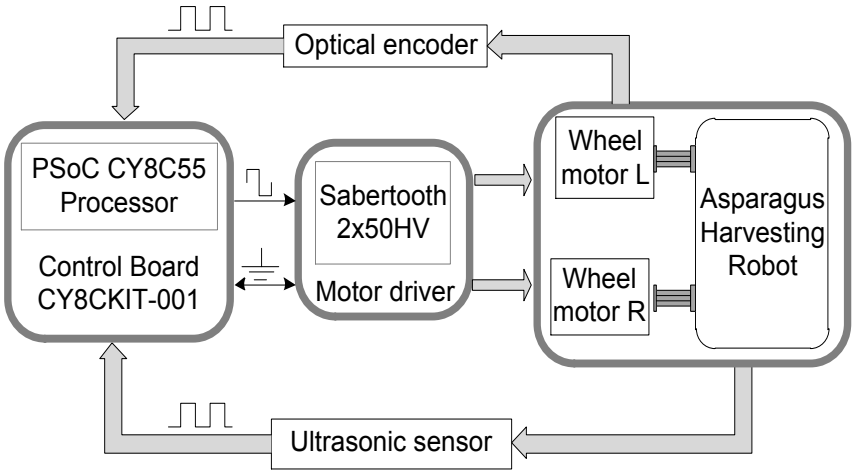

Fig. 7.8: Experimental system.

The two group experimental results were illustrated in Fig. 7.9 and Fig. 7.10. For the first study, the robot started with an initial position of ($S_{Fy}(t_0) = 0.388m$, $S_{Ry}((t_0)) = 0.44m$), which is comparable with the case in Fig. 6.6 in the Section 6.4.2. Fig. 7.10 shows the experimental results for the robot with an initial position of $S_{Fy}(t_0) = 0.335m$, $S_{Ry}\big((t_0)\big) = 0.28m$. To evaluate the guidance performance against external disturbance, a lateral offset of about 1.5cm was introduced at about t = 60s.

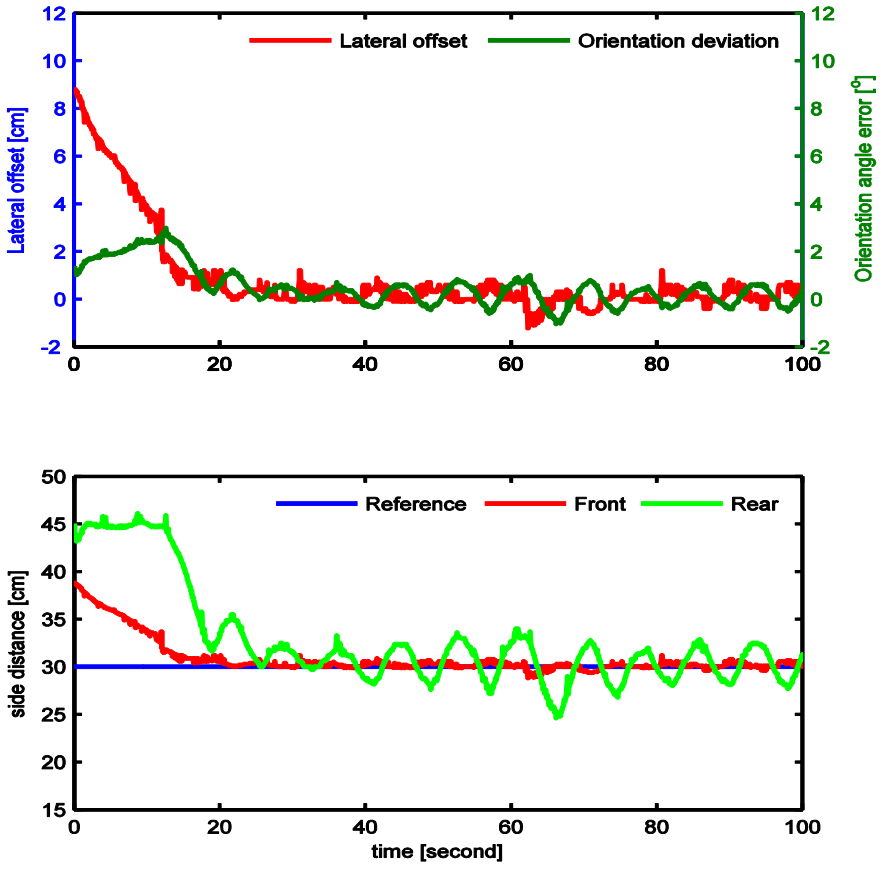

Fig. 7.9: Experimental result of row guiding performance I with $v_{ref} = 0.12m/s$.

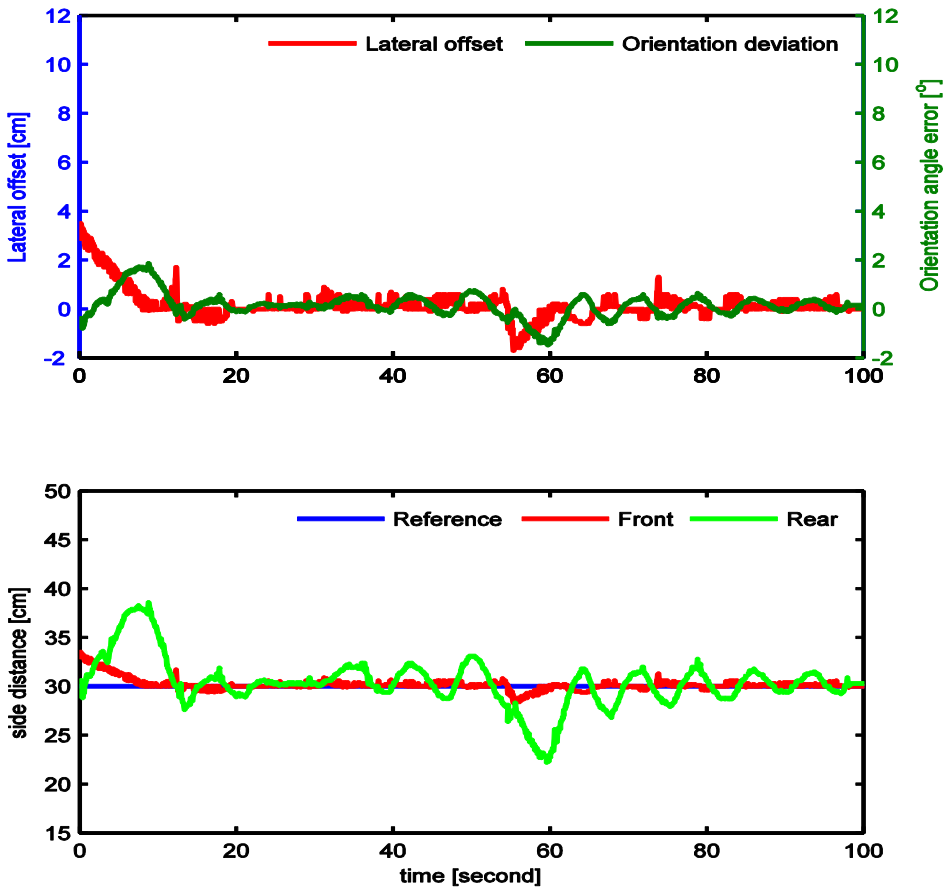

Fig. 7.10: Experimental result of row guiding performance with II $v_{ref} = 0.12m/s$.

It was observed that the lateral offset in Fig. 7.9 decreased continuously to zero. The orientation angle increased before the lateral offset reached zero in that the saturation that set on the orientation angel was adjusted in real-time according to the lateral offset. The introduced track deviation introduced at about $t = 60s$ was also eliminated successfully. In both cases, the experimental results coincide closely with those of the numerical studies. Altogether, all the initial error and the introduced disturbance were successfully eliminated with the proposed practical guidance system. A following precision of ±0.005m for the reference point P of the robot was achieved.

The only difference of the experimental results from the simulation ones is that S_{Ry} (or e_θ) fluctuates continuously around its desired value. It is because e_y is not strictly kept at its desired value in the experimental studies, and the adjustment of the following error is only realized by modifying S_{Ry} (or e_θ) due to the system characteristic. Another impossible reason could be the inevitable misalignment of the ultrasonic sensors. Under this condition, the heading angle would be non-zero with zero lateral offset. To decrease the orientation deviation will increase lateral offset, which will result in fluctuations of the rear distances.

The frequency of the fluctuation depends on the vibration of the lateral offset, and the magnification times of the amplitude with respect to lateral offset is determined by the length of the machine.

7.5 Verification in Field

The on-site tests in the white asparagus field were carried out in middle of May in Colbitz, Sachsen-Anhalt, Germany. The cultivation beds for white asparagus were covered with weeds and also out of shape considerably with the time lapse. The sandy ground was loose due to lasting draught. The required and actual parameters of the test field were shown in Table 7.2. Therefore, the actual situations are not ideal at all. The length of the cultivation bed is about 50m. The headland is circa 5m wide.

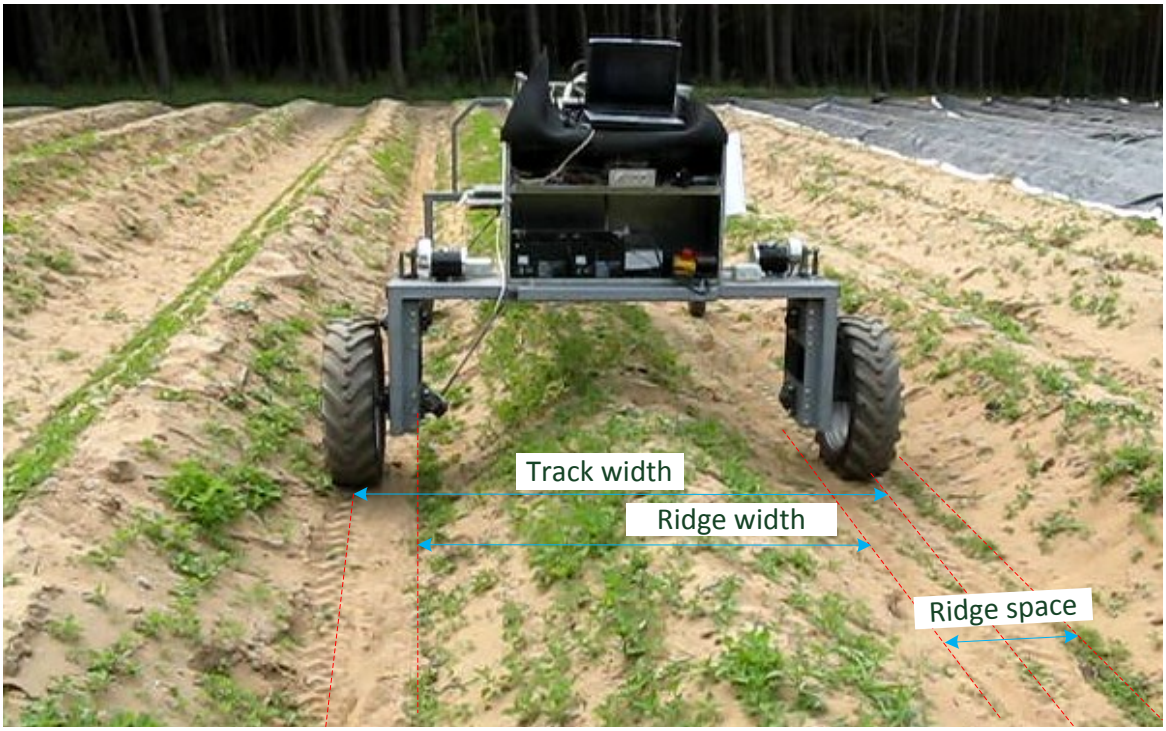

Fig. 7.11: On-site investigation in field

Table 7.2: Cultivation bed

	Requirements (ideal)	Actual situations
Track width [m]	1.9	1.8
Ridge space [m]	≥0.8	0.4~0.5
Ridge width [m]	≤1.1	1.4
Height [m]	0.4~0.7	0.6
Slope of the side surface [degree]	≥50°	≤40°

Pretest was firstly carried out for the field robot without row guidance control strategy. When the drive wheels of the robot subject to different external disturbances caused possibly by rolling resistance or different contact situations between wheels and floor, the linear velocities of the drive wheels will be different. That resulted in an orientation deviation. Without real-time guidance controller, the row following error would be integrated. The worst case for the robot is to drive over the cultivation bed causing damage to the cultivation bed and the asparagus spears.

The row guidance performance of the proposed controller was test with varied situations, varied forward velocities, idle and with load. Fig. 7.12 shows the row following performance of the practical time-optimal control strategy for the robot with a forward linear velocity of 0.12m/s, i.e. 60rpm for the drive motors. The following error and the side distances for the first 100s were illustrated in Fig. 7.12. The field robot started up with an original position of ($S_f(t_0) = 0.29m$, $S_r(t_0) = 0.39m$), where the . It is observed that the orientation deviation e_θ was firstly adjusted to head the right direction by reducing S_r. e_y(i.e. S_f) began to declines only after $e_\theta > 0$. Thereafter, e_y and e_θ converge to zero and fluctuate around zero with the modification of the guidance controller.

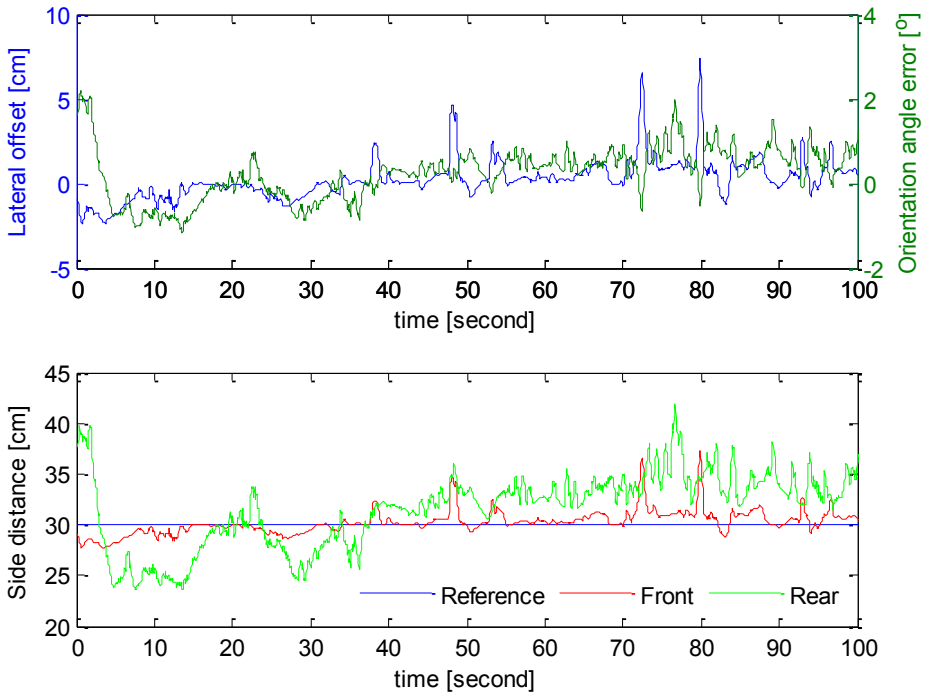

Fig. 7.12: Row guidance performance in the field with $v_{ref} = 0.12m/s$.

A lot of experiments have been carried out in the field. Fig. 7.13 shows the row following performance with the similar initial position but with a higher velocity of 0.2m/s. Fig.

7.14Fig. 7.14 to Fig. 7.15 demonstrate the experimental results of the row guidance performance without load in the field with the forward velocity of 0.4m/s and 0.5m/s, respectively. Fig. 7.16 shows the experimental results for the field robot loaded with 100kg operating with a forward velocity 0.4m/s.

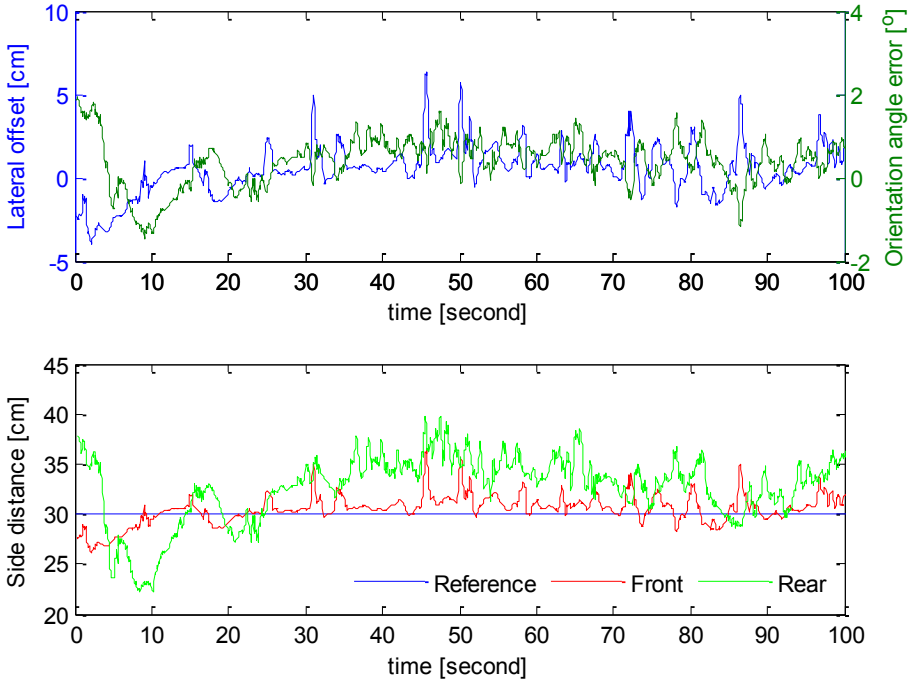

Fig. 7.13: Row guidance performance in the field with $v_{ref} = 0.2m/s$.

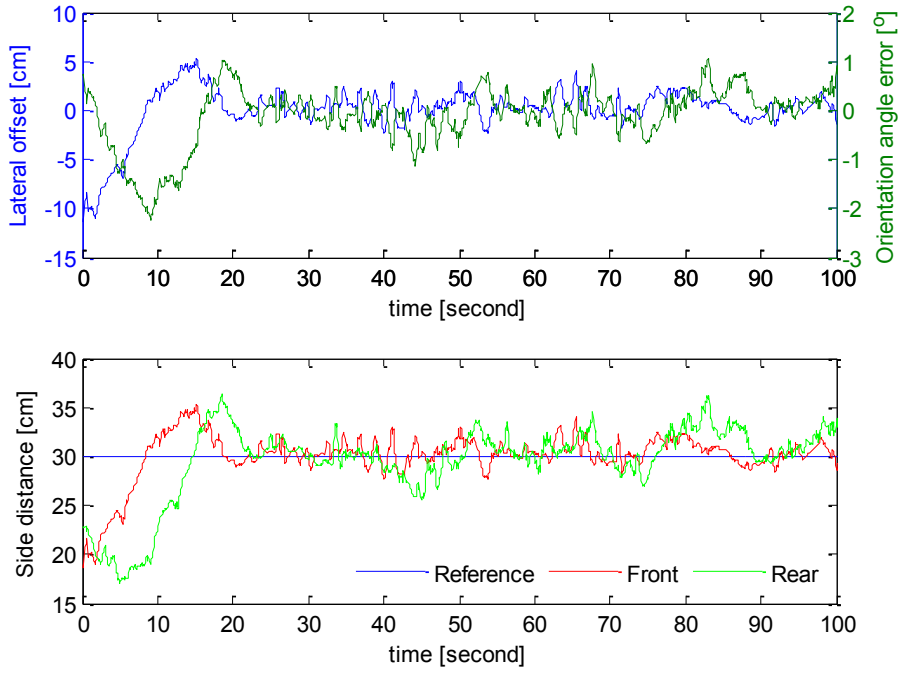

Fig. 7.14: Row guidance performance in the field with $v_{ref} = 0.4m/s$.

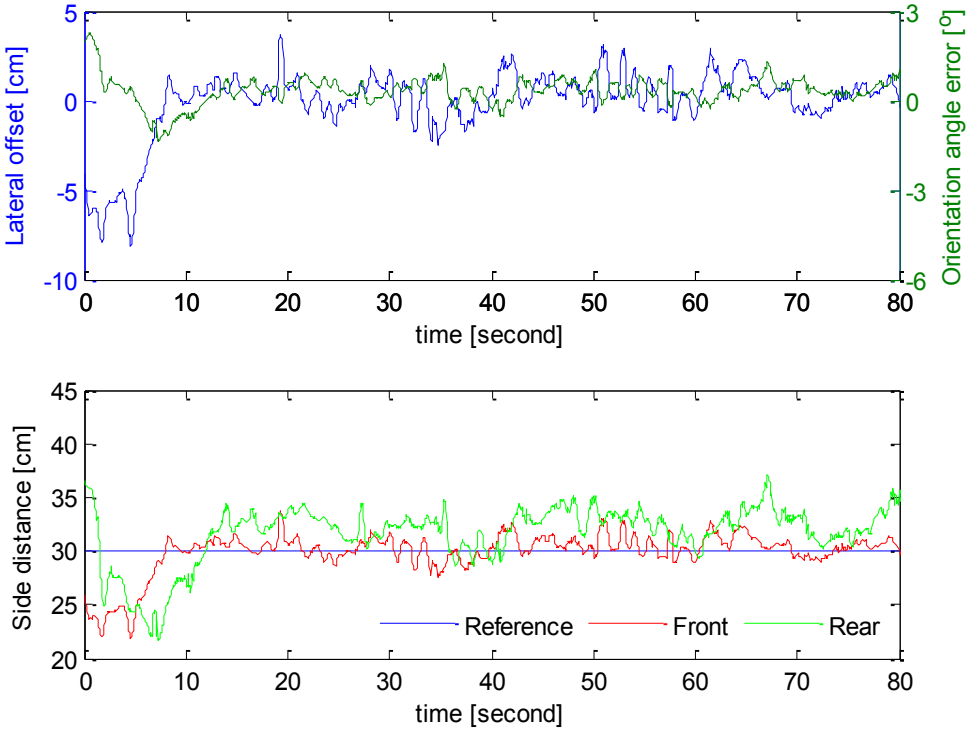

Fig. 7.15: Row guidance performance in the field with $v_{ref} = 0.5m/s$.

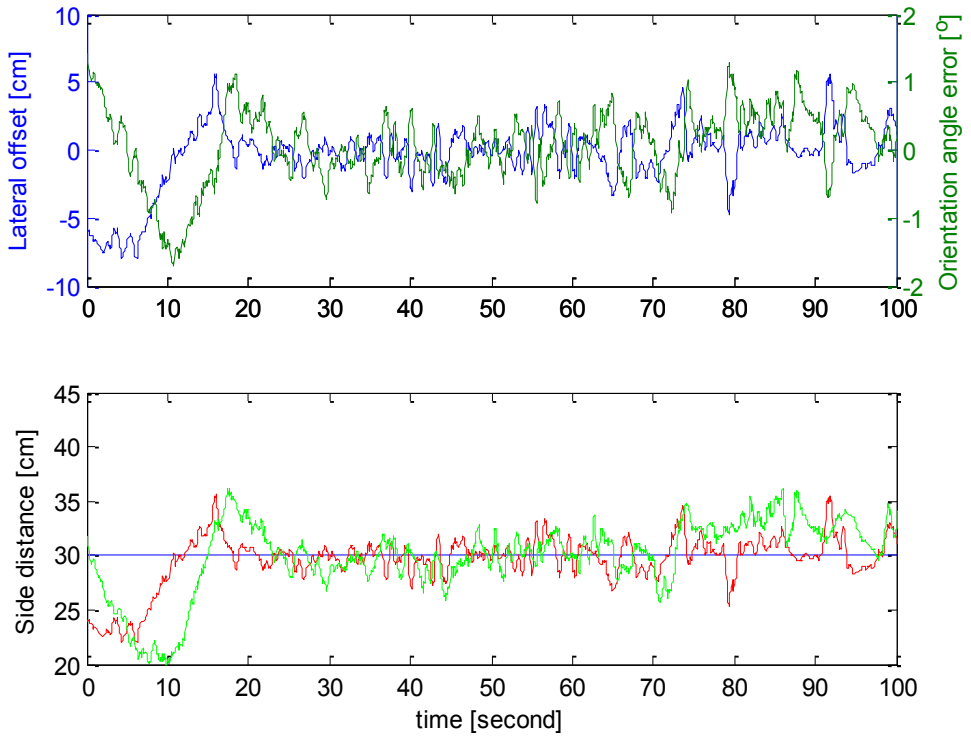

Fig. 7.16: Row guidance performance in the field with $v_{ref} = 0.4m/s$ and a load of 100Kg.

From the experimental results, it is observed that the developing process of the guidance errors and side distances agreed with the simulation results and the prior experimental

results in the laboratory. The field robot converges to its desired trajectory whatever initial positions it starts with. The field robot follows the given cultivation bed with high precision of 0.03m.

The noise is significantly observed in the measurements of the ultrasonic sensors. As is known, the measuring accuracy depends on the echo signal of the emitted ultrasonic waves. When the experimental tests in the field were performed in the later spring, the earth was rather loose due to durable drought. Besides, the test cultivation beds transformed apparently due to long-term exposure in the air. The test situation is considered as worse than normal. Although all of this affected the quality of the echo signal against the cultivation bed and resulted in a weak measuring accuracy, satisfactory row following performance has been achieved with the proposed guidance strategy. We note that slippage was not observed in the in-field experiment. There is no obvious difference between measured distance and the covered distance of the robot that is calculated using the observed velocity. Limited to the available room and the real situations of the asparagus cultivation bed, the turn operation at the headland was performed by hand.

7.6 Discussion

This Chapter was focus on the experimental verification of the proposed time-optimal guidance system. An experimental platform considering automatic and manual operation was setup on the prototype. The automatic row following strategy was performed on a micro-controller development kit with PSoC 5. Since the ultrasonic sensors are only capable of detecting the relative location of the robot with respect to the target cultivation bed, the automatic operation mode is unsuitable for out-row drive. Therefore, manual operation mode is a useful supplement when the information of cultivation bed is not available. A feasible automatic operation for the robot at headland was provided according to the geometrical distribution of the cultivation beds. The function groups were detailed in the software program.

The proposed practical time-optimal row guidance system was firstly evaluated in laboratory. The experimental results coincided very closely with the simulation studies. The satisfactory performance was achieved in the on-side experimental tests in the field. It

has been proved that the suggested row following strategy is highly effective through side distance detection for the robot to follow the given asparagus bed without collision.

8 Conclusions and perspectives

This thesis was focus on the development of a field robot for white asparagus harvest and the automatic row following strategy. Although this research work is focus on the path following control of a wheeled robot for agricultural application, the algorithms to be developed are general enough to be applied to any differential drive mobile robotic machines. In this chapter, the conclusions are firstly drawn. And next some perspectives on the developing improvement for the future are provided.

8.1 Conclusions

The field robot was developed by referring the distribution and dimensions of cultivation beds of white asparagus, as well as the consultation of the farmers of white asparagus plantation. The field robot was determined for a differential-drive mode with two drive wheels integrated with DC motor at the front and two casters at the rear to keep balance. The differential-drive system is cost-effective to be realized and easy to be steered. The features of the cultivation beds, which had a modestly even side surfaces and were built over the ground surface with a height of 50cm, have provided a natural response surface for the ultrasonic signals. Two PING))) ultrasonic sensors have been selected to supervisor the side distances which were used to calculate the actual position of the field robot with respect of the target row.

The row following system of the field robot was developed based on the kinematic model of differential-drive wheeled mobile robots. A typical hierarchical design with two levels was adopted to steer the robot in rows. The high level took charge of coordinating the differential speed of the drive wheels according to the measured following error. The control system at the low level was responsible for the stabilization of the motor speeds. A cascade system, consisting of an inner orientation angle controller and an outer lateral offset controller, was firstly designed using PID method to steer the field robot, where the permitted reference orientation angle was given by the lateral offset controller with a constant saturation limit. Although the initial error and following deviation were successfully eliminated, the potential of the cascade system was not fully exploited. To drive the robot back to the desired trajectory as soon as possible, the time-optimal control for the row guidance system was further exploited using the side distances as the direct controlled variables. The results of the time-optimal control studies illustrated that the

optimal solution was achieved on the boundary of the rear side distance and also depending on the front side distance. However, a practical realization of the time-optimal control method on the micro-controller based on embedded system PSoC 5 was virtually impossible. Resultantly, a mapping between side distances and the row following deviation was observed. The boundary condition of the rear side distance was converted to the limitation on the orientation angle that also depended on the lateral offset. Therefore, an improved cascade system by setting a time-varying limitation on the inner orientation angle controller was applied as a substitute for the time-optimal controller. The effectiveness of row following performance was thoroughly compared in simulation studies. The improved cascade row guidance controller was lastly implemented on the micro-controller. After the successful experimental tests in laboratory, the developed row guidance system of the prototype was further evaluated in the fields. All the experimental results showed that the field robot was capable of following the trajectory given by the target cultivation bed only using two ultrasonic sensors to detect the in-row location of the robot. A satisfactory guidance performance with a precision of ±0.03m has been achieved in the field test.

As a prototype of an automatic field robot for white asparagus harvesting, it is capable of operating automatically along the given cultivation bed. It can also perform the automatic turn operation in well-structured land with enough free space. The alternative manual operation has provided another flexible operation method for the situations where the side distance signals are not available. Therefore, the developed prototype is suitable to be applied as a platform for the further development of an autonomous harvesting machine for white asparagus, and also as an assistant machine to perform the film lift and carriage of the harvested spears.

8.2 Perspectives

Since the field robot is only a prototype as a cost-effective realization of the functions for the first try to accumulate the first experience, there is space to improve or better it.

- Dimension optimization. If the length of the robot can be shorted, there would be more feasible region for the orientation angle, which would make it easier to steer the machine back to the target trajectory faster.
- Installation of an array of ultrasonic sensors. As is known that the measuring surface made up of loose soil or sand could infect the measurement precision of the ultrasonic sensors. Moreover, for the uneven surfaces with stones or clods or coved with weeds, the measurements of the ultrasonic sensors could incorrect or even lost. Array of the ultrasonic sensors can be used to sample not only the distance

information of the robot to the target cultivation bed, but also the distance of the robot to the neighbor beds. With proper data fusion the location of the robot can be determined more exactly.

- Absolute sensors for headland. The precise turn operation at headland requires absolute information of the robot location and the distribution of the cultivation beds. Therefore, additional sensors are essential to be supplemented to get more information of the environment. But additional sensors and advanced technology signify more investment. More research work is needed to get a reasonable compromise between functions and cost-efficiency.

Bibliography

[1] University Bremen, 2012. Report: University Bremen develops automatic asparagus harvester. Nr. 2012057.

[2] M. Asif, S. Amir, A. Israr, and M. Faraz, 2010. A vision system for autonomous weed detection robot. *International Journal of Computer and Electrical Engineering*, vol.2(3), pp.:486–491.

[3] B. Åstrand and A.J. Baerveldt, 2005. A vision based row-following system for agricultural field machinery. *Mechatronics*, vol.15(2), pp.:251–269.

[4] T. Bak, 2001. Vision-gps fusion for guidance of an autonomous vehicle in row crops. *Proceedings of the 14th International Technical Meeting of the Satellite Division of The Institute of Navigation (ION GPS 2001)*, vol.1, pp.:423–451.

[5] T. Bak and H. Jakobsen, 2004. Agricultural robotic platform with four wheel steering for weed detection. *Biosystems Engineering*, vol.87(2), pp.:125–136.

[6] D. Balkcom and M. Mason, 2000. Geometric construction of time optimal trajectories for differential drive robots. In *Fourth Workshop on Algorithmic Foundations of Robotics*, pp.: 1–13.

[7] E.R. Benson, J.F. Reid and Q. Zhang, 2003. Machine vision-based guidance system for agricultural small-grain harvester using cut-edge detection. *Biosystems Engineering*, vol.86(4), pp.:389–398.

[8] J. Billingsley, A. Visala and M. Dunn, 2008. *Springer Handbook of Robotics*. Chapter 16 Robotics in agriculture and forestry, Springer-Verlag, pp: 1065-1077.

[9] J. Borenstein, H.R. Everett and L. Feng, 1996. Where am I? sensors and methods for mobile robot positioning. *University of Michigan*.

[10] J.K. Bourne, 2009. The global food crisis-the end of plenty. *National Geographer*, June, pp.: 26–59.

[11] A. Carullo and M. Parvis, 2001. An ultrasonic sensor for distance measurement in automotive applications. *IEEE Sensors Journal*, vol.1(2), pp.:143.

[12] R.P. Cavalieri, C.D. Clary, R. Folwell, J. Durfey, and T Ball, 2005. Asparagus harvester trials geiger lund selective harvester evaluation. Technical report, Agricultural Research Center, Washington State University.

[13] A.P. Chatzimicahli, I.P.V. Georgilasand, and D. Tourassis, 2009. Design of an advanced prototype robot for white asparagus harvesting. In *IEEE/ASME International Conference on Industrial Advanced Intelligent Mechatronics,*pp.: 887-892.

[14] Y. Chung, C. Park, and F. Harashima, 2001. A position control differential drive wheeled mobile robot. *Industrial Electronics, IEEE Transactions on*, vol.48(4), pp.:853–863.

[15] D. Chwa, 2010. Tracking control of differential-drive wheeled mobile robots using a backstepping-like feedback linearization. *Systems, Man and Cybernetics, Part A: Systems and Humans, IEEE Transactions on*, vol.40(6), pp.:1285–1295.

[16] F. Díaz del Río, G. Jimenez, J.L. Sevillano, S. Vicente, and A. Civit Balcells, 2001. A path following control for unicycle robots. *Journal of Robotic Systems*, vol.18(7), pp.:325–342.

[17] A. De Luca, G. Oriolo, and M. Vendittelli, 2001. Control of wheeled mobile robots: an experimental overview. *Ramsete*, pp.: 181–226.

[18] D. Ehlert, R. Adamek, and H.J. Horn, 2009. Vehicle based laser range finding in crops. *Sensors*, vol.9(5), pp.:3679–3694.

[19] D. Ehlert, M. Heisig, and R. Adamek, 2010. Assessment of a laser scanner on agricultural machinery. *Engineering for Rural Development*, pp.: 32–36.

[20] M. Ehsani, Y. Gao, and A. Emadi, 2009. *Modern Electric, Hybrid Electric, and Fuel Cell Vehicles: Fundamentals, Theory, and Design*, Chapter II Vehicle Fundamentals, CYC Press, pp.: 21–60.

[21] S. Ericson and B. Astrand, 2010. Row-detection on an agricultural field using omnidirectional camera. In *Intelligent Robots and Systems (IROS), In 2010 IEEE/RSJ International Conference on*, pp.: 4982–4987.

[22] F. Espinosa, E. López, R. Mateos, M. Mazo, and R. García, 2001. Advanced and intelligent control techniques applied to the drive control and path tracking systems on a robotic wheelchair. *Autonomous Robots*, vol.11(2), pp.:137–148.

[23] L. Feng, Y. Koren, and J. Borenstein, 1993. A cross-coupling motion for a differential drive mobile robot. *IEEE Transactions on Control Systems*, vol.13(6), pp.: 35–43.

[24] L. Feng, Y. Koren, and J. Borenstein, 1994. A model-reference adaptive motion controller for a differential-drive mobile robot. In *Robotics and Automation, 1994. Proceedings., 1994 IEEE International Conference on*, pp.: 3091–3096.

[25] M.M. Foglia and G. Reina, 2006. Agricultural robot for radicchio harvesting. *Journal of Field Robotics*, vol.23(6-7), pp.:363–377.

[26] P.E. Gill, W. Murray, and M.A. Saunders, 2005. SNOPT: An SQP algorithm for large-scale constrained optimization. *Society for Industrial and Applied Mathematics*, vol.47(1), pp.:99–131.

[27] P. Goel, S.I. Roumeliotis, and G. Sukhatme, 1999. Robust localization using relative and absolute position estimates. *Intelligent Robots and Systems, IROS'99. Proceedings. 1999 IEEE/RSJ International Conference*, vol.2, pp.:1134–1140.

[28] H.W. Griepentrog, C.L. Dühring Jaeger, and D.S. Paraforos, 2013. Robots for field operations with comprehensive multilayer control. *Künstliche Intelligenz*, vol.27(4), pp.:325–333.

[29] R. Grisso, M. Alley, and G. Groover, 2009. Precision farming tools: GPS navigation. *Viginia Cooperative Extension*, pp.: 1–7.

[30] T. Hague, J.A. Marchant, and N.D. Tillett, 2000. Ground based sensing systems for autonomous agricultural vehicles. *Computers and Electronics in Agriculture*, vol.25(1), pp.:11–28.

[31] D. Hest, 2012. New driverless tractor, grain cart systems coming this year. *www.tractorlife.com*, June 13.

[32] Case IH, 2011. V2V from Case IH – harvest more efficiently. *FARMING UK*, http://www.farminguk.com/news/V2V-from-Case-IH-harvest-more-efficiently_19904.html.

[33] Parllax Inc. , 2009. Ping)))™ ultrasonic distance sensor (28015). v1.6, pp.:1–12.

[34] N. Irie, N. Taguchi, T. Horie, and T. Ishimatsu, 2009. Development of asparagus harvester coordinated with 3D vision sensor. *Journal of Robotics and Mechatronics*, vol.21(5), pp.: 583–589.

[35] C. Jeffrey, 2010. An introduction to GNSS- GPS, GLONASS, GALILEO and other global navigation satellite systems. *Published by NovAtel Inc.*.

[36] JohnDeere. John deere machine sync-synchronize your mmachine and logistics for true "on-the-go harvesting": http://www.JohnDeere.com/FarmSigh.

[37] R. Kepner, 1965. Mechanical harvesting feasible for white asparagus. *California Agriculture*, January, pp.:2–5.

[38] Donald E. Kirk, 1998. *Optimal Control Theory: An Introduction*. Dover Publications, Inc., Mineola, New York.

[39] M. Kise, N. Noguchi, K. Ishii, and H. Terao, 2002. The development of the autonomous tractor with steering controller applied by optimal control. In *Proceedings of Automation Technology for Off-Road Equipment (ASAE)*, pp.: 367–373.

[40] M. Kise, N. Noguchi, K. Ishii, and H. Terao, 2002. Enhancement of turning accuracy by path planning for robot tractor. *In: Proc. Automation Technology for Off-road Equipment, ASAE*, pp.:8-11.

[41] M. Kise, Q. Zhang, and F.R. Más, 2005. A stereovision-based crop row detection method for tractor automated guidance. *Biosystems Engineering*, vol.90(4), pp.:357–367.

[42] N. Kondo, M. Monta, and T. Fujiura, 1996. Fruit harvesting robots in Japan. *Advances in Space Research*, vol.18(1), pp.:181–184.

[43] M. Li, K. Imou, K. Wakabayashi, and S. Yokoyama, 2009. Review of research on agricultural vehicle autonomous guidance. *International Journal of Agricultural and Biological Engineering*, vol.2(3), pp.:1–16.

[44] G. Lindhout, 2008. Brabantse wal presents first full-automatic asparagus harvester in the world. *Available: http://www.freshplaza.com/*.

[45] J. Liorens, E. Gil, J. Llop, and A. Escolà, 2011. Ultrasonic and LIDAR sensors for electronic canopy characterization in vineyards: Advances to improve pesticide application methods. *Sensors*, vol.11, pp.:2177–2194.

[46] P. Liu, S. Bi, G. Zang, and W. Wang, 2011. Obstacle avoidance system for agricultural robots based on multi-sensor information fusion. *Computer Science and Network Technology (ICCSNT), 2011 International Conference on*, vol.2, pp.:1181–1185.

[47] J.A. Marchant, T. Hague, and N.D. Tillett, 1997. Row-following accuracy of an autonomous vision-guided agricultural vehicle. *Computers and Electronics in Agriculture*, vol.16(2), pp.:165–175.

[48] S.S. Mehta, T.F. Burks, and W.E. Dixon, 2008. Vision-based localization of a wheeled mobile robot for greenhouse applications: A daisy-chaining approach. *Computers and Electronics in Agriculture*, vol.63(1), pp.:28–37.

[49] M. Monta, N. Kondo, and K.C. Ting, 1998. End-effectors for tomato harvesting robot. *Artificial Intelligence Review*, vol.12(1), pp.:11–25.

[50] P.F. Muir, 1988. Modelling and Control of Wheel Mobile Robots. *PhD thesis*, Department of Electrical and Comupter Engineering, Carnegie Mellon University.

[51] United Nations, 2008. Addressing the global food crisis: key trade, investment and commodity policies in ensuring sustainable food security and alleviating poverty. In *United Nations Conference on Trade and Development*.

[52] M. Nielsen, D. Slaughter, and C. Gliever, 2012. Vision-based 3D peach tree reconstruction for automated blossom thinning. *Industrial Informatics, IEEE Transactions on*, vol. 8(1), pp.:186–196.

[53] N. Noguchil, K. Ishii, and H. Terao, 1997. Development of an agricultural mobile robot using a geomagnetic direction sensor and image sensors. *Journal of Agricultural Engineering Research*, vol. 67, pp.:1–15.

[54] M. Nørremark, H.W. Griepentrog, J. Nielsen, and H.T. Søgaardc, 2008. The development and assessment of the accuracy of an autonomous gps-based system for intra-row mechanical weed control in row crops. *Biosystems*, vol.101(4), pp.:396–410.

[55] Leibniz-Institute of Agricultural Engineering, 2010. Case study: Semi-automatic harvesting of white asparagus. Technical report of Leibniz-Institute of Agricultural Engineering.

[56] T. Oksanen and A. Visala, 2004, An Optimal control of tractor-trailer system in headlands. *Proc. Automation Technology for Off-road Equipment. Kyoto, Japan*, pp.: 255–263.

[57] C. Peiter, 2008. Der Spargelpanther - Raubtier oder zahme Katze. *Available: http://www.ai-solution.de/*.

[58] M. Pham and D. Wang, 2004. A unified nonlinear controller for a platoon of car-like vehicles. In *Proceeding of the 2004 American Control Conference*, vol.3, pp.: 2350–2355.

[59] A.R. Rao, D. Benson, C.L. Darby, and G.T. Huntington, 2011. *User's manual for GPOPS version 4.x: A MATLAB software for solving multiple-phase optimal control problem using hp-adaptive pseudospectral methods.*

[60] J.N. Reed and R.D. Tillett, 1994. Initial experiments in robotic mushroom harvesting. *Mechatronics*, vol.4(3), pp.:265–279.

[61] L.E. Rehder, 2011. Knappes Angebot und hohe Preise prägten die Spargelsaison. *Available: http://www.proplanta.de*.

[62] D.C. Slaughter, D.K. Giles, and D. Downey, 2008. Autonomous robotic weed control systems: A review. *Computers and Electronics in Agriculture*, vol.61(1), pp.:63–78.

[63] J. Sánchez-Hermosilla, F. Rodríguez, R. González, J.L. Guzmán, and M. Berenguel, 2010. A mechatronic description of an autonomous mobile robot for agricultural tasks in greenhouses. *Mobile Robots Navigation*, pp.: 583–608.

[64] P. Soueres and J.P. Laumond, 1996. Shortest path synthesis for a car-like robot. *IEEE Transactions on Automatic Control*, vol.41(5), pp.:672–688.

[65] V. Srinivasan and R. Lumia, 1988. A 3D vision system for robot guidance with structured sine wave illumination. *Intelligent Control, IEEE International Symposium on*, pp.: 196–200.

[66] A. Stoll and H. Dieter Kutzbach, 2000. Guidance of a forage harvester with GPS. *Precision Agriculture*, vol.2(3), pp.:281–291.

[67] B. Åstrand and A.J. Baerveldt, 2002. An agricultural mobile robot with vision-based perception for mechanical weed control. *Autonomous Robots*, vol.13(1), pp.:21–35.

[68] B. Åstrand and A.J. Baerveldt, 2005. A vision based row-following system for agricultural field machinery. *Mechatronics*, vol.15, pp.:251–269.

[69] V. Subramanian, T.E. Burks, and S. Singh, 2005. Autonomous greenhouse sprayer vehicle using machine vision and ladar for steering control. *Applied Engineering in Agriculture*, vol.21(5), pp.:935–943.

[70] V. Subramanian, T.F. Burks, and A.A Arroyo, 2006. Development of machine vision and laser radar based autonomous vehicle guidance systems for citrus grove navigation. *Computers and Electronics in Agriculture*, vol.53(2), pp.:130–143.

[71] H.J. Sussmann and G. Tang, 1991. Shortest paths for the reeds-shepp car: a worked out example of the use of geometric techniques in nonlinear optimal control. In *Research Report SYCON-91-10*.

[72] K. Tanigaki, T. Fujiura, A. Akase, and J. Imagawa, 2008. Cherry-harvesting robot. *Computers and Electronics in Agriculture*, vol.63(1), pp.:65–72.

[73] N.D. Tillett, T. Hague, and S.J. Miles, 2002. Inter-row vision guidance for mechanical weed control in sugar beet. *Computers and Electronics in Agriculture*, vol.33(3), pp.:163–177.

[74] R. Torisu, K. Tanaka and J. Imae, 1997. Optimal path of headland for tractors by optimal control theory. *Journal of the Japanese Society of Agricultural Machinery*, vol.59(4), pp.: 3–10.

[75] R. Torisu, T. Nakatsubo, and J. Imae, 1996. Minimum time control problem of tractor lateral motion. *Journal of the Japanese Society of Agricultural Machinery*, vol.58(5), pp.:5–12.

[76] S.K. Tso and Y.P. Fung, and Y.H. Cheung, 1996. Fuzzy-logic control for differential-wheel-drive AGVs using linear opto-sensor arrays. *Robotics and Automation, 1996 IEEE International Conference on*, vol.3, pp.:2816–2821.

[77] S.D. Tumbo, M. Salyani, J.D. Whitney, T.A. Wheaton, and W.M. Miller, 2002. Investigation of laser and ultrasonic ranging sensors for measurements of citrus canopy volume. *Applied Engineering in Agriculture*, vol.18(3), pp.:367–372.

[78] M. Umeda, S. Kubota and M. Iida, 1999. Development of “stork”, a watermelon-harvesting robot. *Artificial Life and Robotics*, vol.3(3), pp.:143–147.

[79] F. Uwihs, 2008. Nicht selektiver Spargelvollernter. *Available: http://www.spargel-erdbeerprofi.de.*

[80] E.J. Van Henten, J. Hemming, B.A.J. Van Tuijl, J.G. Kornet, J. Meuleman, J. Bontsema, and E.A. Van Os, 2002. An autonomous robot for harvesting cucumbers in greenhouses. *Autonomous Robots*, vol.13(3), pp.:241–258.

[81] D. Wang, G. Xu, and M. Pham, 2001. Look-ahead/behind control of a car-like mobile robot. In *Proc. of the 2001 Robotics and Mechatronics Congress*, pp.:101–106.

[82] H. Wang, Y. Chen, and P. Soueres, 2009. A geometric algorithm to compute time-optimal trajectories for a bidirectional steered robot. *IEEE Transactions on Robotics*, vol.25(2), pp.:399–413.

[83] N. Wang, N. Zhang, and M. Wang, 2006. Wireless sensors in agriculture and food industry - recent development and future perspective. *Computers and Electronics in Agriculture*, vol.50(1), pp.:1–14.

[84] U. Weiss and P. Biber, 2011. Plant detection and mapping for agricultural robots using a 3d lidar senso. *Robotics and Autonomous Systems*, vol. 59(5), pp.:339–345.

[85] F.I. Willrodt, 1924. Steering attachment for tractors, US Patent, No.1506706.

[86] H. Wittel, D. Muhs, D. Jannasch, and J. Vossiek, 2011. Roloff/Matek Maschinenelemente: Normng, Berechnung, Gestaltung - Lehrbuch und Tabellenbuch, Chapter 17 Kettengetriebe, Vieweg + Teubner Verlag, pp.:6 22.

[87] C. Wonneberge, 2005. Erntehilfen in der Spargelernte im Vergleich. *Available: http://www.engelsmachines.nl*.

[88] C. Wuwei, J.K. Mills and S. Wenwu, 2004. A new navigation method for an automatic guided vehicle. *Journal of Robotic Systems*, vol.21(3), pp.:129–139.

[89] O. Yekutieli and F.G. Pegna, 2002. Automatic guidance of a tractor in a vineyard. *Agricultural and Biological Engineers*, pp.: 252–260.

[90] Q. Zhang, J. F. Reid, and N. Noguchi, 1999. Agricultural vehicle navigation using multiple guidance sensors. *In: Proceedings of International Conference on Field and Service Robotics*, pp.: 293–298.

[91] Q. Zhang, J.F. Reid, and N. Noguchi, 2000. Agricultural vehicle navigation using multiple guidance sensors. *SAE Transactions, Journal of Commercial Vehicles*, vol.108, pp.:27–31.

[92] Z.X. Zhu, R. Torisu, J.I. Takeda, E.R Mao and Q. Zhang, 2005. Neural network for estimating vehicle behavior on sloping terrain. *Biosystems Engineering*, vol. 91(4), pp.:403–411.